nature neuroscience

Article

https://doi.org/10.1038/s41593-025-01877-7

Nasal anti-CD3 monoclonal antibody ameliorates traumatic brain injury, enhances microglial phagocytosis and reduces neuroinflammation via IL-10-dependent T_{reg}–microglia crosstalk

Received: 17 October 2022

Accepted: 20 December 2024

A list of authors and their affiliations appears at the end of the paper

Neuroinflammation plays a crucial role in traumatic brain injury (TBI), contributing to both damage and recovery, yet no effective therapy exists to mitigate central nervous system (CNS) injury and promote recovery after TBI. In the present study, we found that nasal administration of an anti-CD3 monoclonal antibody ameliorated CNS damage and behavioral deficits in a mouse model of contusional TBI. Nasal anti-CD3 induced a population of interleukin (IL)-10-producing regulatory T cells (T_{reg} cells) that migrated to the brain and closely contacted microglia. T_{reg} cells directly reduced chronic microglia inflammation and regulated their phagocytic function in an IL-10-dependent manner. Blocking the IL-10 receptor globally or specifically on microglia in vivo abrogated the beneficial effects of nasal anti-CD3. However, the adoptive transfer of IL-10-producing T_{reg} cells to TBI-injured mice restored these beneficial effects by enhancing microglial phagocytic capacity and reducing microglia-induced neuroinflammation. These findings suggest that nasal anti-CD3 represents a promising new therapeutic approach for treating TBI and potentially other forms of acute brain injury.

Traumatic brain injury (TBI) is a leading cause of death and disability, with both direct and indirect costs[1–3]. TBI is implicated in long-term morbidity, including motor deficits, cognitive decline and long-term medical comorbidities and neurodegeneration[4–6]. Current treatments primarily focus on early surgical intervention to limit hematoma expansion and supportive therapy; however, there are few pharmacological interventions to reduce long-term cognitive sequelae post-injury[7–10]. TBI induces a primary mechanical injury followed by a secondary biochemical and cellular response which contributes to neurological impairment[11]. Critically, neuroinflammation is one of the key mechanisms implicated in both the acute and the chronic phases of TBI[12] and, as such, has been identified as an important and potentially modifiable driver of secondary injury in both animal and human studies[13–19]. TBI drives secondary injury via the activation of resident microglia, induction of cytokine release and recruitment of circulating monocytes or lymphocytes to the CNS, which further amplifies pathological inflammation[11,20]. Despite the clear clinical implications, no treatment specifically targets this neuroinflammatory process, partly as the result of the largely unknown molecular and cellular mechanisms that lead to neurological deficits after TBI[20,21]. Therefore, identifying new therapies to address chronic CNS inflammation after TBI represents an important unmet need.

$FoxP3^+$ regulatory T cells (T_{reg} cells) represent a crucial subset of $CD4^+$ T cells that modulate and limit adherent inflammatory responses[22]. There is a growing body of evidence showing that $FoxP3^+$ T_{reg} cells play a critical role in maintaining immune homeostasis and

e-mail: hweiner@rics.bwh.harvard.edu

suppressing immune responses in several acute[23,24] and chronic neurological diseases[25,26]. Experimentally, the depletion of FoxP3$^+$ T$_{reg}$ cells in mice with controlled cortical impact (CCI) injuries leads to increased T cell infiltration, enhanced reactive astrogliosis and exacerbated motor deficits[27]. Conversely, expanding CD4$^+$ FoxP3$^+$ T$_{reg}$ cells through IL-2 treatment has been shown to improve outcomes in animal models of TBI[28]. In humans with TBI, the level of CD4$^+$CD25$^+$FoxP3$^+$ T$_{reg}$ cells positively correlates with clinical outcomes[29]. Together, these studies suggest that inducing T$_{reg}$ cells is a promising approach for the treatment of TBI.

The mucosal immune system is a unique tolerogenic organ that provides a physiological method for inducing T$_{reg}$ cells and is clinically appealing as a result of its apparent lack of toxicity. Our laboratory has investigated the induction of T$_{reg}$ cells by the nasal administration of anti-CD3 monoclonal antibody (aCD3 mAb) and has shown the ameliorating effects of nasal aCD3 in both autoimmune[30] and CNS models of disease, including models of progressive multiple sclerosis (MS)[31] and Alzheimer's disease[32]. Based on this, we investigated whether nasal aCD3 could influence outcomes in relevant TBI models by modulating both systemic and local CNS immune responses.

Accordingly, we demonstrated that nasal aCD3 induces FoxP3$^+$ T$_{reg}$ cells, which ameliorate TBI by modulating CNS innate immunity, enhancing microglia phagocytosis and improving neuropathological and behavioral outcomes post-injury in an IL-10-dependent manner. These findings highlight a new immune-based approach for treating TBI and potentially other types of acute brain injury.

Results

Nasal aCD3 mAb improves cognitive and motor outcomes after TBI

To investigate the therapeutic effect of nasal aCD3 in TBI, we employed the CCI model of TBI, which is known for its accuracy and reproducibility[33], to recapitulate features of moderate-to-severe TBI features, including cerebral contusion, neuroinflammation, blood–brain barrier (BBB) dysfunction and long-term behavioral outcomes. We investigated the therapeutic effects of nasal aCD3 on motor and behavioral outcomes in male mice treated at different times after injury: immediate (4-6 h post-injury), early (3 d post-injury) and delayed (14 d post-injury) (Fig. 1a). Treatment was continued once daily for 7 d, then 3× weekly for up to 1 month after injury (Fig. 1a). In the immediate treatment group, we found improvement in motor function and coordination assessed by the rotarod test (Fig. 1b). Using the Morris water maze (MWM) test, TBI mice treated with aCD3 exhibited near-complete restoration of spatial memory and increased time spent in the target quadrant during the probe trial (Fig. 1b) compared with isotype-treated TBI mice. In addition, we found that male mice treated with immediate nasal aCD3 exhibited less anxious behavior, using the open field test. We found a similar beneficial effect with early treatment (3 d post-injury), except for anxiety (Extended Data Fig. 1a).

We then investigated the effect of delayed (14 d post-injury) nasal aCD3 treatment on behavioral outcomes in male mice and found no improvement in the treated the group compared with the TBI-iso control (Extended Data Fig. 1b). In addition to male mice, we investigated the effects of immediate nasal aCD3 treatment on TBI in female mice. We did not find notable differences in motor or spatial memory testing between the groups after moderate CCI. As reported in the literature, female rodents may outperform males in behavioral tasks after brain injury[34–36]. Thus, we were unable to demonstrate the beneficial effect of nasal aCD3 treatment in female mice at this injury level (Extended Data Fig. 1c).

We then investigated the effect of nasal aCD3 treatment on behavioral outcomes in a more severe form of TBI (3 mm tip diameter and 1.5 mm depth) in both male and female mice. We found improvement in motor function and coordination in the TBI-aCD3 group when compared with TBI-iso control in both sexes (Extended Data Fig. 1d,e). There was partial restoration in spatial memory and increased time spent in the target quadrant during the probe trial in the nasal aCD3-treated mice compared with TBI-iso control in both sexes. Male mice treated with nasal aCD3 exhibited less anxiety-like behavior after severe TBI, but we were unable to assess the beneficial effects of nasal aCD3 in female mice because they did not develop an anxiety phenotype after severe TBI (Extended Data Fig. 1d,e). These data clearly demonstrate that nasal aCD3 improves behavioral outcomes in moderate and severe CCI-induced TBI, with a greater effect being observed in male mice.

Nasal aCD3 mAb ameliorates TBI neuropathology

TBI induces BBB disruption, edema, neuronal death and tissue loss, in addition to the increased production of inflammatory mediators and gliosis[20]. Therefore, we assessed the effects of nasal aCD3 on these neuropathological outcomes (Fig. 1a). We first measured the parenchymal lesion volume in sham-iso, TBI-aCD3 and TBI-iso groups at 7 d post-injury, using 3-tesla magnetic resonance imaging (MRI). We found a reduction in lesion volume in the nasal aCD3-treated group compared with TBI-iso controls (Fig. 1c and Extended Data Fig. 2a). We also measured lesion volume at 1 month post-CCI using hematoxylin and eosin (H&E) staining and, consistent with the MRI, we found a reduction in lesion volume in TBI-aCD3 mice compared with the TBI-iso control (Fig. 1d). Nasal aCD3 also improved BBB integrity at 3 d post-injury compared with the TBI-iso control (Extended Data Fig. 2b). The percentage of brain edema in the ipsilateral and contralateral hemispheres at 3 d post-CCI was reduced in the ipsilateral hemisphere for the TBI-aCD3 group compared with the TBI-iso control (Extended Data Fig. 2c). CCI increased cell death, as measured by TUNEL staining at 7 d after brain injury (Fig. 1e), which was reduced in nasal aCD3 treatment compared with TBI-iso controls. Consistent with previous reports, we found that CCI was associated with an increase in microglia or macrophage activation (Iba-1 staining) at 30 d post-injury compared with sham-iso controls (Fig. 1f)[20,37]. We found that there was a reduction in microgliosis at 30 d post-injury in male mice in both the immediate and the early nasal

Fig. 1 | Nasal aCD3 improves behavioral outcomes and ameliorates neuropathological outcomes in the CCI model of TBI. a, Experimental timeline schematic for treatment regimens (created with BioRender.com). **b**, Behavioral testing (rotarod, MWM test, probe trial, open field for anxiety-like behavior) in the immediate treatment group (sham-iso $n = 8$, TBI-iso $n = 12$, TBI-aCD3 $n = 12$). The MWM test was analyzed by two-factor, repeated-measure, two-way ANOVA (group × time) and others by one-way ANOVA with Tukey's multiple comparisons. Data are shown as mean ± s.e.m. **c**, MRI lesion volume 7 d post-TBI (TBI-iso $n = 5$, TBI-aCD3 $n = 5$), analyzed by two-sided, unpaired Student's t-test. Data are shown as mean ± s.e.m. The red dashes indicate the lesion area. **d**, Lesion volume from H&E-stained brain sections 30 d post-TBI measured with ImageJ (TBI-iso $n = 4$, TBI-aCD3 $n = 4$), analyzed by two-sided, unpaired Student's t-test. Data are shown as mean ± s.e.m. Scale bars, 1,000 µm. **e**, Immunofluorescence of neuronal death 7 d post-TBI at pericontusional cortex (DAPI, blue; TUNEL, red; 7-AAD, green). Scale bars, 200 µm (500 µm for zoomed out). TUNEL-positive cells were quantified using ImageJ (TBI-iso $n = 5$, TBI-aCD3 $n = 5$) and analyzed using two-sided, unpaired Student's t-test. Data are shown as mean ± s.e.m. **f**, Immunofluorescence of Iba-1 at 30 d post-TBI in pericontusional cortex (DAPI, blue; Iba-1, red). Scale bars, 200 µm (500 µm for zoomed out). Iba-1$^+$ cells quantified using ImageJ (sham-iso $n = 4$, TBI-iso $n = 4$, TBI-aCD3 $n = 4$), analyzed by one-way ANOVA with Tukey's multiple comparisons. Data are shown as mean ± s.e.m. **g**, Serum biomarkers 1 d post-TBI measured by Quanterix SiMoA and V-Plex proinflammatory assays (sham-iso $n = 4$, TBI-iso $n = 12$, TBI-aCD3 $n = 12$), analyzed by one-way ANOVA with Tukey's multiple comparisons. Data are shown as box plots (min., max., interquartile range (IQR), median). d.p.i., d post-injury; NS, non-significant. All data represent biological replicates from two independent experiments.

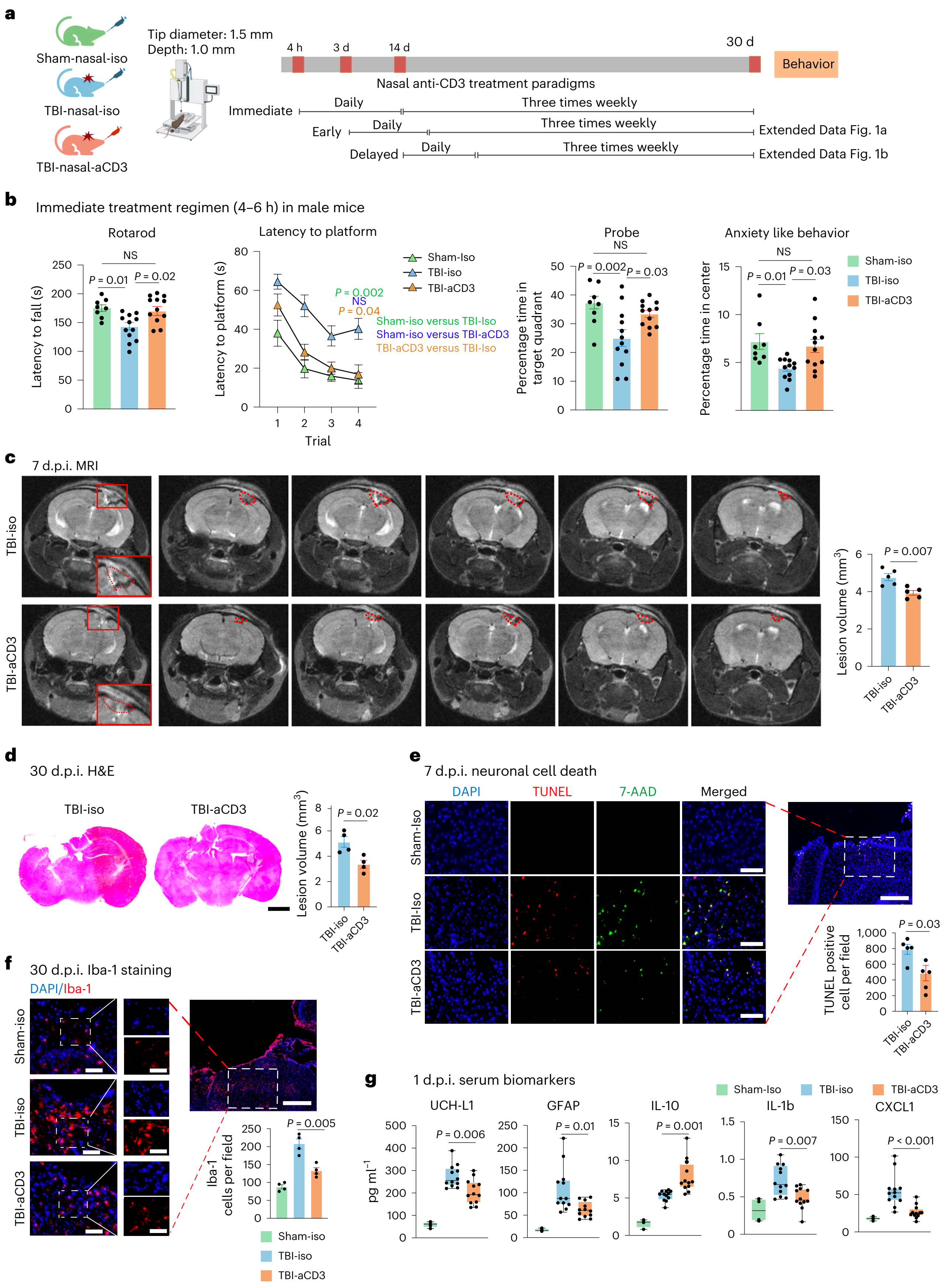
a
Sham-nasal-iso
TBI-nasal-iso
TBI-nasal-aCD3
Tip diameter: 1.5 mm
Depth: 1.0 mm
4 h
3 d
14 d
30 d
Behavior
Nasal anti-CD3 treatment paradigms
Immediate
Daily
Three times weekly
Early
Daily
Three times weekly
Extended Data Fig. 1a
Delayed
Daily
Three times weekly
Extended Data Fig. 1b
b
Immediate treatment regimen (4–6 h) in male mice
Rotarod
Latency to fall (s)
NS
P = 0.01
P = 0.02
Latency to platform
Latency to platform (s)
Trial
Sham-Iso
TBI-iso
TBI-aCD3
P = 0.002
NS
P = 0.04
Sham-iso versus TBI-Iso
Sham-iso versus TBI-aCD3
TBI-aCD3 versus TBI-Iso
Probe
NS
P = 0.002
P = 0.03
Percentage time in target quadrant
Anxiety like behavior
NS
P = 0.01
P = 0.03
Percentage time in center
Sham-iso
TBI-iso
TBI-aCD3
c
7 d.p.i. MRI
TBI-iso
TBI-aCD3
Lesion volume (mm^3)
P = 0.007
TBI-iso
TBI-aCD3
d
30 d.p.i. H&E
TBI-iso
TBI-aCD3
Lesion volume (mm^3)
P = 0.02
TBI-iso
TBI-aCD3
e
7 d.p.i. neuronal cell death
DAPI
TUNEL
7-AAD
Merged
Sham-Iso
TBI-Iso
TBI-aCD3
TUNEL positive cell per field
P = 0.03
TBI-iso
TBI-aCD3
f
30 d.p.i. Iba-1 staining
DAPI/Iba-1
Sham-iso
TBI-iso
TBI-aCD3
Iba-1 cells per field
P = 0.005
Sham-iso
TBI-iso
TBI-aCD3
g
1 d.p.i. serum biomarkers
Sham-Iso
TBI-iso
TBI-aCD3
UCH-L1
pg ml^{-1}
P = 0.006
GFAP
P = 0.01
IL-10
P = 0.001
IL-1b
P = 0.007
CXCL1
P < 0.001

aCD3 groups (Fig. 1f and Extended Data Fig. 2d). Of note, TBI has also been associated with changes in serum biomarkers[38] and we found a reduction in several TBI serum biomarkers in the immediate nasal aCD3 group, including glial fibrillary acidic protein (GFAP), UCH-L1 and the inflammatory cytokines IL-1b and CXCL1 versus controls. It is interesting that we also found an increase in the anti-inflammatory cytokine IL-10 in the immediate nasal aCD3 group versus control animals (Fig. 1g). These markers could be used to assess the efficacy of treatment in humans. As in male mice, we found that nasal aCD3 reduced lesion volume (Extended Data Fig. 2e) and microgliosis at the lesion site in female mice after severe TBI (Extended Data Fig. 2f). These data clearly demonstrate that the behavioral improvements observed in TBI mice treated with nasal aCD3 are associated with enhanced tissue integrity, as indicated by neuropathology and serum biomarkers.

Nasal aCD3 mAb expands central and peripheral T_{reg} cells after TBI

TBI is associated with major changes in the cellular kinetics of both resident and infiltrating cells, which contribute to brain injury. Therefore, to characterize the effect of nasal aCD3 on TBI, we investigated the temporal roles of specific immune cell populations post-injury[20]. We performed flow cytometry analysis on immune cells isolated from cervical lymph nodes (cLNs), meninges and the ipsilateral hemisphere at multiple time points post-TBI. We found that the immediate treatment of nasal aCD3 increased the percentage of total $CD4^+$ T cells and $CD4^+FoxP3^+$ T_{reg} cells in cLNs at 1 d (Extended Data Fig. 3a) and increased the total number of those in the meninges at 2 d post-injury (Fig. 2a,b). Nasal aCD3 also expanded the total number of $CD4^+$ T cells in the brain at 3 and 7 d post-injury and increased $CD4^+FoxP3^+$ T_{reg} cells in the first 30 d post-injury compared with TBI isotype controls (Fig. 2a,b and Extended Data Figs. 3a and 4a). Of note, we did not observe an increase in $CD4^+$ T cells expressing latency-associated peptide (LAP), a membrane-bound transforming growth factor β (TGF-β) compared with the TBI-iso group (Fig. 2c and Extended Data Figs. 3b and 4a). Thus, nasal aCD3 expands T_{reg} cells to control neuroinflammation after TBI.

Nasal aCD3 mAb modulates the innate and adaptive immune response after TBI

Nasal aCD3 also reduced the number of $CD8^+$ cells at 14 and 30 d and helper T cells (T_H1 and T_H17 cells) at day 30 post-injury (Fig. 2c and Extended Data Figs. 3b and 4a). In addition, we found a significant reduction in neutrophil recruitment at day 1, monocytes at day 7 and natural killer cells at days 1 and 14 after CCI in the nasal aCD3 group compared with the TBI-iso controls (Fig. 2d and Extended Data Figs. 3c and 4b,c).

T_{reg} cells induced by nasal aCD3 have a unique immunomodulatory profile

As shown in Fig. 2b, nasal aCD3 increased $CD4^+FoxP3^+$ T_{reg} cells in the first 30 d post-injury compared with TBI isotype controls (Fig. 2b). To elucidate the mechanisms whereby aCD3-induced T_{reg} cells may have contributed to post-TBI recovery, we performed RNA sequencing (RNA-seq) analysis on $CD4^+FoxP3(GFP)^+$ T_{reg} cells isolated from both the pericontusional brain tissue and blood of the sham and injured mice 7 d after CCI (Fig. 2f–k, Extended Data Fig. 5a and Supplementary Table 1). Principal component analysis (PCA) showed that the transcriptomic profile of brain FoxP3 T_{reg} cells was markedly different from blood FoxP3 T_{reg} cells after TBI (Fig. 2f). Consistent with recent reports[23], we found increased expression of multiple immunomodulatory and trophic factor genes (*Il10*, *Spp1*, *Gas6*, *Igf1*, *Dab2*, *Lif*, *Areg*, *Il1r2*, *Irf8*, *Osm*, *Tgfa*, *Ccl8*, and *Hmox1*) in brain-infiltrating T_{reg} cells from TBI mice compared with blood T_{reg} cells from sham mice (Extended Data Fig. 5b).

We first examined the effects of TBI and nasal aCD3 treatment on blood FoxP3 T_{reg} cells (Fig. 2g, Supplementary Table 1). We found that FoxP3 T_{reg} cells isolated from nasally treated aCD3 TBI mice had a unique transcriptomic signature with upregulation of several genes involved in T_{reg} cell proliferation and homeostasis (*Cd47* (ref. 39), *Ndfip1* (ref. 40), *Cd2* (ref. 41)) and T_{reg} cell function (*Lef1* (ref. 42), *Lgals1* (ref. 43) and *Runx1* (ref. 44)). Ingenuity pathway analysis (IPA) revealed IL-10 as a top activated upstream regulator in blood aCD3-induced FoxP3 T_{reg} cells compared with TBI-iso FoxP3 T_{reg} cells along with other transcription factors relevant for T_{reg} cell development and function (*Foxo3* and *Foxo4*)[45] (Extended Data Fig. 5c). Notably, both *Foxo4* and *Stat3* have been reported to regulate IL-10 transcription in $CD4^+$ T_{reg} cells[46].

We then examined the effects of TBI and nasal aCD3 treatment on brain-infiltrating T_{reg} cells (Fig. 2h and Supplementary Table 1). We found both TBI groups (treated and untreated) had upregulated genes enriched in immune regulation (*Spp1*, *Lgals3*, *Arg1*, *Ccl3*, *Ccl8*, *Hmox1*, *Ctsl*, *Lgals1*, and *Il1rn*) (Fig. 2h). In addition, nasal aCD3-induced T_{reg} cells had further increased expression of genes involved in immunomodulation (*Lrp1*, *Tyrobp*, *Cxcl10*, and *Itgam*), regulation of phagocytosis (*Rab31* and *Rab7*), neurotrophic factors (*Igf1* and *Psap*), lipid homeostasis (*Abca1* and *Lpl*) and other genes required for T_{reg} cell immunosuppressive function (*Dab2* (ref. 47), *Plau*[48] and *Lgmn*[49]). Gene set enrichment analysis (GSEA) and IPA revealed enrichment of biological pathways involved in migration, regulation of immune response, phagocytosis, neurogenesis, homeostasis and secretory functions in brain TBI-aCD3-FoxP3 T_{reg} cells compared with brain sham-iso controls (Fig. 2i) and TBI-iso-FoxP3 T_{reg} cells (Fig. 2j). Similar to blood $FoxP3^+$ T_{reg} cells, IPA identified IL-10 and Stat3 among the most activated upstream regulators of T_{reg} cells in the brain of TBI mice treated with nasal aCD3 (Fig. 2k and Extended Data Fig. 5d). The IL-10–Stat3 axis has been reported as playing a role in the immune tolerance conferred by T_{reg} cells[50]; consistent with this, flow cytometry analysis of brain T_{reg} cells showed upregulation of IL-10 expression in aCD3-treated animals compared with TBI-iso controls (Fig. 2l). Taken together, these findings demonstrate that peripheral and central T_{reg} cells possess unique immunomodulatory profiles associated with the amelioration of TBI via nasal aCD3 treatment.

Fig. 2 | Nasal aCD3 expands FoxP3 T_{reg} cells and modulates the adaptive immune response. a,**b**, Flow cytometry analysis and quantification of $CD4^+$ (**a**) and $CD4^+FoxP3^+$ (**b**) T_{reg} cells in the meninges and ipsilateral hemisphere at 1, 3, 7, 14 and 30 d (D) after TBI and treatment. **c**, Quantification of $CD4^+$ subsets at the same time points. **d**, Analysis of $CD11b^+$-infiltrated cells across these intervals. Groups included sham-iso ($n = 4$), TBI-iso ($n = 6$) and TBI-aCD3 ($n = 6$). Data are analyzed by one-way ANOVA with Tukey's multiple comparisons for every individual timepoint. Data are shown as mean ± s.e.m. representing biological replicates from two independent experiments per timepoint for **a**–**d**. **e**, Immunofluorescence of meninges (2 d post-TBI) and brain (7 d post-TBI) samples from FoxP3-GFP mice with DAPI (blue), CD3 (pink), FoxP3 (green). Scale bars, 100 µm. IHC, immunohistochemistry. **f**, PCA plot of brain and blood T_{reg} cells 7 d post-TBI. Brain and blood samples are pools of 5 mice and sham-iso brain samples are pools of 20 mice. Due to the low number of $FoxP3^+$ cells recruited to the brain and ethical considerations, we limited the study to two biological replicates, following practices from previous studies in the field[23]. Despite this limitation, the consistent and robust results observed support the validity of our findings. **g**,**h**, Heatmaps of DEGs from blood (**g**) and brain (**h**) T_{reg} cells at 7 d post-TBI using DESeq2 (FDR-corrected $P < 0.05$, $n = 2$ pooled samples per group). **i**, GSEA of GOBP 7 d post-TBI for brain T_{reg} cells. The asterisks indicate enriched terms ($q < 0.05$). NES, normalized enrichment score. **j**, IPA analysis of DEGs from brain T_{reg} cells in TBI-aCD3 versus TBI-iso using DESeq2 analysis (two-sided Wald's test, FDR-corrected $P < 0.05$). One-sided Fisher's exact test was used: $^*P < 0.05$, $^{**}P < 0.01$, $^{***}P < 0.001$. Results with FDR-corrected $P < 0.05$ were selected. **k**, Predicted upstream regulators using IPA for TBI-aCD3 versus TBI-iso. **l**, Quantification of $FoxP3^+IL\text{-}10^+$ T_{reg} cells in the ipsilateral hemisphere 7 d post-TBI. Groups included sham-iso ($n = 4$), TBI-iso ($n = 6$) and TBI-aCD3 ($n = 6$). Data are shown as box plots (min., max., IQR, median), analyzed by one-way ANOVA with Tukey's multiple comparisons. Data are from biological replicates and represent two independent experiments.

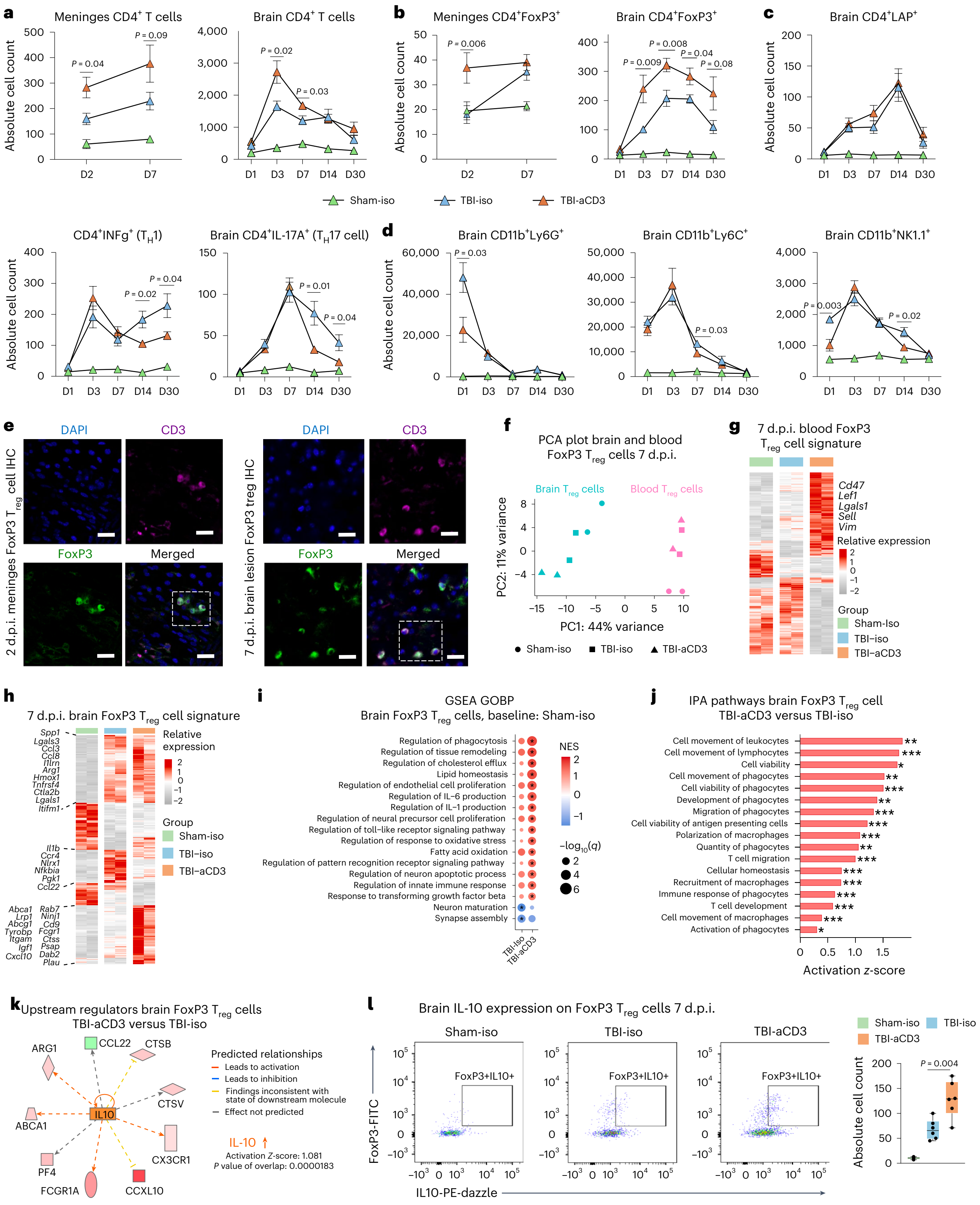
a
Meninges CD4+ T cells
Brain CD4+ T cells
Absolute cell count
P = 0.04
P = 0.09
P = 0.02
P = 0.03
D2
D7
D1
D3
D14
D30
b
Meninges CD4+FoxP3+
Brain CD4+FoxP3+
P = 0.006
P = 0.008
P = 0.009
P = 0.04
P = 0.08
c
Brain CD4+LAP+
Sham-iso
TBI-iso
TBI-aCD3
CD4+INFg+ (TH1)
Brain CD4+IL-17A+ (TH17 cell)
P = 0.04
P = 0.02
P = 0.01
d
Brain CD11b+Ly6G+
Brain CD11b+Ly6C+
Brain CD11b+NK1.1+
P = 0.03
P = 0.003
P = 0.02
e
DAPI
CD3
FoxP3
Merged
2 d.p.i. meninges FoxP3 Treg cell IHC
7 d.p.i. brain lesion FoxP3 treg IHC
f
PCA plot brain and blood FoxP3 Treg cells 7 d.p.i.
Brain Treg cells
Blood Treg cells
PC2: 11% variance
PC1: 44% variance
● Sham-iso
■ TBI-iso
▲ TBI-aCD3
g
7 d.p.i. blood FoxP3 Treg cell signature
Cd47
Lef1
Lgals1
Sell
Vim
Relative expression
Group
Sham-Iso
TBI-iso
TBI-aCD3
h
7 d.p.i. brain FoxP3 Treg cell signature
Spp1
Lgals3
Ccl3
Ccl8
Il1rn
Arg1
Hmox1
Tnfrsf4
Ctla2b
Lgals1
Itifm1
Il1b
Ccr4
Nlrx1
Nfkbia
Pgk1
Ccl22
Abca1
Lrp1
Abcg1
Tyrobp
Itgam
Igf1
Cxcl10
Rab7
Ninj1
Cd9
Fcgr1
Ctss
Psap
Dab2
Plau
Relative expression
Group
Sham-iso
TBI-iso
TBI-aCD3
i
GSEA GOBP
Brain FoxP3 Treg cells, baseline: Sham-iso
Regulation of phagocytosis
Regulation of tissue remodeling
Regulation of cholesterol efflux
Lipid homeostasis
Regulation of endothelial cell proliferation
Regulation of IL-6 production
Regulation of IL-1 production
Regulation of neural precursor cell proliferation
Regulation of toll-like receptor signaling pathway
Regulation of response to oxidative stress
Fatty acid oxidation
Regulation of pattern recognition receptor signaling pathway
Regulation of neuron apoptotic process
Regulation of innate immune response
Response to transforming growth factor beta
Neuron maturation
Synapse assembly
NES
-log10(q)
TBI-iso
TBI-aCD3
j
IPA pathways brain FoxP3 Treg cell TBI-aCD3 versus TBI-iso
Cell movement of leukocytes **
Cell movement of lymphocytes ***
Cell viability *
Cell movement of phagocytes **
Cell viability of phagocytes ***
Development of phagocytes **
Migration of phagocytes ***
Cell viability of antigen presenting cells ***
Polarization of macrophages ***
Quantity of phagocytes **
T cell migration ***
Cellular homeostasis ***
Recruitment of macrophages ***
Immune response of phagocytes ***
T cell development ***
Cell movement of macrophages ***
Activation of phagocytes *
Activation z-score
k
Upstream regulators brain FoxP3 Treg cells TBI-aCD3 versus TBI-iso
ARG1
CCL22
CTSB
CTSV
ABCA1
IL10
CX3CR1
PF4
FCGR1A
CCXL10
Predicted relationships
Leads to activation
Leads to inhibition
Findings inconsistent with state of downstream molecule
Effect not predicted
IL-10 ↑
Activation Z-score: 1.081
P value of overlap: 0.0000183
l
Brain IL-10 expression on FoxP3 Treg cells 7 d.p.i.
Sham-iso
TBI-iso
TBI-aCD3
FoxP3+IL10+
FoxP3-FITC
IL10-PE-dazzle
Absolute cell count
P = 0.004

Nasal aCD3 mAb modulates the microglial inflammation after TBI

Microglia play a critical role in TBI pathogenesis and their adherent activation contributes to long-term functional deficits after TBI[20]. Nasal aCD3 treatment increased the migration of FoxP3$^+$ T$_{reg}$ cells to the meninges and CCI lesion site (Fig. 2e), where they were found to be in close contact with microglial dendrites after injury (Fig. 3a). Thus, to further elucidate the effects of TBI and immediate nasal aCD3 treatment on the microglial inflammatory profile post-injury, we performed RNA-seq analysis on sorted microglial single-cell suspensions from the ipsilateral hemisphere of the mouse brains, using the microglia-specific 4D4$^+$ antibody[51] (Extended Data Fig. 6a) at 7 and 30 d post-CCI (Fig. 3b and Supplementary Table 2). In analyzing the highest expressed genes in the sham-iso, TBI-iso and TBI-aCD3 microglial groups, we found that multiple microglial genes, including *Cx3cr1, Hexb* and *Tmem119*, were among the highest expressed (Extended Data Fig. 6b). A heatmap of the microglial gene signature demonstrated that the TBI-iso and TBI-aCD3 groups had overall similar transcriptomic profiles at 7 d, yet with demonstration of early upregulation of anti-inflammatory genes such as *Cx3cr1*, *CD33*, *Hspa1a*, and *Hspa1b*, whereas there was a clear modulation of the microglial transcriptomic signature in TBI-aCD3 group toward the sham-iso phenotype at 30 d post-injury (Fig. 3c and Supplementary Table 2), including the downregulation of microglial proinflammatory genes (*Il6*, *Il18*, *Cd36*, *Ifitm3*, and *Lgals1*) and upregulation of key homeostatic genes (*Tgfbr2*, *Adgrg1*, *Mertk*, *Rhob*, *Atp8a2*, *Abcc3*, *Fscn1*, *Pde3b*, *Inpp4b*, and *Cmklr1*).

Microglia possess a unique transcriptomic signature that enables them to perform sensing, homeostatic and housekeeping functions, which vary according to the brain's physiological or pathological state[52]. To determine the effects of TBI and nasal anti-CD3 on these essential microglial functions, we examined the microglial sensome dataset for genes and pathways involved in each of these functions[53]. At 7 d post-TBI, we found that microglia from the nasal aCD3-treated group, compared with TBI-iso, were associated with increased expression of homeostatic and sensing genes involved in pattern recognition receptors (*Tlr1*), Fc receptors (*Cmtm7*), Siglec receptors (*Cd33*), cell–cell interaction (*Cd84* and *Lag3*) and chemokine receptors (*Cx3cr1*) (Fig. 3d). *Cd33* and *Lag3* were among the most significantly differentially expressed genes (DEGs) in the TBI aCD3-treated group compared with TBI-iso control at 7 d post-injury. CD33 activity has been implicated in processes including microglial endogenous ligand receptors and sensors, adhesion processing of immune cells and inhibition of cytokines release by monocytes[54,55]. Lymphocyte activation gene-3 (*Lag3*) regulates T cell expansion and limits the duration and intensity of the immune response[56]. Moreover, the TBI aCD3-treated group exhibited downregulation of *Cd14*, a key regulator of microglial proinflammatory responses to injury[57]. At 30 d post-injury, we found that nasal aCD3 treatment was associated with increased expression of several transforming growth factor β (TGF-β)-signaling genes, including *Smad3*, *Tgfbr1* and *Tgfbr2* compared with TBI-iso control (Fig. 3c,d and Supplementary Table 2)[58]. TGF-β is required for maintaining the microglial homeostatic state[59] and modulating microglia-mediated inflammation after acute brain injury[60]. Nasal aCD3 treatment was also associated with decreased expression of sensing genes involved in cytokine receptor (*Tnfrsf17*), FC receptor (*Fcgr1*, *Fcgr4*, *Fcgr3*, and *Fcer1g*) and pattern recognition receptors (*Cd74*, *Tlr6*, *Upk1b*, and *Selplg*) compared with TBI-iso control (Fig. 3d).

We then performed GSEA comparing the TBI groups with sham-iso controls at 7 and 30 d post-injury. At 7 d post-injury, we observed an upregulation in pathways involved in oxidative stress and neuron apoptosis in the TBI-iso group compared with the sham-iso group. The TBI-aCD3-treated animals had less upregulation of genes in these pathways and more upregulation in microglial pathways involved in the regulation of anti-inflammatory IL-10 production, phagocytosis and tolerance induction at 7 d post-injury (Fig. 3e). At 30 d post-TBI, we found enrichment of pathways involved in proinflammatory mechanisms (IL-6, IL-1 and tumor necrosis factor production), adaptive immune response, T cell cytotoxicity and cell killing pathways in the TBI-iso control compared with the sham-iso group. However, TBI-aCD3-treated animals had less upregulation of genes in these proinflammatory pathways and more upregulation in biological pathways involved in regulation of phagocytosis and cytokine production (Fig. 3e).

Previous studies have suggested an association between microglia-mediated chronic inflammation after TBI and subsequent chronic neurodegeneration[20,52]. To investigate this relationship, we analyzed the expression levels of inflammatory response genes and genes characteristic of disease-associated microglia (DAMs)[61] and neurodegenerative microglia (MGnDs)[51] in all three groups at 30 d post-injury. We found that the TBI-iso microglia had a unique proinflammatory response (Fig. 3f) and a DAM or MGnD signature (Fig. 3g), because we found increased expression of key proinflammatory (*Casp1*, *Nfkbia*, *C5ar1*, *Lyz1*, *Ifitm3*, *Il6*, *Lyz2*, *Cd86*, and *Irgm1*), DAM-1 and -2 genes (*B2m*, *Cstb*, *Cd52*, *Cd9*, *Cst7*, *Fth1*, *Ccl6*, and *Tyrobp*) and MGnD microglial genes (*Cybb*, *Gpnmb*, *Lgals3*, and *Clec7a*)[51,61]. Importantly, several of these genes were downregulated in nasal aCD3-treated mice, approaching expression levels observed in the sham group (Fig. 3f-g).

Consistent with the microglial transcriptomic data, quantitative PCR with reverse transcription (RT–qPCR) from ipsilateral hemisphere sorted microglia (Fig. 3h) and brain tissue (Extended Data Fig. 6c) revealed that, compared with the TBI-iso control, nasal aCD3 treatment increased the expression of the anti-inflammatory cytokine *Il10* in both microglia and brain tissue at 7 d post-injury. Moreover, treatment reduced several proinflammatory markers in microglia (*Clec7a*, *Tlr2*, *Il1b*, *Tnf*, *Cd86*, and *Il18*) and brain tissue (*Il6*, *Tnf*, *Ifng*, *Il17a*, and *Ccl5*) at 30 d post-injury. Of note, mice treated with nasal aCD3 showed upregulation of brain-derived neurotrophic factor (*Bdnf*), a neurotrophin that has a critical role in neuronal survival and is involved in synaptic plasticity, learning and memory[62], compared with the TBI-iso control, at 1 month post-injury (Extended Data Fig. 6c).

Fig. 3 | Nasal aCD3 modulates the microglial inflammatory response after TBI. **a**, Immunofluorescence of ipsilateral brain lesion (7 d post-TBI) from FoxP3-GFP mice for DAPI (blue), CD3 (pink), FoxP3 (green) and Iba-1 (red) showing FoxP3 T$_{reg}$ cells in close proximity to Iba-1. Scale bars, 100 µm and 50 µm for the enlarged image. **b**, Experimental timeline schematic for microglial bulk RNA-seq at 7 and 30 d after TBI and treatment (created with BioRender.com). **c**, Heatmap of DEGs from microglia at 7 and 30 d post-TBI identified using DESeq2 analysis (two-sided LRT, $n = 4$ mice per group, FDR-corrected $P < 0.05$). **d**, Microglial core sensome genes at 7 and 30 d in TBI-aCD3 versus TBI-iso. Genes are colored by their function[53,107,108]. Emboldened DEGs have an asterisk: FDR-corrected $P < 0.05$; $^*P < 0.05$ (DESeq2 analysis, two-sided Wald's test, $n = 4$ mice per group). **e**, GSEA of GOBP at 7 and 30 d post-TBI based on the following pairwise comparisons: TBI-iso versus sham-iso and TBI-aCD3 versus sham-iso; the asterisk indicates enriched terms (q-value < 0.05). NES, normalized enrichment score. **f**, Heatmap of genes involved in inflammatory response from microglia at 30 d post-TBI. Genes identified with an FDR-corrected $P < 0.05$ using DESeq2 analysis are indicated by an asterisk (two-sided LRT, $n = 4$ mice per group). Genes were identified from the GOBP term inflammatory response as well as microglial inflammatory genes[89]. **g**, Heatmap of DAM and MGnD genes at 30 d post-TBI. Genes identified with an FDR-corrected $P < 0.05$ using DESeq2 analysis are indicated by an asterisk (two-sided LRT, $n = 4$ mice per group). Genes were identified based on the previous work of our group and others[51,61]. **h**, RT–qPCR of microglia sorted from the ipsilateral hemisphere at 7 and 30 d post-TBI. Expression was normalized to glyceraldehyde 3-phosphate dehydrogenase (GAPDH) and presented relative to that of sham-iso animals (sham-iso $n = 4$, TBI-iso $n = 5$, TBI-aCD3 $n = 5$), analyzed by one-way ANOVA with Tukey's multiple comparisons. Data are shown as mean ± s.e.m. All data are biological replicates and represent two independent experiments.

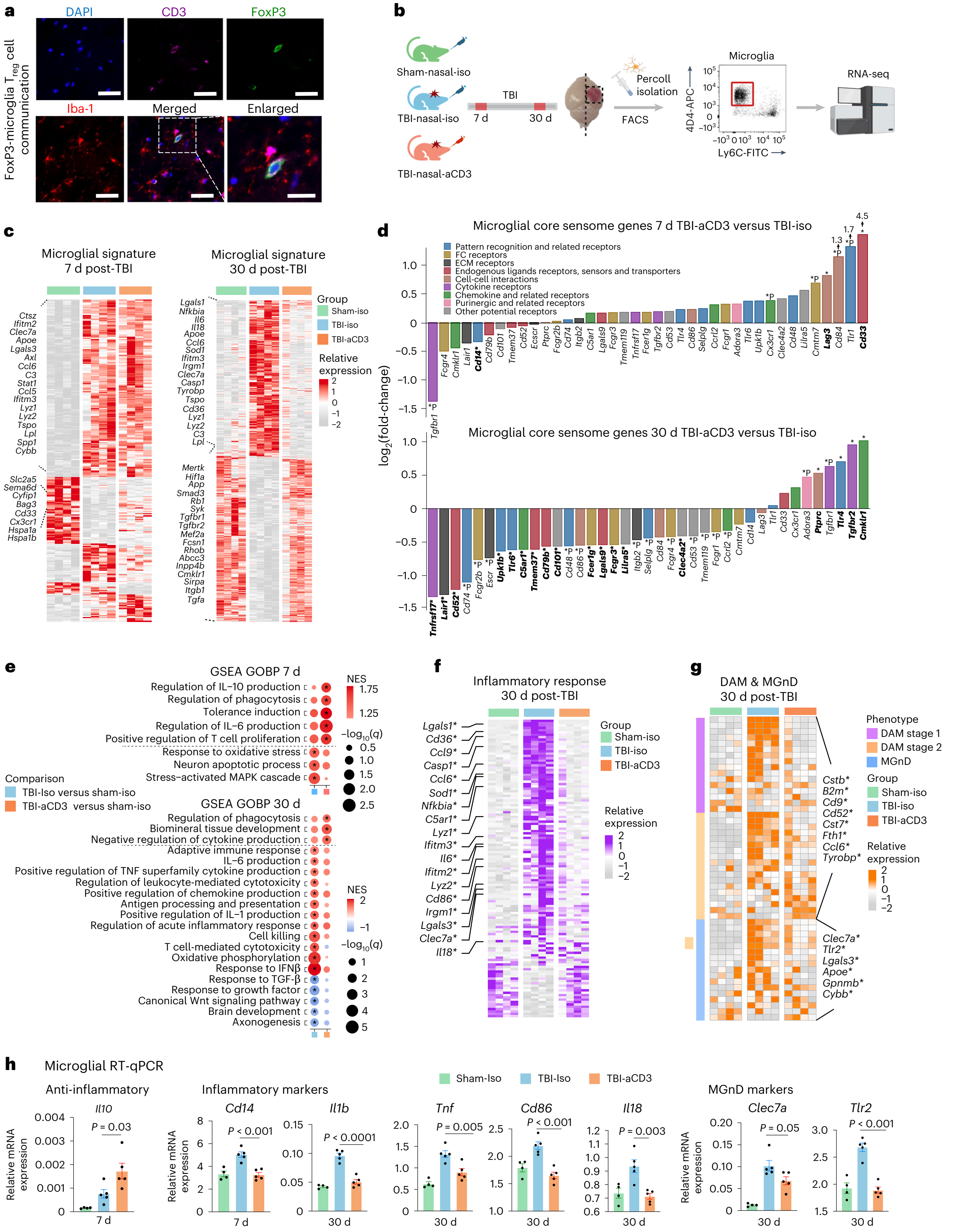
a
FoxP3-microglia T_{reg} cell communication
DAPI
CD3
FoxP3
Iba-1
Merged
Enlarged
b
Sham-nasal-iso
TBI-nasal-iso
TBI-nasal-aCD3
TBI
7 d
30 d
Percoll isolation
FACS
Microglia
4D4-APC
Ly6C-FITC
RNA-seq
c
Microglial signature 7 d post-TBI
Ctsz
Ifitm2
Clec7a
Apoe
Lgals3
Axl
Ccl6
C3
Stat1
Ccl5
Ifitm3
Lyz1
Lyz2
Tspo
Lpl
Spp1
Cybb
Slc2a5
Sema6d
Cyfip1
Bag3
Cd33
Cx3cr1
Hspa1a
Hspa1b
Microglial signature 30 d post-TBI
Lgals1
Nfkbia
Il6
Il18
Apoe
Ccl6
Sod1
Ifitm3
Irgm1
Clec7a
Casp1
Tyrobp
Tspo
Cd36
Lyz1
Lyz2
C3
Lpl
Mertk
Hif1a
App
Smad3
Rb1
Syk
Tgfbr1
Tgfbr2
Mef2a
Fcsn1
Rhob
Abcc3
Inpp4b
Cmklr1
Sirpa
Itgb1
Tgfa
Group
Sham-iso
TBI-iso
TBI-aCD3
Relative expression
2
1
0
−1
−2
d
Microglial core sensome genes 7 d TBI-aCD3 versus TBI-iso
Pattern recognition and related receptors
FC receptors
ECM receptors
Endogenous ligands receptors, sensors and transporters
Cell-cell interactions
Cytokine receptors
Chemokine and related receptors
Purinergic and related receptors
Other potential receptors
log2(fold-change)
1.0
0.5
0
−0.5
−1.0
−1.5
4.5
1.7
1.3
Tgfbr1
Fcgr4
Cmklr1
Lair1
Cd14*
Cd79b
Cd101
Tmem37
Cd52
Ptprc
Escr
Fcgr2b
Cd74
Itgb2
C5ar1
Lgals9
Fcgr3
Tmem119
Tnfrsf17
Fcer1g
Tgfbr2
Cd53
Tlr4
Cd86
Selplg
Ccrl2
Fcgr1
Adora3
Tlr6
Upk1b
Cx3cr1
Clec4a2
Cd48
Lilra5
Cmtm7
Lag3
Cd84
Tlr1
Cd33
Microglial core sensome genes 30 d TBI-aCD3 versus TBI-iso
Tnfrsf17*
Lair1*
Cd52*
Cd74
Fcgr2b
Escr
Upk1b*
Tlr6*
C5ar1*
Tmem37*
Cd79b*
Cd101*
Cd48
Cd86
Fcer1g*
Lgals9*
Fcgr3*
Lilra5*
Itgb2
Selplg
Cd84
Fcgr4
Clec4a2*
Cd53
Tmem119
Fcgr1
Ccrl2
Cmtm7
Cd14
Lag3
Tlr1
Cd33
Cx3cr1
Adora3
Ptprc
Tgfbr1
Tlr4
Tgfbr2
Cmklr1
e
GSEA GOBP 7 d
Regulation of IL−10 production
Regulation of phagocytosis
Tolerance induction
Regulation of IL−6 production
Positive regulation of T cell proliferation
Response to oxidative stress
Neuron apoptotic process
Stress−activated MAPK cascade
NES
1.75
1.25
−log10(q)
0.5
1.0
1.5
2.0
2.5
Comparison
TBI-Iso versus sham-iso
TBI-aCD3 versus sham-iso
GSEA GOBP 30 d
Regulation of phagocytosis
Biomineral tissue development
Negative regulation of cytokine production
Adaptive immune response
IL−6 production
Positive regulation of TNF superfamily cytokine production
Regulation of leukocyte-mediated cytotoxicity
Positive regulation of chemokine production
Antigen processing and presentation
Positive regulation of IL−1 production
Regulation of acute inflammatory response
Cell killing
T cell-mediated cytotoxicity
Oxidative phosphorylation
Response to IFNβ
Response to TGF-β
Response to growth factor
Canonical Wnt signaling pathway
Brain development
Axonogenesis
NES
2
−1
−log10(q)
1
2
3
4
5
f
Inflammatory response 30 d post-TBI
Lgals1*
Cd36*
Ccl9*
Casp1*
Ccl6*
Sod1*
Nfkbia*
C5ar1*
Lyz1*
Ifitm3*
Il6*
Ifitm2*
Lyz2*
Cd86*
Irgm1*
Lgals3*
Clec7a*
Il18*
Group
Sham-iso
TBI-iso
TBI-aCD3
Relative expression
2
1
0
−1
−2
g
DAM & MGnD 30 d post-TBI
Phenotype
DAM stage 1
DAM stage 2
MGnD
Group
Sham-iso
TBI-iso
TBI-aCD3
Cstb*
B2m*
Cd9*
Cd52*
Cst7*
Fth1*
Ccl6*
Tyrobp*
Clec7a*
Tlr2*
Lgals3*
Apoe*
Gpnmb*
Cybb*
Relative expression
2
1
0
−1
−2
h
Microglial RT-qPCR
Sham-Iso
TBI-Iso
TBI-aCD3
Anti-inflammatory
Il10
P = 0.03
Relative mRNA expression
0.004
0.003
0.002
0.001
0
7 d
Inflammatory markers
Cd14
P < 0.001
8
6
4
2
0
7 d
Il1b
P < 0.0001
0.15
0.10
0.05
0
30 d
Tnf
P = 0.005
2.0
1.5
1.0
0.5
0
30 d
Cd86
P < 0.001
2.5
2.0
1.5
1.0
30 d
Il18
P = 0.003
1.2
1.1
1.0
0.9
0.8
0.7
0.6
30 d
MGnD markers
Clec7a
P = 0.05
0.20
0.15
0.10
0.05
0
30 d
Tlr2
P < 0.001
3.0
2.5
2.0
1.5
30 d

To further investigate whether delaying the therapeutic window of nasal anti-CD3 to 3 d post-injury would still modulate the microglial transcriptomic profile at 30 d post-injury, we performed bulk RNA-seq on isolated microglia from mice treated with nasal aCD3 or isotype control from day 3 to day 30 (early treatment) post-injury (Supplementary Table 2). We found that the early treatment paradigm also modulated the microglial transcriptomic signature in the TBI-aCD3 group toward the sham-iso phenotype (Extended Data Fig. 6d) and was associated with decreased expression of several proinflammatory and DAM or MGnD genes (*Lpl*, *Lyz1*, *Nfkbia*, *Irgm1*, *Lyz2* and *Apoe*) (Extended Data Fig. 6e). Consistent with this, GSEA analysis revealed that the early nasal aCD3 treatment paradigm was also associated with downregulation in several inflammatory response and immune response-related pathways compared with TBI-iso (Extended Data Fig. 6f). In line with these results, RT–qPCR of ipsilateral brain tissue demonstrated a reduction in several proinflammatory genes including *Il6*, *Il18* and *Tnf* in TBI-aCD3 compared with TBI-iso controls (Extended Data Fig. 6g).

To assess the effect of nasal aCD3 treatment on microglia inflammation in female mice after severe TBI, we performed bulk RNA-seq on sorted microglia at 30 d post-injury (Supplementary Table 2). We found a similar therapeutic effect in female mice with the TBI-aCD3 microglial transcriptomic profile reverting to that of sham mice, associated with a reduced inflammatory and DAM or MGnD profile relative to TBI-iso mice controls (Extended Data Fig. 6h,i). RT–qPCR of ipsilateral brain tissue showed consistent findings (Extended Data Fig. 6j). Taken together, these findings demonstrate that nasal aCD3 shifts microglia from a pathogenic, disease-associated phenotype to a beneficial, homeostatic phenotype.

Nasal aCD3 increases microglia phagocytosis in an IL-10-dependent manner

Acute brain injury leads to neuronal cell death and the release of substantial amounts of myelin and cell debris, which subsequently trigger a persistent and intense inflammatory response that may impede neurological recovery. Microglia and macrophages play an important role in debris removal and modulating the immune response post-injury[20]. However, uncontrolled phagocytosis may lead to progressive brain damage and worsening cognitive and memory impairments[63]. We found that TBI-aCD3-treated animals had increased upregulation in biological pathways involved in regulation of phagocytosis (Fig. 3e) and a distinct upregulated phagocytic signature at 7 d post-injury (Fig. 4a), with increased expression of several key microglial phagocytosis regulators at 30 d post-TBI, including *Mertk*[64], *Sirpa*[65] and *Tlr4* (ref. 66), compared with TBI-iso microglia (Supplementary Table 2). To functionally assess the phagocytic capacity of microglia after TBI (with and without nasal aCD3 treatment), we performed an in vivo experiment in which the TBI-induced lesion was injected with either labeled apoptotic neurons or phosphate-buffered saline (PBS) on day 6 post-injury for 16 h and on day 7 post-injury for 4 h post-injection experiments (Fig. 4b). In line with our microglial transcriptomic data, aCD3-treated animals had higher microglial phagocytic capacity to uptake apoptotic neurons at both 4 and 16 h post-injection compared with the TBI-iso group (Fig. 4c,d and Extended Data Fig. 7a,b). To elucidate the mechanism by which nasal aCD3 enhanced microglial phagocytic capacity after TBI, we performed bulk RNA-seq on phagocytic and nonphagocytic microglia isolated at 4 and 16 h post-injection from TBI-iso and TBI-aCD3 groups at 7 d post-TBI (Supplementary Table 3). At 4 h post-injection, we observed a distinct microglial transcriptomic signature for phagocytic TBI-aCD3 microglia, characterized by the upregulation of several key phagocytosis genes (Fig. 4e). Compared with nonphagocytic TBI-iso microglia, phagocytic TBI-aCD3 microglia were associated with increased expression of genes involved in the recognition and engulfment (eat me and find me signals) of apoptotic cells and debris (*Mertk*[67], *Mrc1* (ref. 68), *Abca1* (ref. 67), *Lrp1* (ref. 67), and *Stab1* (ref. 69)), digestion and degradation of engulfed material including lysosomal machinery (*Rab27a*[70], *Smcr8* (ref. 71), *Clec16a*[72], and *Vps8* (ref. 73)), lipid metabolism (*Apoc1* (ref. 74), *Olr1* (ref. 75) and *Ldlr*[76]), cytoskeleton dynamics pathways (*Myo1e*[77]) and regulation of microglial phagocytosis (*Tspo*[78], *Qk*[79] and *Pik3cg*[80]) (Fig. 4e,f and Supplementary Table 3). Consistent with these findings, GSEA analysis of phagocytic TBI-aCD3 microglia compared with nonphagocytic TBI-iso microglia showed enrichment for pathways involved in phagocytosis, along with other pathways pertinent for the phagocytic process such as endocytosis, pattern recognition and cell migration, all of which were not upregulated in the phagocytic TBI-iso microglia (Fig. 4g). In addition, compared with phagocytic TBI-iso microglia, phagocytic TBI-aCD3 microglia had increased upregulation of antigen presentation and IL-10 pathways (Fig. 4h). IPA analysis revealed IL-10 as a top regulator and signaling pathway in aCD3-treated phagocytic microglia post-TBI (Fig. 4h,i). We found a similar pattern of increased expression of phagocytosis machinery-related genes and pathways at 16 h post-injection (Extended Data Fig. 7c) and also observed that phagocytic TBI-aCD3 microglia had a more homeostatic and a less inflammatory (disease-associated) profile compared with phagocytic TBI-iso microglia (Extended Data Fig. 7d,e and Supplementary Table 3).

To investigate the role of IL-10 in the regulation of microglia phagocytic capacity after TBI, we repeated the in vivo microglia phagocytosis assay using IL-10 knockout (KO) mice (Fig. 4j). We found that the increased phagocytic capacity of TBI-aCD3 microglia at 4 h post-injection was significantly attenuated in the IL-10 KO TBI-aCD3 microglial group. Collectively, these findings demonstrate that nasal aCD3 treatment increases the phagocytic machinery of microglia after acute TBI, in an IL-10-dependent manner. In addition, we found that the phagocytic capacity of wild-type (WT) TBI-iso microglia was significantly reduced in the IL-10 KO TBI-iso microglia group, demonstrating the importance of IL-10 in microglial phagocytic function after TBI.

Fig. 4 | Nasal aCD3 increased microglial phagocytic capacity after TBI in an IL-10-dependent manner. a, Heatmap of microglial phagocytosis genes 7 d after TBI. Genes identified with FDR-corrected $P < 0.05$ using DESeq2 analysis are indicated by an asterisk (two-sided LRT, $n = 4$ mice per group). Genes were identified from the GOBP term phagocytosis and microglial phagocytosis genes[51,61]. **b**, Schematic presenting a phagocytosis functional study (created with BioRender.com). **c**, Immunofluorescence of lesion (7 d post-TBI) for apoptotic neurons (blue) and P2ry12 (red) showing engulfment of apoptotic neurons by P2ry12. Scale bars, 100 µm and 50 µm for the enlarged image. **d**, Phagocytosis experiment where mice were injected with labeled apoptotic neurons and sacrificed 4 h post-injection. The gating strategy shows phagocytic positive microglia and data are shown as box plots (min., max., IQR, median) and $n = 5$ mice per group were used. Data were analyzed by two-sided, unpaired Student's *t*-test. **e**, Clustered heatmap of DEGs of aggregated samples for phagocytic (+P) and nonphagocytic (−P) microglia 7 d post-TBI and 4 h post-injection of apoptotic neurons identified using DESeq2 analysis (two-sided LRT, $n = 3$-4 mice per group, FDR-corrected $P < 0.05$). **f**, Bar plots with $\log_2$(fold-changes) of genes from **e** pertinent to microglial phagocytosis and related functions in the following comparisons: TBI-iso (+P) versus TBI-iso (−P) and TBI-aCD3 (+P) versus TBI-Iso (−P). **g**, GSEA analysis of GOBP 7 d post-TBI and 4 h post-injection of apoptotic neurons based on pairwise comparisons: TBI-iso (+P) versus TBI-Iso (−P), TBI-aCD3 (+P) versus TBI-Iso (−P) and TBI-aCD3 (−P) versus TBI-Iso (−P). The asterisk indicates enriched terms (q-value < 0.05). **h**, Selected top canonical pathways from IPA analysis of DEGs in phagocytic TBI-aCD3 microglia compared with phagocytic and nonphagocytic TBI-iso microglial groups at 7 d post-TBI and 4 h post-injection of apoptotic neurons. **i**, Predicted upstream regulator in TBI-aCD3 (+P) versus TBI-iso (−P). **j**, Phagocytosis experiment with similar design to **b**. Data are shown as box plots (min., max., IQR, median) and $n = 5$ mice per group were used. The data were analyzed by one-way ANOVA with Tukey's multiple comparisons. All data are biological replicates and represent two independent experiments.

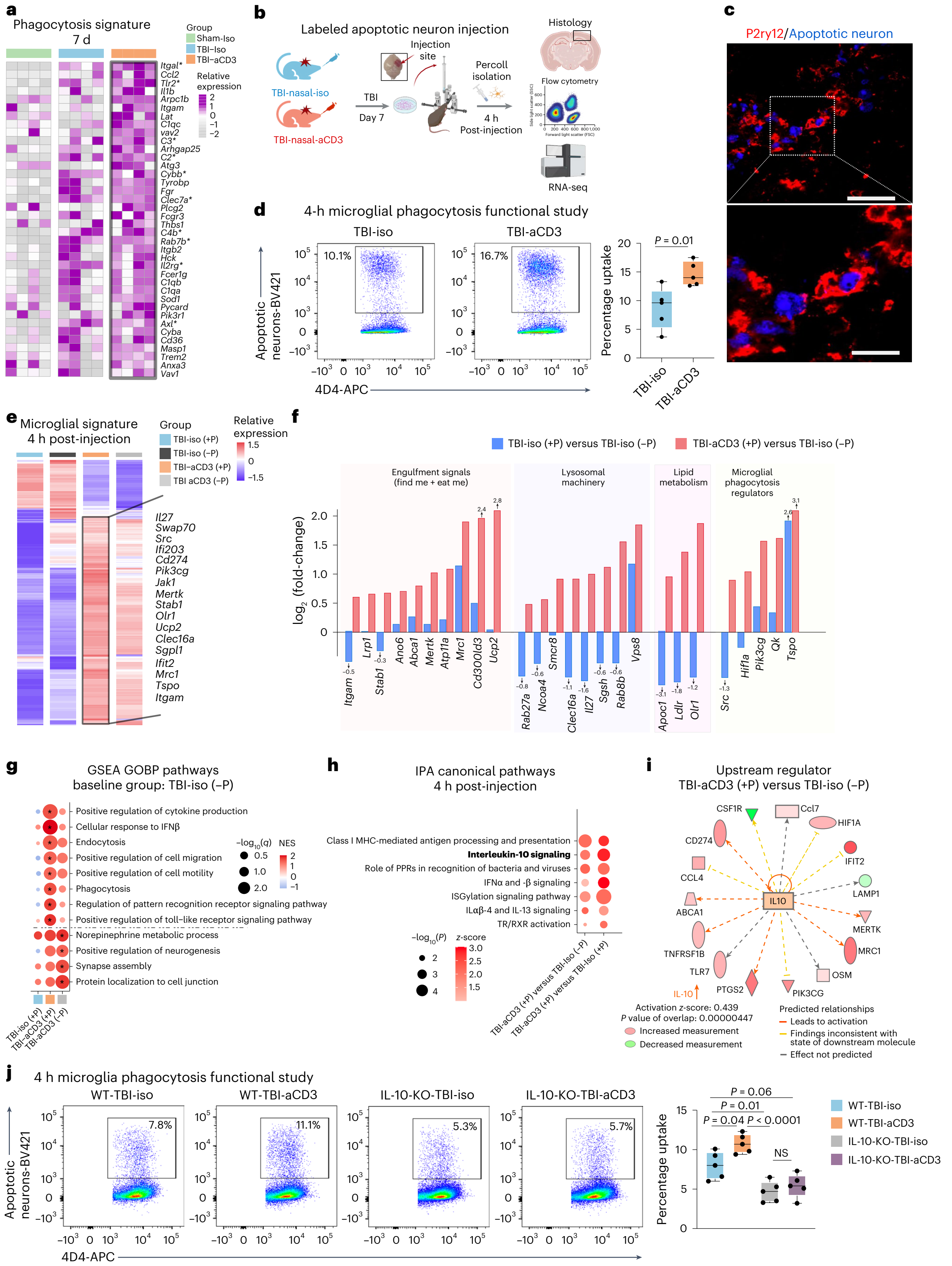
a
Phagocytosis signature
7 d
Group
Sham-Iso
TBI-Iso
TBI-aCD3
Relative expression
2
1
0
−1
−2
Itgal*
Ccl2
Tlr2*
Il1b
Arpc1b
Itgam
Lat
C1qc
vav2
C3*
Arhgap25
C2*
Atg3
Cybb*
Tyrobp
Fgr
Clec7a*
Plcg2
Fcgr3
Thbs1
C4b*
Rab7b*
Itgb2
Hck
Il2rg*
Fcer1g
C1qb
C1qa
Sod1
Pycard
Pik3r1
Axl*
Cyba
Cd36
Masp1
Trem2
Anxa3
Vav1
b
Labeled apoptotic neuron injection
TBI-nasal-iso
TBI-nasal-aCD3
TBI
Day 7
Injection site
Histology
Percoll isolation
4 h
Post-injection
Flow cytometry
RNA-seq
c
P2ry12/Apoptotic neuron
d
4-h microglial phagocytosis functional study
TBI-iso
TBI-aCD3
10.1%
16.7%
Apoptotic neurons-BV421
4D4-APC
Percentage uptake
P = 0.01
TBI-iso
TBI-aCD3
e
Microglial signature
4 h post-injection
Group
TBI-iso (+P)
TBI-iso (−P)
TBI-aCD3 (+P)
TBI aCD3 (−P)
Relative expression
1.5
0
−1.5
Il27
Swap70
Src
Ifi203
Cd274
Pik3cg
Jak1
Mertk
Stab1
Olr1
Ucp2
Clec16a
Sgpl1
Ifit2
Mrc1
Tspo
Itgam
f
TBI-iso (+P) versus TBI-iso (−P)
TBI-aCD3 (+P) versus TBI-iso (−P)
Engulfment signals (find me + eat me)
Lysosomal machinery
Lipid metabolism
Microglial phagocytosis regulators
$\log_2$ (fold-change)
Itgam
Lrp1
Stab1
Ano6
Abca1
Mertk
Atp11a
Mrc1
Cd300ld3
Ucp2
Rab27a
Ncoa4
Smcr8
Clec16a
Il27
Sgsh
Rab8b
Vps8
Apoc1
Ldlr
Olr1
Src
Hif1a
Pik3cg
Qk
Tspo
g
GSEA GOBP pathways
baseline group: TBI-iso (−P)
Positive regulation of cytokine production
Cellular response to IFNβ
Endocytosis
Positive regulation of cell migration
Positive regulation of cell motility
Phagocytosis
Regulation of pattern recognition receptor signaling pathway
Positive regulation of toll-like receptor signaling pathway
Norepinephrine metabolic process
Positive regulation of neurogenesis
Synapse assembly
Protein localization to cell junction
$-\log_{10}(q)$
NES
TBI-iso (+P)
TBI-aCD3 (+P)
TBI-aCD3 (−P)
h
IPA canonical pathways
4 h post-injection
Class I MHC-mediated antigen processing and presentation
Interleukin-10 signaling
Role of PPRs in recognition of bacteria and viruses
IFNα and -β signaling
ISGylation signaling pathway
ILα β-4 and IL-13 signaling
TR/RXR activation
$-\log_{10}(P)$
z-score
TBI-aCD3 (+P) versus TBI-iso (−P)
TBI-aCD3 (+P) versus TBI-iso (+P)
i
Upstream regulator
TBI-aCD3 (+P) versus TBI-iso (−P)
CSF1R
Ccl7
HIF1A
CD274
IFIT2
CCL4
LAMP1
ABCA1
IL10
MERTK
TNFRSF1B
MRC1
TLR7
OSM
PTGS2
PIK3CG
IL-10
Activation z-score: 0.439
P value of overlap: 0.00000447
Increased measurement
Decreased measurement
Predicted relationships
Leads to activation
Findings inconsistent with state of downstream molecule
Effect not predicted
j
4 h microglia phagocytosis functional study
WT-TBI-iso
WT-TBI-aCD3
IL-10-KO-TBI-iso
IL-10-KO-TBI-aCD3
7.8%
11.1%
5.3%
5.7%
Apoptotic neurons-BV421
4D4-APC
Percentage uptake
P = 0.06
P = 0.01
P = 0.04
P < 0.0001
NS
WT-TBI-iso
WT-TBI-aCD3
IL-10-KO-TBI-iso
IL-10-KO-TBI-aCD3

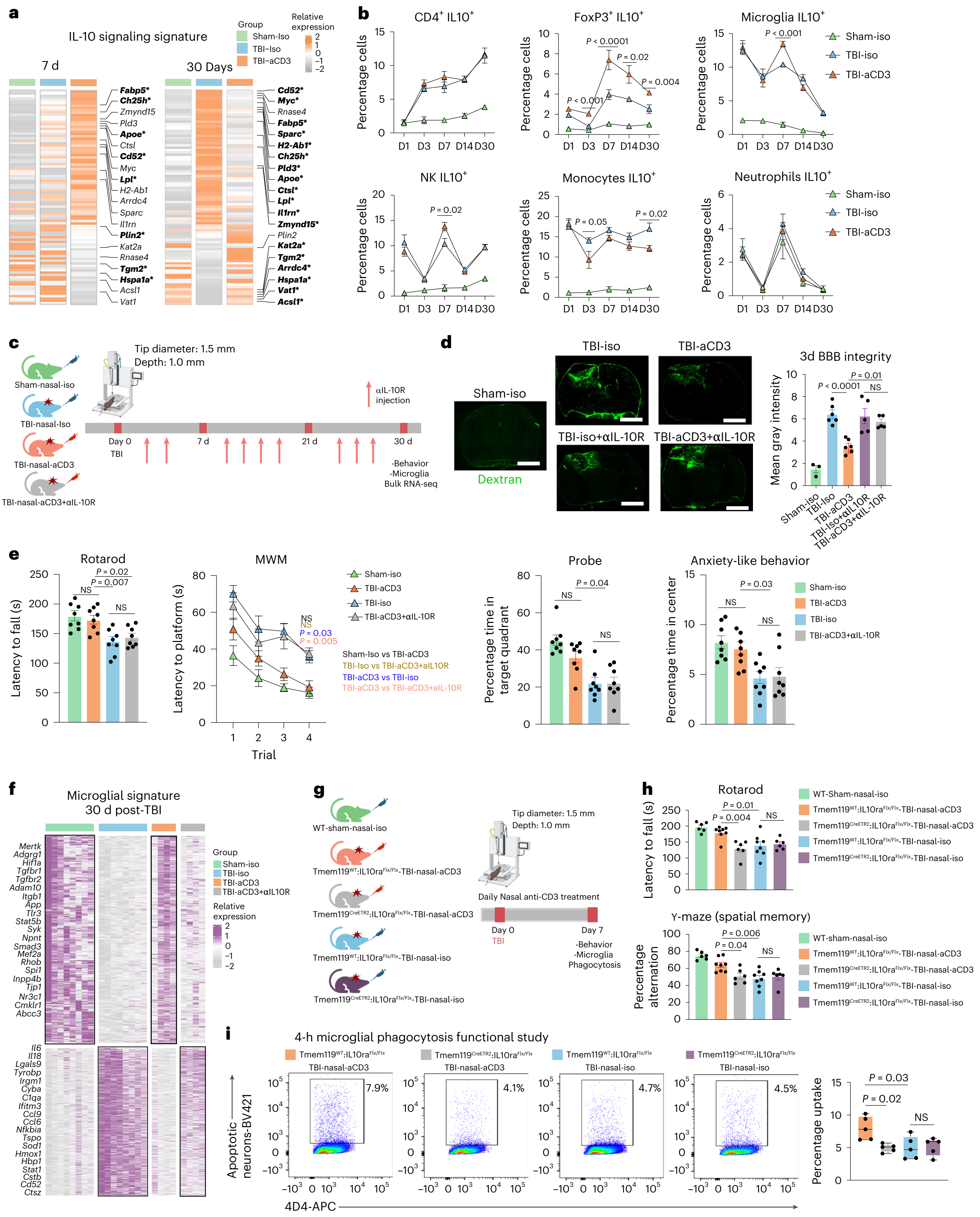
a
IL-10 signaling signature
Group
Sham-Iso
TBI-Iso
TBI-aCD3
Relative expression
2
1
0
−1
−2
7 d
30 Days
Fabp5*
Ch25h*
Zmynd15
Pld3
Apoe*
Ctsl
Cd52*
Myc
Lpl*
H2-Ab1
Arrdc4
Sparc
Il1rn
Plin2*
Kat2a
Rnase4
Tgm2*
Hspa1a*
Acsl1
Vat1
Cd52*
Myc*
Rnase4
Fabp5*
Sparc*
H2-Ab1*
Ch25h*
Pld3*
Apoe*
Ctsl*
Lpl*
Il1rn*
Zmynd15*
Plin2
Kat2a*
Tgm2*
Arrdc4*
Hspa1a*
Vat1*
Acsl1*
b
CD4+ IL10+
FoxP3+ IL10+
Microglia IL10+
NK IL10+
Monocytes IL10+
Neutrophils IL10+
Percentage cells
D1 D3 D7 D14 D30
P < 0.0001
P = 0.02
P < 0.001
P = 0.004
P < 0.001
P = 0.02
P = 0.05
P = 0.02
Sham-iso
TBI-iso
TBI-aCD3
c
Sham-nasal-iso
TBI-nasal-Iso
TBI-nasal-aCD3
TBI-nasal-aCD3+αIL-10R
Tip diameter: 1.5 mm
Depth: 1.0 mm
αIL-10R injection
Day 0 TBI
7 d
21 d
30 d
-Behavior
-Microglia
Bulk RNA-seq
d
Sham-iso
TBI-iso
TBI-aCD3
TBI-iso+αIL-10R
TBI-aCD3+αIL-10R
Dextran
3d BBB integrity
Mean gray intensity
P < 0.0001
P = 0.01
NS
Sham-iso
TBI-Iso
TBI-aCD3
TBI-iso+αIL10R
TBI-aCD3+αIL-10R
e
Rotarod
Latency to fall (s)
P = 0.02
P = 0.007
NS
NS
MWM
Latency to platform (s)
Trial
NS
NS
P = 0.03
P = 0.005
Sham-iso
TBI-aCD3
TBI-iso
TBI-aCD3+αIL-10R
Sham-Iso vs TBI-aCD3
TBI-Iso vs TBI-aCD3+αIL10R
TBI-aCD3 vs TBI-iso
TBI-aCD3 vs TBI-aCD3+αIL-10R
Probe
Percentage time in target quadrant
P = 0.04
NS
NS
Anxiety-like behavior
Percentage time in center
P = 0.03
NS
NS
Sham-iso
TBI-aCD3
TBI-iso
TBI-aCD3+αIL-10R
f
Microglial signature 30 d post-TBI
Mertk
Adgrg1
Hif1a
Tgfbr1
Tgfbr2
Adam10
Itgb1
App
Tlr3
Stat5b
Syk
Npnt
Smad3
Mef2a
Rhob
Spi1
Inpp4b
Tjp1
Nr3c1
Cmklr1
Abcc3
Il6
Il18
Lgals9
Tyrobp
Irgm1
Cyba
C1qa
Ifitm3
Ccl9
Ccl6
Nfkbia
Tspo
Sod1
Hmox1
Hbp1
Stat1
Cstb
Cd52
Ctsz
Group
Sham-iso
TBI-iso
TBI-aCD3
TBI-aCD3+αIL10R
Relative expression
2
1
0
−1
−2
g
WT-sham-nasal-iso
Tmem119WT:IL10raFlx/Flx-TBI-nasal-aCD3
Tmem119CreETR2:IL10raFlx/Flx-TBI-nasal-aCD3
Tmem119WT:IL10raFlx/Flx-TBI-nasal-iso
Tmem119CreETR2:IL10raFlx/Flx-TBI-nasal-iso
Tip diameter: 1.5 mm
Depth: 1.0 mm
Daily Nasal anti-CD3 treatment
Day 0
TBI
Day 7
-Behavior
-Microglia
Phagocytosis
h
Rotarod
Latency to fall (s)
P = 0.01
P = 0.004
NS
Y-maze (spatial memory)
Percentage alternation
P = 0.006
P = 0.04
NS
WT-Sham-nasal-iso
Tmem119WT:IL10raFlx/Flx-TBI-nasal-aCD3
Tmem119CreETR2:IL10raFlx/Flx-TBI-nasal-aCD3
Tmem119WT:IL10raFlx/Flx-TBI-nasal-iso
Tmem119CreETR2:IL10raFlx/Flx-TBI-nasal-iso
i
4-h microglial phagocytosis functional study
Tmem119WT:IL10raFlx/Flx TBI-nasal-aCD3
Tmem119CreETR2:IL10raFlx/Flx TBI-nasal-aCD3
Tmem119WT:IL10raFlx/Flx TBI-nasal-iso
Tmem119CreETR2:IL10raFlx/Flx TBI-nasal-iso
7.9%
4.1%
4.7%
4.5%
Apoptotic neurons-BV421
4D4-APC
Percentage uptake
P = 0.03
P = 0.02
NS

Fig. 5 | Nasal aCD3 ameliorates TBI microglial inflammation and functional outcomes in an IL-10-dependent manner. a, Heatmap of genes of aggregated samples involved in the IL-10 pathway for microglia at 7 and 30 d post-TBI. Genes identified with an FDR-corrected $P < 0.05$ using DESeq2 analysis are emboldened and indicated by an asterisk (two-sided LRT, $n = 4$ mice per group). Genes were identified from the literature[109]. **b**, IL-10 expression (flow cytometry) in different cells at different time points post-TBI and treatment in the ipsilateral hemisphere (sham-iso $n = 4$, TBI-iso $n = 6$, TBI-aCD3 $n = 6$), analyzed by one-way ANOVA with Tukey's multiple comparisons for individual time points. Data are shown as mean ± s.e.m. NK, natural killer cell. **c**, Experimental timeline of anti-IL-10R-blocking mAbs (aIL-10R) (created with BioRender.com). **d**, Dextran 70-kDa (green) for measurement of BBB permeability (3 d post-TBI). Scale bars, 1,000 µm. Data are shown as mean ± s.e.m. (sham-iso $n = 3$, $n = 6$ for the rest of the groups), analyzed by one-way ANOVA with Tukey's multiple comparisons. **e**, Behavioral testing (rotarod, MWM, probe trial, OF for anxiety-like behavior). The MWM was analyzed by two-factor, repeated-measures, two-way ANOVA (group × time) and the others by one-way ANOVA with Tukey's multiple comparisons. Data are shown as mean ± s.e.m. ($n = 8$ mice per group). **f**, Clustered heatmap DEGs at 30 d post-TBI identified using DESeq2 analysis (two-sided LRT, $n = 4$–8 mice per group, FDR-corrected $P < 0.05$). The microglial data at 30 d post-TBI from Fig. 3c were integrated. **g**, Experimental timeline for the microglia-specific IL-10ra KO (created with BioRender.com). **h**, Behavioral testing of rotarod and Y-maze assessed between the groups. Data are shown as mean ± s.e.m. (WT sham-nasal-iso $n = 6$, Tmem119^{WT}:IL-10ra$^{Flx/Flx}$-TBI-Nasal-aCD3 $n = 8$, Tmem119^{CreETR2}:IL-10ra$^{Flx/Flx}$TBI-Nasal-aCD3 $n = 6$, Tmem119^{WT}:IL-10ra$^{Flx/Flx}$-TBI-nasal-iso $n = 8$, Tmem119 ^{CreETR2}:IL-10ra$^{Flx/Flx}$TBI-nasal-iso $n = 6$). Analysis was by one-way ANOVA with Tukey's multiple comparisons. **i**, Phagocytosis experiment with a similar design to Fig. 4b. Data are shown as box plots (min., max., IQR, median; $n = 5$ mice per group), analyzed by one-way ANOVA with Tukey's multiple comparisons. All data are biological replicates and represent two independent experiments.

Nasal aCD3 ameliorates TBI outcomes via IL-10/IL-10R signaling in microglia

IL-10 is a potent anti-inflammatory cytokine produced by T_{reg} cells that acts on many cell types as a result of the presence of IL-10 receptor (IL-10R) on almost all hematopoietic cells[81]. IL-10 signaling is critical to maintain microglia under a homeostatic phenotype, because genetic depletion of IL-10 under proinflammatory conditions results in increased release of proinflammatory cytokines and chemokines[82]. We found a clear upregulation of the microglial IL-10-cytokine gene expression signature in TBI-aCD3 microglia group at 7 days post-CCI as compared to Sham-Iso and TBI-Iso controls (Fig. 5a). We also found that nasal aCD3 induced IL-10-secreting T_{reg} cells (from day 3 to day 30 post-injury) (Fig. 5b and Extended Data Fig. 8a) and increased IL-10 expression in both microglia and brain tissue derived from the site of injury (Fig. 3h and Extended Data Fig. 6c). We then investigated whether IL-10 played a role in the beneficial effects of nasal aCD3 by administering anti-IL-10R (aIL-10R)-blocking antibody intraperitoneally (i.p.) every 3 d post-injury (Fig. 5c) and investigating the behavioral outcomes and BBB disruption in sham-iso, TBI-iso, TBI-aCD3 and TBI-aCD3+aIL-10R groups. We found that the improvements in BBB disruption (Fig. 5d) and motor coordination functions, spatial memory and anxiety-like behavior observed in TBI-aCD3 were abrogated by blocking IL-10R (TBI-aCD3+aIL-10R group) (Fig. 5e).

We next investigated the impact of blocking IL-10R on the microglial inflammatory transcriptomic profile by performing RNA-seq on sorted microglia from the ipsilateral hemisphere of the brain (Extended Data Fig. 6a) at 1 month post-CCI (Fig. 3b and Supplementary Table 4). We found that the modulatory effect of nasal aCD3 on microglia was abrogated by blocking IL-10 as shown in the microglial heatmap signature (Fig. 5f). At 1 month post-CCI, similar to the transcriptomic signature of TBI-iso control, microglia from the TBI-aCD3+aIL-10R group had a more proinflammatory profile compared with sham-iso and the TBI-aCD3 group and was associated with decreased expression of homeostatic markers such as *Mertk*, *Tgfbr2*, *Atp8a2*, and *Adgrg1* (Fig. 5f and Supplementary Table 4).

We hypothesized that the beneficial effect of the T_{reg} cells induced by nasal aCD3 was dependent on IL10R signaling in microglia. We thus investigated this hypothesis by using IL-10R$^{flox/flox}$Tmem119^{CreETR2} conditional and tamoxifen-induced KO mice and littermate controls (Extended Data Fig. 8b). We investigated the effects of microglial IL-10R ablation on the behavioral and microglial phagocytic capacity at 7 d post-TBI (Fig. 5g). We found that tamoxifen-treated TBI-aCD3-IL-10R$^{flox/flox}$Tmem119^{CreETR2} mice exhibited worse motor and cognitive outcomes (Fig. 5h) and reduced microglial phagocytic capacity (Fig. 5i) compared with tamoxifen-treated TBI-aCD3 littermate controls, further supporting the role for IL-10 in modulating the microglial gene signature after nasal aCD3 treatment. Taken together, these data clearly demonstrate a critical role for IL-10/IL-10R signaling in augmenting microglial phagocytic capacity and ameliorating disease in TBI.

Nasal aCD3-induced CD4$^+$FoxP3$^+$ T_{reg} cells ameliorate neuroinflammation and TBI outcomes

In the days to weeks after TBI, lymphocytes appear at the lesion site and both effector T cells and T_{reg} cells infiltrate the injured brain[83–86]. We found that nasal aCD3 expanded FoxP3$^+$ T_{reg} cells at the injury site from day 3 to day 30 post-injury compared with the TBI-iso controls (Fig. 2b) and that nasal aCD3 improved behavioral and neuropathological outcomes of TBI by decreasing microglial inflammation (Figs. 1b and 3c). Thus, we next investigated whether these beneficial outcomes were dependent on T_{reg} cells by employing multiple experimental approaches including adoptive transfer experiments (discussed here) and an ex vivo T_{reg} cell–microglia transwell co-culture system and T_{reg} cell depletion

Fig. 6 | Nasal aCD3-induced CD4$^+$FoxP3$^+$ T_{reg} cells attenuate the CNS inflammatory response, increase microglial phagocytosis and improve behavioral outcomes after TBI. a, Experimental timeline of adoptive transfer (created with BioRender.com). **b**, Behavioral testing of rotarod and Y-maze assessed. Data are shown as mean ± s.e.m. (sham-DPBS $n = 6$, TBI-aCD3-FoxP3 $n = 8$, TBI-iso FoxP3 $n = 8$, TBI-aCD3-FoxP3$^-$ $n = 8$) and analyzed by one-way ANOVA with Tukey's multiple comparisons. **c**, Clustered heatmap of unique and shared DEGs of aggregated samples from microglia at 7 d post-TBI on the following comparisons: TBI-iso FoxP3 versus TBI-aCD3-FoxP3$^-$ and TBI-aCD3-FoxP3 versus TBI-aCD3-FoxP3$^-$. Clusters were functionally annotated using enriched GOBP terms (q-value < 0.05). DEGs were identified using DESeq2 analysis (two-sided Wald's test, $n = 3$ mice per group, FDR-corrected $P < 0.05$). **d**, GSEA analysis of Hallmark pathways at 7 d post-TBI for the following: TBI-iso FoxP3 versus TBI-aCD3-FoxP3$^-$ and TBI-aCD3-FoxP3 versus TBI-aCD3-FoxP3$^-$. The asreisk indicates enriched terms (q-value < 0.05). **e**, Predicted upstream regulators (IPA analysis) in TBI-aCD3-FoxP3 versus TBI-aCD3-FoxP3$^-$. **f**, GSEA analysis of Hallmark pathways comparing TBI-aCD3-FoxP3 versus TBI-iso FoxP3. **g**, Predicted upstream regulator (IPA analysis) in TBI-aCD3-FoxP3 versus TBI-Iso FoxP3. **h**, RT–qPCR of microglia sorted from the ipsilateral hemisphere 7 d post-TBI. Expression was normalized to GAPDH and presented relative to sham-DPBS mice. Data are shown as mean ± s.e.m., $n = 3$–4 mice per group and analyzed by one-way ANOVA with Tukey's multiple comparisons. **i**, Phagocytosis experiment with similar design to Fig. 4b. Data are shown as box plots (min., max., IQR, median), $n = 4$ mice per group and analyzed by one-way ANOVA with Tukey's multiple comparisons. **j**, Schematic representing microglia and T_{reg} cell transwell co-culture (created with BioRender.com). Microglia were isolated 24 h post-TBI and cultured with FoxP3 T_{reg} cells from either nasal aCD3 or isotype-treated TBI mice for 7 d. **j**, RT–qPCR of microglia, expression normalized to GAPDH. Data are shown as mean ± s.e.m., $n = 4$ conditions per group and analyzed by one-way ANOVA with Tukey's multiple comparisons. All data and conditions are biological replicates and represent two independent experiments.

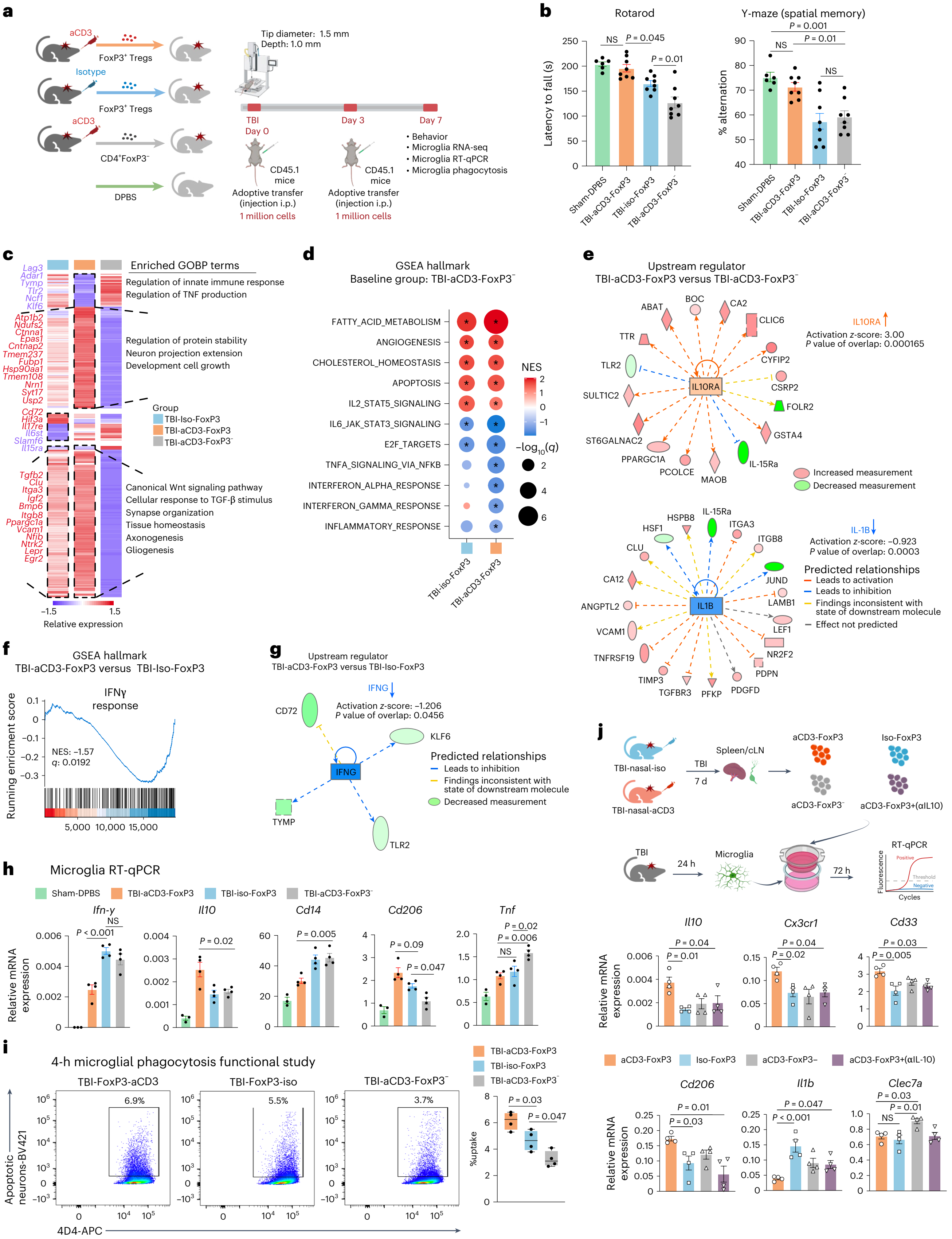
a
aCD3
FoxP3+ Tregs
Isotype
FoxP3+ Tregs
aCD3
CD4+FoxP3−
DPBS
Tip diameter: 1.5 mm
Depth: 1.0 mm
TBI
Day 0
Day 3
Day 7
CD45.1 mice
Adoptive transfer (injection i.p.)
1 million cells
• Behavior
• Microglia RNA-seq
• Microglia RT-qPCR
• Microglia phagocytosis
b
Rotarod
Latency to fall (s)
NS
P = 0.045
P = 0.01
Y-maze (spatial memory)
% alternation
P = 0.001
P = 0.01
NS
Sham-DPBS
TBI-aCD3-FoxP3
TBI-iso-FoxP3
TBI-aCD3-FoxP3−
c
Enriched GOBP terms
Regulation of innate immune response
Regulation of TNF production
Regulation of protein stability
Neuron projection extension
Development cell growth
Canonical Wnt signaling pathway
Cellular response to TGF-β stimulus
Synapse organization
Tissue homeostasis
Axonogenesis
Gliogenesis
Lag3 Adar1 Tymp Tlr2 Ncf1 Klf6
Atp1b2 Ndufs2 Ctnna1 Epas1 Cntnap2 Tmem237 Fubp1 Hsp90aa1 Tmem108 Nrn1 Syt17 Usp2
Cd72 Hif3a Il17re Il6st Slamf6 Il15ra
Tgfb2 Clu Itga3 Igf2 Bmp6 Itgb8 Ppargc1a Vcam1 Nfib Ntrk2 Lepr Egr2
Group
TBI-Iso-FoxP3
TBI-aCD3-FoxP3
TBI-aCD3-FoxP3−
−1.5 1.5
Relative expression
d
GSEA hallmark
Baseline group: TBI-aCD3-FoxP3−
FATTY_ACID_METABOLISM
ANGIOGENESIS
CHOLESTEROL_HOMEOSTASIS
APOPTOSIS
IL2_STAT5_SIGNALING
IL6_JAK_STAT3_SIGNALING
E2F_TARGETS
TNFA_SIGNALING_VIA_NFKB
INTERFERON_ALPHA_RESPONSE
INTERFERON_GAMMA_RESPONSE
INFLAMMATORY_RESPONSE
NES
2 1 0 −1
−log10(q)
2 4 6
TBI-iso-FoxP3
TBI-aCD3-FoxP3
e
Upstream regulator
TBI-aCD3-FoxP3 versus TBI-aCD3-FoxP3−
IL10RA
Activation z-score: 3.00
P value of overlap: 0.000165
ABAT BOC CA2 CLIC6 TTR CYFIP2 TLR2 CSRP2 SULT1C2 FOLR2 ST6GALNAC2 GSTA4 PPARGC1A PCOLCE MAOB IL-15Ra
Increased measurement
Decreased measurement
IL1B
Activation z-score: −0.923
P value of overlap: 0.0003
HSPB8 IL-15Ra HSF1 ITGA3 ITGB8 CLU CA12 JUND LAMB1 ANGPTL2 LEF1 VCAM1 NR2F2 TNFRSF19 PDPN TIMP3 TGFBR3 PFKP PDGFD
Predicted relationships
Leads to activation
Leads to inhibition
Findings inconsistent with state of downstream molecule
Effect not predicted
f
GSEA hallmark
TBI-aCD3-FoxP3 versus TBI-Iso-FoxP3
IFNγ response
Running enrichment score
NES: −1.57
q: 0.0192
5,000 10,000 15,000
g
Upstream regulator
TBI-aCD3-FoxP3 versus TBI-Iso-FoxP3
IFNG
Activation z-score: −1.206
P value of overlap: 0.0456
CD72 KLF6 TYMP TLR2
Predicted relationships
Leads to inhibition
Findings inconsistent with state of downstream molecule
Decreased measurement
h
Microglia RT-qPCR
Sham-DPBS TBI-aCD3-FoxP3 TBI-iso-FoxP3 TBI-aCD3-FoxP3−
Ifn-γ Il10 Cd14 Cd206 Tnf
Relative mRNA expression
P < 0.001
NS
P = 0.02
P = 0.005
P = 0.09
P = 0.047
P = 0.02
P = 0.006
NS
i
4-h microglial phagocytosis functional study
TBI-FoxP3-aCD3 6.9%
TBI-FoxP3-iso 5.5%
TBI-aCD3-FoxP3− 3.7%
Apoptotic neurons-BV421
4D4-APC
%uptake
P = 0.03
P = 0.047
j
TBI-nasal-iso
TBI-nasal-aCD3
TBI 7 d
Spleen/cLN
aCD3-FoxP3
Iso-FoxP3
aCD3-FoxP3−
aCD3-FoxP3+(αIL10)
TBI 24 h
Microglia
72 h
RT-qPCR
Fluorescence
Positive
Threshold
Negative
Cycles
Il10 Cx3cr1 Cd33
Cd206 Il1b Clec7a
Relative mRNA expression
P = 0.04 P = 0.01
P = 0.04 P = 0.02
P = 0.03 P = 0.005
P = 0.01 P = 0.03
P = 0.047 P < 0.001
P = 0.03 P = 0.01 NS
aCD3-FoxP3 Iso-FoxP3 aCD3-FoxP3− aCD3-FoxP3+(αIL-10)

experiments (discussed below). In the experiments involving adoptive transfer, we found that the adoptive transfer of CD4$^+$FoxP3$^+$ T$_{\mathrm{reg}}$ cells from aCD3-treated mice improved motor function and coordination and restored spatial memory when compared with mice that received either CD4$^+$FoxP3$^+$ T$_{\mathrm{reg}}$ cells from TBI-iso mice or CD4$^+$ T cells depleted of T$_{\mathrm{reg}}$ cells from anti-CD3-treated mice at 7 d post-TBI (Fig. 6b). We then performed RNA-seq on microglia isolated from the ipsilateral hemisphere of TBI-aCD3-FoxP3$^+$, TBI-iso-Foxp3$^+$ and TBI-aCD3-FoxP3$^-$ green fluorescent protein (GFP) groups at 7 d post-TBI (Supplementary Table 5). We found that TBI-aCD3-FoxP3$^+$ microglia had a distinct transcriptomic profile when compared with other groups (Fig. 6c). GSEA analysis comparing TBI-aCD3-FoxP3$^+$ microglia with TBI-aCD3-FoxP3$^-$ microglia demonstrated that the TBI-aCD3-FoxP3$^+$ microglia were associated with downregulation of several proinflammatory pathways including interferon (IFN)γ and IFNα (Fig. 6d). IPA revealed IL-10Ra as one of the top activated upstream regulators and IL-1b as one of the top inhibited upstream regulators in TBI-aCD3-FoxP3$^+$ microglia compared with TBI-aCD3-FoxP3$^-$ microglia (Fig. 6e). IFNγ was one of the most downregulated regulators in TBI-aCD3-FoxP3$^+$ microglia compared with TBI-iso-FoxP3$^+$ microglia (Fig. 6f,g). Consistent with the microglial transcriptomic data, RT–qPCR of TBI-aCD3-FoxP3$^+$, microglia from the lesion site showed reduction in proinflammatory cytokines (*Inf-γ*, *Cd14* and *Tnf*) and increased expression of homeostatic (*Cd206*) and anti-inflammatory cytokines (such as *Il10*) compared with the two other groups studied (Fig. 6h). Importantly, we also found that adoptive transfer of CD4$^+$FoxP3$^+$ T$_{\mathrm{reg}}$ cells from aCD3-treated mice increased microglial phagocytic capacity at 7 d post-injury compared with the two other groups (Fig. 6i). The microglial phagocytic capacity was also increased in mice that received CD4$^+$FoxP3$^+$ T$_{\mathrm{reg}}$ cells from TBI-iso-mice compared with mice that received FoxP3$^-$ cells from aCD3-treated mice, indicating the importance of CD4$^+$FoxP3$^+$ T$_{\mathrm{reg}}$ cells in increasing microglial phagocytic function after TBI.

To assess the beneficial effects of T$_{\mathrm{reg}}$ cells on behavioral outcomes and microglial inflammation at more chronic time points (30 d) post-TBI, we employed an alternative approach where total splenic T cells (CD45.2$^+$CD4$^+$) isolated from TBI-iso (iso-total CD4$^+$) and TBI-nasal aCD3-treated mice (aCD3-total CD4$^+$) and CD45.2$^+$CD4$^+$FoxP3$^-$ GFP cells isolated from aCD3-treated animals (aCD3-FoxP3$^-$ GFP) post-CCI were transferred i.p. into untreated but CCI-injured congenic CD45.1-expressing mice (Extended Data Figs. 8c and 9a). Adoptive transfer was performed at three time points post-CCI with each mouse receiving 2.5×10^6 cells per injection. We found improvement in motor function and coordination, restoration of spatial memory and increased time spent in the target quadrant during the probe trial in mice that received total CD4$^+$ T cells from aCD3-treated mice compared with mice that received CD4$^+$ T cells depleted of T$_{\mathrm{reg}}$ cells at 30 d post-TBI (Extended Data Fig. 9b). We performed flow cytometric analyses to track adoptively transferred cells in recipient mice by transferring cells from CD45.2 mice into CD45.1 mice and found CD45.2 transferred cells in all organs analyzed (Extended Data Fig. 9c). We then performed RNA-seq on microglia isolated from the ipsilateral hemisphere of iso-total CD4$^+$, aCD3-total CD4$^+$ and aCD3-FoxP3$^-$ GFP groups at 30 d post-TBI (Supplementary Table 5). A heatmap signature showed a distinct microglial transcriptomic signature of aCD3-total CD4$^+$ compared with iso-total CD4$^+$ and aCD3-FoxP3$^-$ GFP groups at 30 d post-CCI (Extended Data Fig. 9d). GSEA pathway analysis demonstrated that the aCD3-total CD4$^+$ group was associated with the upregulation of neuron development pathways and the downregulation of several proinflammatory pathways involved in innate and adaptive immune responses, immune effector processes and antigen presentation compared with the iso-total CD4$^+$ group, all of which were not notably upregulated in the aCD3-FoxP3$^-$ GFP group (Extended Data Fig. 9e). Similarly, the aCD3-total CD4$^+$ group was associated with a downregulation of the innate immune response pathway when compared with the aCD3-FoxP3$^-$ GFP group (Extended Data Fig. 9f,g), where IPA analysis demonstrated IL-10 as a top activated upstream regulator and IFNγ as a top inhibited upstream regulator (Extended Data Fig. 9h). Consistent with the microglial transcriptomic data, RT–qPCR of the ipsilateral hemisphere showed an increase in the expression of several anti-inflammatory cytokines (*Il10* and *Il2*), and growth factors including *Gdnf* at 1 month post-CCI in the aCD3-total CD4$^+$ group compared with the iso-total CD4$^+$ and aCD3-FoxP3$^-$ GFP groups (Extended Data Fig. 9i). Taken together, these data demonstrate a critical role for FoxP3$^+$ T$_{\mathrm{reg}}$ cells in augmenting microglia phagocytic capacity and ameliorating disease in TBI.

CD4$^+$Foxp3$^+$ T$_{\mathrm{reg}}$ cells suppress microglial inflammatory and homeostatic markers in vitro

To further investigate the interaction between T$_{\mathrm{reg}}$ cells and microglia after TBI, we employed an ex vivo transwell co-culture system in which microglia were isolated from the ipsilateral hemisphere of CCI mice 24 h after injury and T$_{\mathrm{reg}}$ cells were isolated from spleens of a separate cohort of mice subjected to CCI and treated with nasal aCD3 or isotype control for 7 d (Fig. 6j). Microglia were placed in the lower chamber and T$_{\mathrm{reg}}$ cells in the upper chamber and we performed RT–qPCR of microglia 72 h after incubation. We found an increase in anti-inflammatory and homeostatic markers (*Il10*, *Cx3cr1* and *Cd206*) and a reduction in the proinflammatory marker *Il1b* in the TBI-aCD3 microglia, which are consistent with our in vivo microglial transcriptomic data at 7 d post-TBI. This effect was lost by blocking IL-10 in vitro which is also consistent with what we observed following in vivo Il-10 neutralization (Fig. 5).

IL-10-producing T$_{\mathrm{reg}}$ cells modulate microglial phagocytosis, neuroinflammation and TBI outcomes

FoxP3 T$_{\mathrm{reg}}$ cells play a critical role in suppressing CNS inflammation in acute stroke and chronic neurological diseases[87] and, as shown above, we found that adoptive transfer of FoxP3 T$_{\mathrm{reg}}$ cells from nasal aCD3-treated mice ameliorated TBI and IL-10 is an important factor in this process. We then asked whether IL-10 produced by T$_{\mathrm{reg}}$ cells was

Fig. 7 | IL-10-producing T$_{\mathrm{reg}}$ cells play a critical role in modulating microglia and improving recovery post-TBI. a, Experimental timeline of FoxP3-DTR T$_{\mathrm{reg}}$ cell depletion (created with BioRender.com). **b**, Behavioral testing of rotarod and Y-maze was assessed between the groups. Data are shown as mean ± s.e.m., $n = 6$ mice per group and analyzed by one-way ANOVA with Tukey's multiple comparisons. **c**, RT–qPCR of microglia sorted from the ipsilateral hemisphere 7 d post-TBI. Expression was normalized to GAPDH. Data are shown as mean ± s.e.m., $n = 4$ mice per group and analyzed by one-way ANOVA with Tukey's multiple comparisons. **d**, Phagocytosis experiment with similar design to Fig. 4b. Data are shown as box plots (min,. max., IQR, median), $n = 5$ mice per group and analyzed by one-way ANOVA with Tukey's multiple comparisons. **e**, Schematic representing validation of *Il10* expression (created with BioRender.com). RT–qPCR of *Il10* expression was done for FoxP3$^+$Thy1.1$^+$- and FoxP3$^+$Thy1.1$^-$-sorted cells and expression was normalized to GAPDH. Data are shown as mean ± s.e.m., $n = 3$ mice per group and analyzed by two-sided, unpaired Student's *t*-test. **f**, Schematic representing adoptive transfer experiment (created with BioRender.com). Expression of Thy1.1 on FoxP3 was analyzed between the two groups. Data are shown as mean ± s.e.m., $n = 3$ sample per group and analyzed by two-sided, unpaired Student's *t*-test. Each sample was a pool of five injured hemispheres. **g**, Schematic representing experimental timeline of adoptive transfer experiment. **h**, Behavioral testing of rotarod and Y-maze assessed between the groups. Data are shown as mean ± s.e.m, $n = 6$ mice per group and analyzed by one-way ANOVA with Tukey's multiple comparisons. **i**, RT–qPCR of microglia sorted from the ipsilateral hemisphere 7 d post-TBI. Expression was normalized to GAPDH. Data are shown as mean ± s.e.m., $n = 4$ mice per group and analyzed by one-way ANOVA with Tukey's multiple comparisons. **j**, Phagocytosis experiment with similar design to Fig. 4b. Data are shown as box plots (min., max., IQR, median), $n = 4$ mice per group and analyzed by one-way ANOVA with Tukey's multiple comparisons. All data are biological replicates and represent two independent experiments.

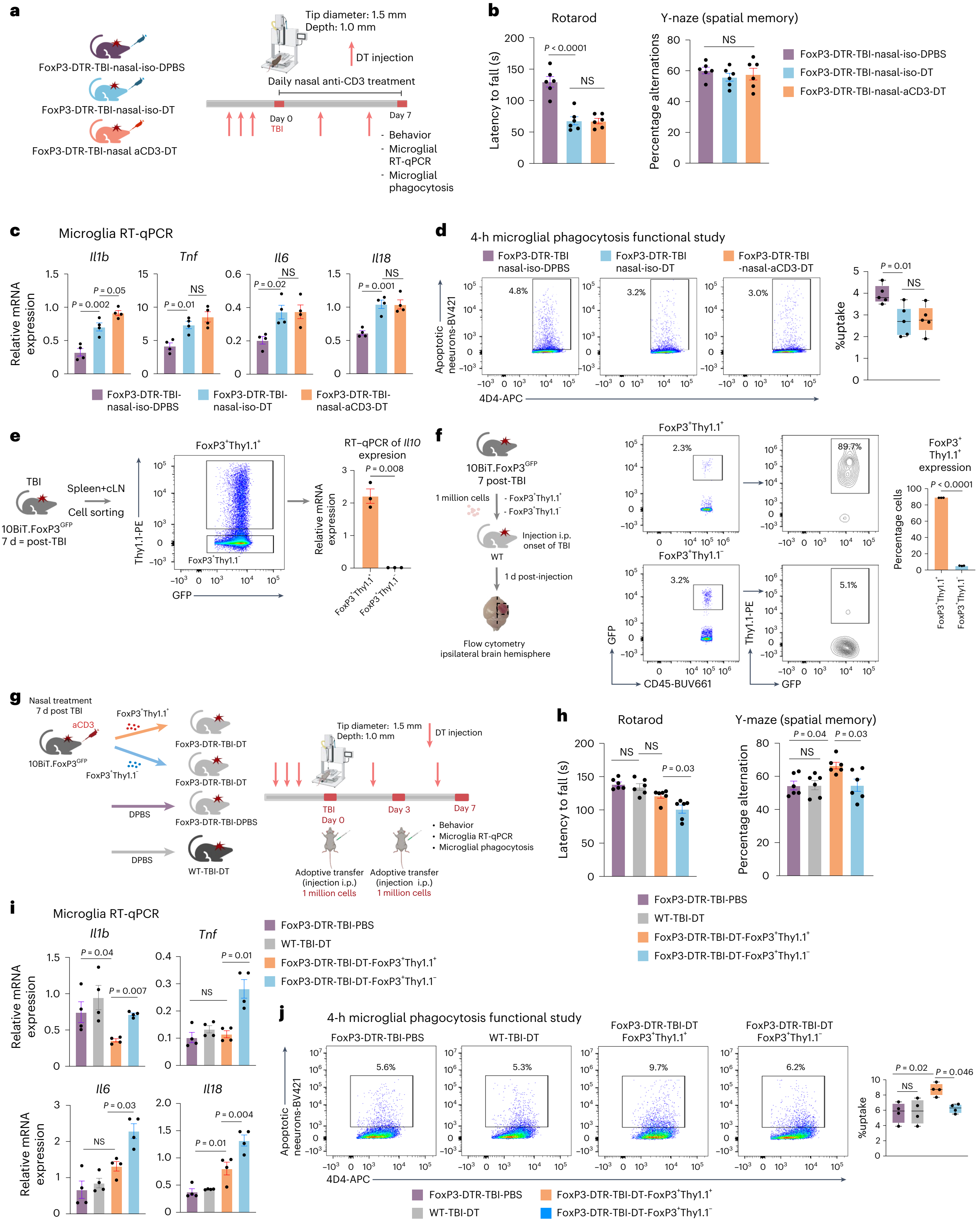
a
FoxP3-DTR-TBI-nasal-iso-DPBS
FoxP3-DTR-TBI-nasal-iso-DT
FoxP3-DTR-TBI-nasal aCD3-DT
Tip diameter: 1.5 mm
Depth: 1.0 mm
DT injection
Daily nasal anti-CD3 treatment
Day 0
TBI
Day 7
- Behavior
- Microglial RT-qPCR
- Microglial phagocytosis
b
Rotarod
Latency to fall (s)
P < 0.0001
NS
Y-naze (spatial memory)
Percentage alternations
NS
FoxP3-DTR-TBI-nasal-iso-DPBS
FoxP3-DTR-TBI-nasal-iso-DT
FoxP3-DTR-TBI-nasal-aCD3-DT
c
Microglia RT-qPCR
Il1b
Tnf
Il6
Il18
Relative mRNA expression
P = 0.05
P = 0.002
NS
P = 0.01
NS
P = 0.02
NS
P = 0.001
FoxP3-DTR-TBI-nasal-iso-DPBS
FoxP3-DTR-TBI-nasal-iso-DT
FoxP3-DTR-TBI-nasal-aCD3-DT
d
4-h microglial phagocytosis functional study
FoxP3-DTR-TBI nasal-iso-DPBS
FoxP3-DTR-TBI nasal-iso-DT
FoxP3-DTR-TBI -nasal-aCD3-DT
4.8%
3.2%
3.0%
Apoptotic neurons-BV421
4D4-APC
%uptake
P = 0.01
NS
e
TBI
10BiT.FoxP3GFP
7 d = post-TBI
Spleen+cLN
Cell sorting
FoxP3+Thy1.1+
FoxP3+Thy1.1−
Thy1.1-PE
GFP
RT–qPCR of Il10 expression
Relative mRNA expression
P = 0.008
FoxP3+Thy1.1+
FoxP3+Thy1.1−
f
10BiT.FoxP3GFP
7 post-TBI
1 million cells
- FoxP3+Thy1.1+
- FoxP3+Thy1.1−
Injection i.p. onset of TBI
WT
1 d post-injection
Flow cytometry ipsilateral brain hemisphere
FoxP3+Thy1.1+
2.3%
89.7%
FoxP3+Thy1.1−
3.2%
5.1%
GFP
CD45-BUV661
Thy1.1-PE
GFP
FoxP3+ Thy1.1+ expression
Percentage cells
P < 0.0001
FoxP3+Thy1.1+
FoxP3+Thy1.1−
g
Nasal treatment
7 d post TBI
aCD3
10BiT.FoxP3GFP
FoxP3+Thy1.1+
FoxP3+Thy1.1−
FoxP3-DTR-TBI-DT
FoxP3-DTR-TBI-DT
DPBS
FoxP3-DTR-TBI-DPBS
DPBS
WT-TBI-DT
Tip diameter: 1.5 mm
Depth: 1.0 mm
DT injection
TBI
Day 0
Day 3
Day 7
• Behavior
• Microglia RT-qPCR
• Microglial phagocytosis
Adoptive transfer (injection i.p.) 1 million cells
Adoptive transfer (injection i.p.) 1 million cells
h
Rotarod
Latency to fall (s)
NS
NS
P = 0.03
Y-maze (spatial memory)
Percentage alternation
P = 0.04
P = 0.03
NS
FoxP3-DTR-TBI-PBS
WT-TBI-DT
FoxP3-DTR-TBI-DT-FoxP3+Thy1.1+
FoxP3-DTR-TBI-DT-FoxP3+Thy1.1−
i
Microglia RT-qPCR
Il1b
P = 0.04
P = 0.007
Tnf
P = 0.01
NS
Il6
P = 0.03
NS
Il18
P = 0.004
P = 0.01
Relative mRNA expression
FoxP3-DTR-TBI-PBS
WT-TBI-DT
FoxP3-DTR-TBI-DT-FoxP3+Thy1.1+
FoxP3-DTR-TBI-DT-FoxP3+Thy1.1−
j
4-h microglial phagocytosis functional study
FoxP3-DTR-TBI-PBS
5.6%
WT-TBI-DT
5.3%
FoxP3-DTR-TBI-DT FoxP3+Thy1.1+
9.7%
FoxP3-DTR-TBI-DT FoxP3+Thy1.1−
6.2%
Apoptotic neurons-BV421
4D4-APC
%uptake
P = 0.02
P = 0.046
NS
FoxP3-DTR-TBI-PBS
WT-TBI-DT
FoxP3-DTR-TBI-DT-FoxP3+Thy1.1+
FoxP3-DTR-TBI-DT-FoxP3+Thy1.1−

responsible for this effect. To address this question, we first depleted FoxP3 T_{reg} cells using FoxP3-DTR transgenic mice that express the diphtheria toxin receptor (DTR) under control of the *FoxP3* promoter and then investigated the role of IL-10-producing T_{reg} cells in TBI by using a dual reporter system that involved the gene encoding IL-10 and transcriptomic factor FoxP3 (10BiT.FoxP3^{GFP})[88] which allowed us to sort IL-10^{+} and IL-10^{-} T_{reg} cells. In the first FoxP3 T_{reg} cell depletion experiment, DT was injected 3 d before CCI and repeated every 3 d until 7 d after CCI or sham operation (Fig. 7a and Extended Data Fig. 10a). We found that the depletion of FoxP3 T_{reg} cells worsened motor function as measured by rotarod behavioral testing (Fig. 7b) and exacerbated microglial inflammation (Fig. 7c). We also observed increased expression of proinflammatory microglial markers including *Il1b*, *Tnf*, *Il6*, and *Il18*, as measured by RT–qPCR. Most importantly, we found that the depletion of FoxP3 T_{reg} cells reduced microglial phagocytic capacity to uptake dead neurons (Fig. 7d), highlighting their pivotal role in regulating microglial phagocytosis. Based on these results, we then investigated the role of IL-10-producing T_{reg} cells in TBI by using a dual reporter system that involved the gene encoding IL-10 and 10BiT.FoxP3^{GFP} (ref. 88) that allowed us to sort IL-10^{+} and IL-10^{-} T_{reg} cells (Fig. 7e-f). We assessed the effect of IL-10^{+} and IL-10^{-} T_{reg} cells by adoptive transfer of these cells to FoxP3-depleted mice (Fig. 7g and Extended Data Fig. 10b). We observed that DT has similar behavior outcomes in WT TBI DT mice and the FoxP3 TBI DT-PBS group (Fig. 7h). However, we found that the adoptive transfer of IL-10^{+} T_{reg} cells was associated with improvements in motor function measured by rotarod and spatial memory measured by the Y-maze compared with the mice that received IL-10^{-} T_{reg} cells (Fig. 7h). Moreover, IL-10^{+} T_{reg} cells attenuated the microglial inflammatory response with reduction in proinflammatory markers such as *Il1b*, *Tnf*, *Il6*, and *Il18* compared with IL-10^{-} T_{reg} cells (Fig. 7i). Most importantly, adoptive transfer of IL-10^{+} T_{reg} cells enhanced the microglial phagocytosis of dead neurons (Fig. 7j), indicating their critical role in modulating microglial inflammation and augmenting microglial phagocytosis. Thus, IL-10 plays a critical role in the beneficial effect of nasal aCD3-induced FoxP3 T_{reg} cells on TBI.

Discussion

Neuroinflammation plays a crucial role in both acute and chronic stages of TBI and contributes to secondary injury[11,20]. Our study demonstrates that nasal aCD3-induced IL-10^{+}FoxP3^{+} T_{reg} cells promoted cognitive and motor recovery from TBI, enhanced microglia phagocytosis and reduced neuroinflammation via IL-10-dependent T_{reg} cell–microglia crosstalk.

Microglia play a critical role in neuroinflammation after TBI and their activation contributes to long-term functional deficits and neurodegeneration[20]. We previously identified a time-dependent change in the microglial transcriptomic phenotype after contusional brain injury with reduced homeostasis, housekeeping and sensing tissue damage in the early stages and the development of a proinflammatory state over time[89]. Microglia also play a role in recovery by migrating to sites of neuronal death to phagocytose dead or dying cells or debris, and participate in synaptic remodeling to minimize neuronal injury and restore tissue integrity in the injured brain[52]. In the present study, nasal aCD3-induced FoxP3^{+} T_{reg} cells enhanced the phagocytic, homeostatic, sensing and housekeeping microglial phenotype in the acute stage of injury. Transcriptomic analyses and functional studies demonstrated that nasal aCD3 increased the microglial phagocytic capacity to uptake apoptotic neurons post-injury in an IL-10-dependent manner. Importantly, we found that IL-10-producing FoxP3^{+} T_{reg} cells play a critical role in augmenting microglial phagocytic capacity after TBI. We also found that aCD3 modulation of microglia at the lesion site is involved in controlling synaptic pruning and remodeling and myelin homeostasis. The expression of *Bdnf*, a key mediator of synaptic plasticity, which increases neuronal TrkB phosphorylation at the site of injury[90], was increased in the aCD3-treated mice.

In the chronic phase of TBI, nasal aCD3-induced FoxP3^{+} T_{reg} cells regulated the function of microglia from a phagocytic phenotype in the acute stages to a homeostatic and less inflammatory phenotype. It also decreased the expression of MGnD and DAM genes, which are associated with neurodegeneration[51], toward homeostatic levels seen in sham-treated animals at 30 d post-injury. By removing cellular debris by phagocytosis early after injury and releasing neurotrophic factors and anti-inflammatory cytokines, microglia contribute to the reduced cell death and improved behavioral and neuropathological outcomes observed after nasal aCD3 treatment of TBI.

Studies have shown T lymphocyte infiltration into the brain after TBI[91]. T_{reg} cells comprise a population of CD4^{+} T cells that include FoxP3^{+} T_{reg} cells and FoxP3^{-} T_{reg} cells, the latter of which includes T_H3 and Type 1 regulatory T (T_r1) cells[92]. Depletion of FoxP3^{+} T_{reg} cells increased T cell CNS infiltration and expression of inflammatory IFNγ after TBI[27]. However, the function of the interaction between T_{reg} cells and microglia is largely unknown. Our transcriptomic analyses of peripheral and brain-infiltrating T_{reg} cells revealed that they were reprogrammed in favor of the mobilization, immunoregulation and cell–cell interactions, especially the activation of phagocytes. Consistent with a recent study in stroke[23], brain-infiltrating T_{reg} cells exhibited higher expression of genes involved in immunoregulatory and trophic factors which were enhanced with nasal aCD3. Adoptive transfer of total CD4, CD4^{+}FoxP3^{+} T_{reg} cells and, most importantly, CD4^{+}FoxP3^{+}IL-10^{+} T_{reg} cells from nasal aCD3-treated mice modulated the microglial response and improved behavioral and neuropathological outcomes. We reported that nasal aCD3 treatment in a progressive experimental autoimmune encephalitis (EAE) model of MS[27] and a model of lupus[30] induced an IL-10-dependent CD4^{+}LAP^{+}FoxP3^{+} T_{reg} cell response. In our nasal aCD3 TBI studies, we did not observe an increase in LAP^{+} T cells, although we did observe expansion of CD4^{+}FoxP3^{+} T_{reg} cells and IL-10^{+}FoxP3^{+} T_{reg} cells. These differences may be related to distinct regulatory mechanisms induced by acute injury such as TBI versus an autoimmune inflammatory process such as EAE or lupus, although, in both instances, nasal aCD3 induced a T_{reg} cell phenotype that ameliorated disease.

T_{reg} cells exert their immunoregulatory functions after TBI by secreting regulatory cytokines such as IL-10 (ref. 93), IL-4 and TGF-β[94,95]. IL-10 is an anti-inflammatory cytokine that plays a role in resolution of neuroinflammation after brain injury[93]. The expression of IL-10 in the brain increases with acute brain injury, promoting neurological recovery by multiple mechanisms, including inhibiting microglia or macrophage cytokine production, reducing the activation of effector T cells, monocytes and macrophages, and promoting neuronal and glial cell survival[93,96,97]. Clinical studies have shown that IL-10 levels increase after TBI[98,99]. Preclinical studies have shown that IL-10$^{-/-}$ female mice have worse inflammation and motor and cognitive function post-CCI[100]. IL-10 pharmacological formulations reduce lesion volume and improve functional outcomes after TBI[101,102]. However, the role of IL-10 in T_{reg} cell–microglia crosstalk and its effects on microglial function after TBI have not been explored. We found that nasal aCD3 mAb induced IL-10-producing FoxP3^{+} T_{reg} cells that migrated to the CNS to downregulate microglial activation and improve behavior in an IL-10-dependent manner. Specific blocking of the IL-10R in vivo in microglia reversed the therapeutic effects of nasal aCD3 mAb, reduced microglial phagocytic capacity and contributed to a chronic microglial activation state. These results demonstrate the important role of T_{reg} cell–microglial crosstalk via IL-10 in the treatment of TBI using nasal aCD3.

A major challenge for the treatment of TBI is to induce T_{reg} cells in a fashion that is nontoxic and translatable to the clinic. Approaches such as infusion of cord blood T_{reg} cells, astrocytes engineered to produce IL-2 and mesenchymal stromal cells have demonstrated preclinical benefit, but are difficult to translate to the clinic[87,103]. Nasal aCD3 is a unique immunotherapeutic approach to induce T_{reg} cells to downregulate CNS inflammation and could be given immediately after TBI. Foralumab, a fully human aCD3 mAb, has been successfully given to humans and has demonstrated immunomodulatory effects with minimal toxicity[104–106]. A pilot trial in individuals with mild-to-moderate COVID-19 reduced lung inflammation and blood inflammatory biomarkers without side effects[105,106] and nasal foralumab is being studied in individuals with progressive MS.

In conclusion, our study identifies nasal aCD3 as a new therapeutic approach for treating TBI. Nasal aCD3 induces T_{reg} cells that enhance the phagocytic capacity of microglia to clear dead neurons, modulate the CNS innate and adaptive immune responses, and promote functional recovery in an IL-10-dependent manner. This approach has potential applications for the treatment of TBI and other types of acute brain injury, such as stroke.

Online content

Any methods, additional references, Nature Portfolio reporting summaries, source data, extended data, supplementary information, acknowledgements, peer review information; details of author contributions and competing interests; and statements of data and code availability are available at https://doi.org/10.1038/s41593-025-01877-7.

References

1. Faul, M. & Coronado, V. Epidemiology of traumatic brain injury. *Handb. Clin. Neurol.* **127**, 3–13 (2015).
2. Centers for Disease Control and Prevention. *Surveillance Report of Traumatic Brain Injury-related Emergency Department Visits, Hospitalizations, and Deaths—United States, 2014* (CDC, 2019).
3. Taylor C. A., Bell, J. M., Breiding, M. J. & Xu L. Traumatic brain injury-related emergency department visits, hospitalizations, and deaths, United States 2007 and 2013. *MMWR Surveill. Summ.* **66**, 1–16 (2017).
4. Shively, S., Scher, A. I., Perl, D. P. & Diaz-Arrastia, R. Dementia resulting from traumatic brain injury: what is the pathology? *Arch. Neurol.* **69**, 1245–1251 (2012).
5. Izzy, S. et al. Association of traumatic brain injury with the risk of developing chronic cardiovascular, endocrine, neurological, and psychiatric disorders. *JAMA Netw. Open* **5**, e229478 (2022).
6. Izzy, S. et al. Long-term risk of cardiovascular disease after traumatic brain injury: screening and prevention. *Lancet Neurol.* **22**, 959–970 (2023).
7. Langlois, J. A., Rutland-Brown, W. & Wald, M. M. The epidemiology and impact of traumatic brain injury: a brief overview. *J. Head Trauma Rehabil.* **21**, 375–378 (2006).
8. Gordon, W. A. et al. Traumatic brain injury rehabilitation: state of the science. *Am. J. Phys. Med. Rehabil.* **85**, 343–382 (2006).
9. McCrory, P. et al. Consensus statement on concussion in sport: the 3rd International Conference on Concussion in Sport held in Zurich, November 2008. *J. Athl. Train.* **44**, 434–448 (2009).
10. Helmick, K., Members of Consensus Conference. Cognitive rehabilitation for military personnel with mild traumatic brain injury and chronic post-concussional disorder: results of April 2009 consensus conference. *NeuroRehabilitation* **26**, 239–255 (2010).
11. Needham, E. J. et al. The immunological response to traumatic brain injury. *J. Neuroimmunol.* **332**, 112–125 (2019).
12. Algattas, H. & Huang, J. H. Traumatic brain injury pathophysiology and treatments: early, intermediate, and late phases post-injury. *Int. J. Mol. Sci.* **15**, 309–341 (2013).
13. Davalos, D. et al. ATP mediates rapid microglial response to local brain injury in vivo. *Nat. Neurosci.* **8**, 752–758 (2005).
14. Nimmerjahn, A., Kirchhoff, F. & Helmchen, F. Resting microglial cells are highly dynamic surveillants of brain parenchyma in vivo. *Science* **308**, 1314–1318 (2005).
15. Roth, T. L. et al. Transcranial amelioration of inflammation and cell death after brain injury. *Nature* **505**, 223–228 (2014).
16. Fourgeaud, L. et al. TAM receptors regulate multiple features of microglial physiology. *Nature* **532**, 240–244 (2016).
17. Ramlackhansingh, A. F. et al. Inflammation after trauma: microglial activation and traumatic brain injury. *Ann. Neurol.* **70**, 374–383 (2011).
18. Mannix, R. C. & Whalen, M. J. Traumatic brain injury, microglia, and Beta amyloid. *Int. J. Alzheimers Dis.* **2012**, 608732 (2012).
19. Schimmel, S. J., Acosta, S. & Lozano, D. Neuroinflammation in traumatic brain injury: a chronic response to an acute injury. *Brain Circ.* **3**, 135–142 (2017).
20. Jassam, Y. N., Izzy, S., Whalen, M., McGavern, D. B. & El Khoury, J. Neuroimmunology of traumatic brain injury: time for a paradigm shift. *Neuron* **95**, 1246–1265 (2017).
21. Simon, D. W. et al. The far-reaching scope of neuroinflammation after traumatic brain injury. *Nat. Rev. Neurol.* **13**, 171–191 (2017).
22. Sakaguchi, S., Yamaguchi, T., Nomura, T. & Ono, M. Regulatory T cells and immune tolerance. *Cell* **133**, 775–787 (2008).
23. Shi, L. et al. Treg cell-derived osteopontin promotes microglia-mediated white matter repair after ischemic stroke. *Immunity* **54**, 1527–1542 e1528 (2021).
24. Benakis, C. et al. T cells modulate the microglial response to brain ischemia. *eLife* https://doi.org/10.7554/eLife.82031 (2022).
25. Baruch, K. et al. Breaking immune tolerance by targeting Foxp3$^+$ regulatory T cells mitigates Alzheimer's disease pathology. *Nat. Commun.* **6**, 7967 (2015).
26. Olson, K. E., Mosley, R. L. & Gendelman, H. E. The potential for treg-enhancing therapies in nervous system pathologies. *Clin. Exp. Immunol.* **211**, 108–121 (2023).
27. Kramer, T. J. et al. Depletion of regulatory T cells increases T cell brain infiltration, reactive astrogliosis, and interferon-gamma gene expression in acute experimental traumatic brain injury. *J. Neuroinflam.* **16**, 163 (2019).
28. Gao, W. et al. IL-2/anti-IL-2 complex attenuates inflammation and BBB disruption in mice subjected to traumatic brain injury. *Front. Neurol.* **8**, 281 (2017).
29. Li, M. et al. Role of regulatory T cell in clinical outcome of traumatic brain injury. *Chin. Med. J.* **128**, 1072–1078 (2015).
30. Wu, H. Y., Quintana, F. J. & Weiner, H. L. Nasal anti-CD3 antibody ameliorates lupus by inducing an IL-10-secreting $CD4^+CD25^-LAP^+$ regulatory T cell and is associated with down-regulation of IL-$17^+CD4^+ICOS^+CXCR5^+$ follicular helper T cells. *J. Immunol.* **181**, 6038–6050 (2008).
31. Mayo, L. et al. IL-10-dependent Tr1 cells attenuate astrocyte activation and ameliorate chronic central nervous system inflammation. *Brain* **139**, 1939–1957 (2016).
32. Lopes, J. R. et al. Nasal administration of anti-CD3 monoclonal antibody ameliorates disease in a mouse model of Alzheimer's disease. *Proc. Natl Acad. Sci. USA* **120**, e2309221120 (2023).
33. Smith, D. H. et al. Pre-clinical traumatic brain injury common data elements: toward a common language across laboratories. *J. Neurotrauma* **32**, 1725–1735 (2015).
34. Wagner, A. K. et al. Evaluation of estrous cycle stage and gender on behavioral outcome after experimental traumatic brain injury. *Brain Res.* **998**, 113–121 (2004).
35. Monaco, C. M. et al. Environmental enrichment promotes robust functional and histological benefits in female rats after controlled cortical impact injury. *Exp. Neurol.* **247**, 410–418 (2013).
36. Xiong, Y. et al. Role of gender in outcome after traumatic brain injury and therapeutic effect of erythropoietin in mice. *Brain Res.* **1185**, 301–312 (2007).
37. Alam, A. et al. Cellular infiltration in traumatic brain injury. *J. Neuroinflam.* **17**, 328 (2020).
38. Richter, S. et al. Serum biomarkers identify critically ill traumatic brain injury patients for MRI. *Criti. Care* **26**, 369 (2022).
39. Van, V. Q. et al. Cutting edge: CD47 controls the in vivo proliferation and homeostasis of peripheral CD4+ CD25+ Foxp3+ regulatory T cells that express CD103. *J. Immunol.* **181**, 5204–5208 (2008).

40. Layman, A. A. K. et al. Ndfip1 restricts mTORC1 signalling and glycolysis in regulatory T cells to prevent autoinflammatory disease. *Nat. Commun.* **8**, 15677 (2017).
41. Kashiwakura, Y. et al. CD2-mediated regulation of peripheral CD4$^+$CD25$^+$ regulatory T-cell apoptosis accompanied by down-regulation of Bim. *Immunology* **139**, 48–60 (2013).
42. Xing, S. et al. Tcf1 and Lef1 are required for the immunosuppressive function of regulatory T cells. *J. Exp. Med.* **216**, 847–866 (2019).
43. Garin, M. I. et al. Galectin-1: a key effector of regulation mediated by CD4+CD25+ T cells. *Blood* **109**, 2058–2065 (2007).
44. Ono, M. et al. Foxp3 controls regulatory T-cell function by interacting with AML1/Runx1. *Nature* **446**, 685–689 (2007).
45. Ohkura, N. & Sakaguchi, S. Foxo1 and Foxo3 help Foxp3. *Immunity* **33**, 835–837 (2010).
46. Fu, W. et al. Foxo4- and Stat3-dependent IL-10 production by progranulin in regulatory T cells restrains inflammatory arthritis. *FASEB J.* **31**, 1354–1367 (2017).
47. Jain, N. et al. Cutting edge: Dab2 is a FOXP3 target gene required for regulatory T cell function. *J. Immunol.* **183**, 4192–4196 (2009).
48. He, F. et al. PLAU inferred from a correlation network is critical for suppressor function of regulatory T cells. *Mol. Syst. Biol.* **8**, 624 (2012).
49. Probst-Kepper, M. et al. GARP: a key receptor controlling FOXP3 in human regulatory T cells. *J. Cell. Mol. Med.* **13**, 3343–3357 (2009).
50. Schmetterer, K. G. & Pickl, W. F. The IL-10/STAT3 axis: contributions to immune tolerance by thymus and peripherally derived regulatory T-cells. *Eur. J. Immunol.* **47**, 1256–1265 (2017).
51. Krasemann, S. et al. The TREM2-APOE pathway drives the transcriptional phenotype of dysfunctional microglia in neurodegenerative diseases. *Immunity* **47**, 566–581 e569 (2017).
52. Hickman, S., Izzy, S., Sen, P., Morsett, L. & El Khoury, J. Microglia in neurodegeneration. *Nat. Neurosci.* **21**, 1359–1369 (2018).
53. Hickman, S. E. et al. The microglial sensome revealed by direct RNA sequencing. *Nat. Neurosci.* **16**, 1896–1905 (2013).
54. Crocker, P. R., McMillan, S. J. & Richards, H. E. CD33-related siglecs as potential modulators of inflammatory responses. *Ann. N. Y. Acad. Sci.* **1253**, 102–111 (2012).
55. Crocker, P. R., Paulson, J. C. & Varki, A. Siglecs and their roles in the immune system. *Nat. Rev. Immunol.* **7**, 255–266 (2007).
56. Workman, C. J. & Vignali, D. A. The CD4-related molecule, LAG-3 (CD223), regulates the expansion of activated T cells. *Eur. J. Immunol.* **33**, 970–979 (2003).
57. Janova, H. et al. CD14 is a key organizer of microglial responses to CNS infection and injury. *Glia* **64**, 635–649 (2016).
58. Zoller, T. et al. Silencing of TGFbeta signalling in microglia results in impaired homeostasis. *Nat. Commun.* **9**, 4011 (2018).
59. Butovsky, O. et al. Identification of a unique TGF-beta-dependent molecular and functional signature in microglia. *Nat. Neurosci.* **17**, 131–143 (2014).
60. Taylor, R. A. et al. TGF-beta1 modulates microglial phenotype and promotes recovery after intracerebral hemorrhage. *J. Clin. Invest.* **127**, 280–292 (2017).
61. Keren-Shaul, H. et al. A unique nicroglia type associated with restricting development of Alzheimer's disease. *Cell* **169**, 1276–1290.e1217 (2017).
62. Miranda, M., Morici, J. F., Zanoni, M. B. & Bekinschtein, P. Brain-derived neurotrophic factor: a key molecule for memory in the healthy and the pathological brain. *Front. Cell Neurosci.* **13**, 363 (2019).
63. Neher, J. J. et al. Phagocytosis executes delayed neuronal death after focal brain ischemia. *Proc. Natl Acad. Sci. USA* **110**, E4098–E4107 (2013).
64. Healy, L. M. et al. MerTK Is a functional regulator of myelin phagocytosis by human myeloid cells. *J. Immunol.* **196**, 3375–3384 (2016).
65. Wu, C., Yang, L., Youngblood, H., Liu, T. C. & Duan, R. Microglial SIRPalpha deletion facilitates synapse loss in preclinical models of neurodegeneration. *Neurosci. Bull.* **38**, 232–234 (2022).
66. Rajbhandari, L. et al. Toll-like receptor 4 deficiency impairs microglial phagocytosis of degenerating axons. *Glia* **62**, 1982–1991 (2014).
67. Park, S. Y. & Kim, I. S. Engulfment signals and the phagocytic machinery for apoptotic cell clearance. *Exp. Mol. Med.* **49**, e331 (2017).
68. Li, W. Eat-me signals: keys to molecular phagocyte biology and 'appetite' control. *J. Cell. Physiol.* **227**, 1291–1297 (2012).
69. Moon, B., Yang, S., Moon, H., Lee, J. & Park, D. After cell death: the molecular machinery of efferocytosis. *Exp. Mol. Med.* **55**, 1644–1651 (2023).
70. Dou, Y. et al. Microglial migration mediated by ATP-induced ATP release from lysosomes. *Cell Res.* **22**, 1022–1033 (2012).
71. Amick, J., Roczniak-Ferguson, A. & Ferguson, S. M. C9orf72 binds SMCR8, localizes to lysosomes, and regulates mTORC1 signaling. *Mol. Biol. Cell* **27**, 3040–3051 (2016).
72. Smits, D. J. et al. CLEC16A interacts with retromer and TRIM27, and its loss impairs endosomal trafficking and neurodevelopment. *Hum. Genet.* **142**, 379–397 (2023).
73. Jonker, C. T. H. et al. Vps3 and Vps8 control integrin trafficking from early to recycling endosomes and regulate integrin-dependent functions. *Nat. Commun.* **9**, 792 (2018).
74. Wang, N. et al. Opposing effects of apoE2 and apoE4 on microglial activation and lipid metabolism in response to demyelination. *Mol. Neurodegener.* **17**, 75 (2022).
75. Filipello, F. et al. Defects in lysosomal function and lipid metabolism in human microglia harboring a TREM2 loss of function mutation. *Acta Neuropathol.* **145**, 749–772 (2023).
76. Shi, Y. et al. Overexpressing low-density lipoprotein receptor reduces tau-associated neurodegeneration in relation to apoE-linked mechanisms. *Neuron* **109**, 2413–2426.e2417 (2021).
77. Barger, S. R. et al. Membrane-cytoskeletal crosstalk mediated by myosin-I regulates adhesion turnover during phagocytosis. *Nat. Commun.* **10**, 1249 (2019).
78. Fairley, L. H. et al. Mitochondrial control of microglial phagocytosis by the translocator protein and hexokinase 2 in Alzheimer's disease. *Proc. Natl Acad. Sci. USA* **120**, e2209177120 (2023).
79. Ren, J. et al. Qki is an essential regulator of microglial phagocytosis in demyelination. *J. Exp. Med.* https://doi.org/10.1084/jem.20190348 (2021).
80. Schmidt, C. et al. Phosphoinositide 3-kinase gamma mediates microglial phagocytosis via lipid kinase-independent control of cAMP. *Neuroscience* **233**, 44–53 (2013).
81. Karaca, N. E. et al. Early diagnosis and hematopoietic stem cell transplantation for IL10R deficiency leading to very early-onset inflammatory bowel disease are essential in familial cases. *Case Rep. Immunol.* **2016**, 5459029 (2016).
82. Laffer, B. et al. Loss of IL-10 promotes differentiation of microglia to a M1 phenotype. *Front. Cell Neurosci.* **13**, 430 (2019).
83. Loftspring, M. C., McDole, J., Lu, A., Clark, J. F. & Johnson, A. J. Intracerebral hemorrhage leads to infiltration of several leukocyte populations with concomitant pathophysiological changes. *J. Cereb. Blood Flow Metab.* **29**, 137–143 (2009).
84. Mracsko, E. et al. Leukocyte invasion of the brain after experimental intracerebral hemorrhage in mice. *Stroke* **45**, 2107–2114 (2014).
85. Guo, F. Q. et al. Study of relationship between inflammatory response and apoptosis in perihematoma region in patients with intracerebral hemorrhage]. *Zhongguo Wei Zhong Bing Ji Jiu Yi Xue* **18**, 290–293 (2006).

86. Zhang, W., Wu, Q., Hao, S. & Chen, S. The hallmark and crosstalk of immune cells after intracerebral hemorrhage: Immunotherapy perspectives. *Front. Neurosci.* **16**, 1117999 (2022).
87. Yshii, L. et al. Astrocyte-targeted gene delivery of interleukin 2 specifically increases brain-resident regulatory T cell numbers and protects against pathological neuroinflammation. *Nat. Immunol.* **23**, 878–891 (2022).
88. Maynard, C. L. et al. Regulatory T cells expressing interleukin 10 develop from Foxp3+ and Foxp3- precursor cells in the absence of interleukin 10. *Nat. Immunol.* **8**, 931–941 (2007).
89. Izzy, S. et al. Time-dependent changes in microglia transcriptional networks following traumatic brain injury. *Front. Cell Neurosci.* **13**, 307 (2019).
90. Houlton, J., Abumaria, N., Hinkley, S. F. R. & Clarkson, A. N. Therapeutic potential of neurotrophins for repair after brain injury: a helping hand from biomaterials. *Front. Neurosci.* **13**, 790 (2019).
91. Xu, L. et al. T-cell infiltration, contribution and regulation in the central nervous system post-traumatic injury. *Cell Prolif.* **54**, e13092 (2021).
92. Curotto de Lafaille, M. A. & Lafaille, J. J. Natural and adaptive foxp3+ regulatory T cells: more of the same or a division of labor? *Immunity* **30**, 626–635 (2009).
93. Garcia, J. M. et al. Role of interleukin-10 in acute brain injuries. *Front. Neurol.* **8**, 244 (2017).
94. Tiemessen, M. M. et al. CD4+CD25+Foxp3+ regulatory T cells induce alternative activation of human monocytes/macrophages. *Proc. Natl Acad. Sci. USA* **104**, 19446–19451 (2007).
95. Zhao, W., Beers, D. R., Liao, B., Henkel, J. S. & Appel, S. H. Regulatory T lymphocytes from ALS mice suppress microglia and effector T lymphocytes through different cytokine-mediated mechanisms. *Neurobiol. Dis.* **48**, 418–428 (2012).
96. Strle, K. et al. Interleukin-10 in the brain. *Crit. Rev. Immunol.* **21**, 427–449 (2001).
97. Moore, K. W., de Waal Malefyt, R., Coffman, R. L. & O'Garra, A. Interleukin-10 and the interleukin-10 receptor. *Annu. Rev. Immunol.* **19**, 683–765 (2001).
98. Schneider Soares, F. M. et al. Interleukin-10 is an independent biomarker of severe traumatic brain injury prognosis. *Neuroimmunomodulation* **19**, 377–385 (2012).
99. Kirchhoff, C. et al. Cerebrospinal IL-10 concentration is elevated in non-survivors as compared to survivors after severe traumatic brain injury. *Eur. J. Med. Res.* **13**, 464–468 (2008).
100. Chen, X. et al. Interleukin-10 mediates the neuroprotection of hyperbaric oxygen therapy against traumatic brain injury in mice. *Neuroscience* **266**, 235–243 (2014).
101. Kline, A. E. et al. Acute systemic administration of interleukin-10 suppresses the beneficial effects of moderate hypothermia following traumatic brain injury in rats. *Brain Res.* **937**, 22–31 (2002).
102. Lee, H. F., Lee, T. S. & Kou, Y. R. Anti-inflammatory and neuroprotective effects of triptolide on traumatic brain injury in rats. *Respir. Physiol. Neurobiol.* **182**, 1–8 (2012).
103. Caplan, H. W. et al. Combination therapy with Treg and mesenchymal stromal cells enhances potency and attenuation of inflammation after traumatic brain injury compared to monotherapy. *Stem Cells* **39**, 358–370 (2021).
104. Chitnis, T. et al. Nasal administration of anti-CD3 monoclonal antibody modulates effector CD8+ T cell function and induces a regulatory response in T cells in human subjects. *Front. Immunol.* **13**, 956907 (2022).
105. Moreira, T. G. et al. Nasal administration of anti-CD3 monoclonal antibody (foralumab) reduces lung inflammation and blood inflammatory biomarkers in mild to moderate COVID-19 patients: a pilot study. *Front. Immunol.* **12**, 709861 (2021).
106. Moreira, T. G. et al. Nasal administration of anti-CD3 mAb (foralumab) downregulates NKG7 and increases TGFB1 and GIMAP7 expression in T cells in subjects with COVID-19. *Proc. Natl Acad. Sci. USA* **120**, e2220272120 (2023).
107. Hickman, S. E. & El Khoury, J. Analysis of the microglial sensome. *Methods Mol. Biol.* **2034**, 305–323 (2019).
108. Galatro, T. F. et al. Transcriptomic analysis of purified human cortical microglia reveals age-associated changes. *Nat. Neurosci.* **20**, 1162–1171 (2017).
109. Xue, J. et al. Transcriptome-based network analysis reveals a spectrum model of human macrophage activation. *Immunity* **40**, 274–288 (2014).

Saef Izzy[1,2,3], Taha Yahya[1,2,3], Omar Albastaki[1,2,3], Hadi Abou-El-Hassan[2], Michael Aronchik[1,2], Tian Cao[1,2], Marilia Garcia De Oliveira[2], Kuan-Jung Lu[1,2], Thais G. Moreira[2], Patrick da Silva[2], Masen L. Boucher[4], Leah C. Beauchamp[2], Danielle S. LeServe[2], Wesley Nogueira Brandao[2], Ana Carolina Durão[2], Toby Lanser[2], Federico Montini[2], Joon-Hyuk Lee[2], Joshua D. Bernstock[5], Megha Kaul[2], Gabriel Pasquarelli-do-Nascimento[2], Kusha Chopra[2], Rajesh Krishnan[2], Rebekah Mannix[4], Rafael M. Rezende[2], Francisco J. Quintana[2], Oleg Butovsky[2] & Howard L. Weiner[2] ✉

[1]Immunology of Brain Injury Program, Brigham & Women's Hospital, Harvard Medical School, Boston, MA, USA. [2]Ann Romney Center for Neurologic Diseases, Brigham & Women's Hospital, Harvard Medical School, Boston, MA, USA. [3]Divisions of Stroke, Cerebrovascular, and Critical Care Neurology, Department of Neurology, Brigham and Women's Hospital, Harvard Medical School, Boston, MA, USA. [4]Boston Children's Hospital, Harvard Medical School, Boston, MA, USA. [5]Department of Neurosurgery, Brigham and Women's Hospital, Harvard Medical School, Boston, MA, USA.
✉e-mail: hweiner@rics.bwh.harvard.edu

Methods

Experimental animals

Studies were performed using 8- to 12-week-old C57BL6J mice (Jackson Laboratories cat. no. 000664), B6.CD45.1 mice (Jackson Laboratory, cat. no. 002014), FoxP3-GFP mice (Jackson Laboratory, cat. no. 023800), FoxP3-DTR mice (Jackson Laboratory, cat. no. 016958), IL-10 KO mice (Jackson Laboratory, cat. no. 002251), Tmem119-Cre^{ETR2} mice (Jackson Laboratory, cat. no. 031820), IL-10ra^{Flx} mice (Jackson Laboratory, cat. no. 028146) and 10BiT.FoxP3^{GFP} (kindly provided by V. Kuchroo)[88]. All mice were housed under specific pathogen-free conditions, with free access to food and water. All animals were housed in temperature (20 °C) and humidity (60%)-controlled rooms, maintained on a 12 h:12 h light:dark cycle (lights on at 07:00). Mice were euthanized by CO_2 inhalation. The Institutional Animal Care and Use Committee at Harvard Medical School and Brigham and Women's Hospital has all experimental procedures involving animals.

Treatment with aCD3 mAb

Mice were nasally treated with a daily dose, immediately (4–6 hours) and for some experiments early (3 days) or delayed (7 days) post TBI, of 1 µg per mouse hamster immunoglobulin G (IgG) CD3-specific antibody (BioXCell, clone no. 145-2C11) or hamster IgG control antibody (BioXCell) dissolved in PBS and henceforth every other day after the first week until the experimental endpoint. For some experiments, mice were given 0.5 mg of monoclonal anti-IL-10R-blocking antibody (BioXCell, clone 1B1.3A), by intraperitoneal injection at the onset of TBI and henceforth every third day until the experimental endpoint.

Conditional genetic deletion of IL-10Ra in microglia

To induce Cre-recombinase expression, a dose of tamoxifen (150 mg per kg of body weight) in corn oil was injected i.p. for 5 d consecutively. IL-10Ra$^{flx/flx}$ was crossed with Tmem119-Cre^{ETR2} mice[110]. Recombination was induced in Tmem119-Cre^{ETR2}:IL-10Ra$^{flx/flx}$ mice and Tmem119-Cre^{WT}:IL-10Ra$^{flx/flx}$ littermates were used as controls. A washout period of 2 weeks was implemented after the last tamoxifen injection before starting any experiment.

FoxP3 cell depletion

Depletion of FoxP3 was done as previously described[23]. In short, DT (0.05 µg per g body weight) was injected i.p. 3 d before TBI and was repeated every 3 d to maintain FoxP3 depletion until sacrifice.

Controlled cortical impact

A CCI model was used as previously described[111]. Mice were anesthetized with 4.5% isoflurane (Anaquest) in 70% nitrous oxide and 30% oxygen using a Fluotec 3 vaporizer (Colonial Medical). The mice were placed in a stereotaxic frame and a 5-mm craniotomy was made over the right somatosensory cortex using a drill and a trephine. The bone flap was removed and discarded and a pneumatic cylinder with a 1.5- or 3-mm flat tip impounder and velocity 6 m s^{-1}, depth 1.0 or 1.5 mm and dwell time of 0.8 s was used to induce CCI (Impact One, Leica Biosystems). The scalp was sutured closed and the mice were returned to their cages to recover.

Behavioral studies

Open field testing. The open field (OF) test is used to measure general locomotor activity and anxiety-like behavior of the animals[112]. The OF square chambers are made of blue Plexiglas with dimensions of 30 × 38 × 40 cm^3. For each testing session, the animal was allowed to explore the chamber for 15 min. A computer-assisted tracking system and software (EthoVision XT, v.14, Noldus Information Technology) was used to record the behavior of the animals throughout the testing session. The percentage time spent in the center was measured.

Rotarod. The rotarod was carried out as previously described[31]. Mice were placed on a rotarod apparatus (Ugo Basile, cat. no. 7650), accelerating from 4 rpm to 60 rpm in 300 s. Each animal was given three trials and the times when the animal would no longer be able to hold on were recorded and averaged for analysis of motor function.

Morris water maze. The MWM was used to measure spatial learning and memory by training mice to use spatial cues to find a hidden platform to escape water[113]. The MWM apparatus is a circular pool with a diameter of 130 cm and depth of 50 cm. During the first day, the platform was visible and the animals were given three trials to find it. During the 4-d training period, mice received three trials per day learning how to find the hidden platform. Then 24 h after the last training day, a probe trial was performed in which the platform was removed and mice were allowed to swim for up to 60 s. The amount of time spent by the animal to find the platform and the time spent in the target quadrant for the probe trial were calculated using Noldus EthoVision XT tracking software.

Y-maze. The Y-maze was used to assess spatial working memory in mice. The test was conducted as previously described[114]. In short, the mice were placed in the center of the maze and given 5 min to explore all three arms, the number of triads (triplets of consecutive arm entries of ABC, BCA and CAB) were counted to the percentage alternation. The ratio of correct choice was determined by the equation: Percentage alternations = ((No. of alternations)/(Total arm entries − 2)) × 100 (ref. 115).

BBB permeability 70-kDa FITC-dextran

A 70-kDa FITC-dextran (Sigma-Aldrich, cat. no. 46945) was used to measure BBB permeability as described in previous studies[116,117], with modifications: 0.2 mg of 70-kDa FITC-dextran per g of body weight was injected retro-orbitally[118,119]. Then, 10 min post-70-kDa FITC-dextran administration, the mouse was euthanized with a lethal dose of xylazine and ketamine cocktail (450 mg kg^{-1} and 45 mg kg^{-1}) i.p. with a 29-gauge insulin pen. The mouse was transcardially perfused with 50 ml of PBS. The whole brain was removed and stored at −80 °C (ref. 120). Cryoprotected and flash-frozen brains were coronally sectioned (16-µm-thick serial sections, 300 µm apart)[116]. The brain sections were captured by a Leica DMi8 wide-field microscope. FITC-dextran visualization was done under a 488-nm excitation wavelength laser. For each mouse, we obtained five to six continued section slices from the brain tissue's front, middle and posterior sections. An investigator blind to the experimental design manually measured the *I* mean gray value of the dextran tracer-positive area found in the brain parenchyma using ImageJ.

Brain edema

Brains were removed at 72 h after CCI, bisected into left and right hemispheres and each hemisphere was weighed (wet weight). Brains were then dried at 60 °C for 48 h and dry weights were obtained. The percentage of brain water content was expressed as ((wet − dry weight)/(wet weight)) × 100% as previously described[121].

Magnetic resonance imaging

Imaging was done using a 7.0T Bruker BioSpect USR. In brief, mice were gently handled and placed in an isoflurane anesthesia chamber. Then the mice were placed inside the imaging apparatus with their nose in front of tubes releasing 2% isoflurane. Electrocardiogram (ECG) leads were placed on the animal's paws and a pneumatic pillow sensor placed under the abdomen for continuous ECG and respiratory rate monitoring of the anesthetized animal. These waveforms were closely monitored throughout magnetic resonance imaging (MRI) by the MRI operator. The animal was placed on an MRI-compatible bed, which was placed inside the magnet for imaging. The imaging sessions lasted between 15 min and 60 min. Mice were then returned to their cages and monitored continuously after being returned to their cages before returning to a fully alert status. The following parameters were obtained to generate the T2 sequence images: slice thickness: 0.5 mm; repetition time: 3,000 ms; echo time: 50 ms; no. of averages: 3; spacing between slices: 0.5 mm; echo train length: 8; acquisition matrix: 200 × 200; flip angle: 90°; and field of view: 20 mm. Serial Images were viewed and analyzed using the three-dimensional (3D) Slicer platform[122].

Immunohistochemistry

Animals were anesthetized with CO_2 until the respiration rate slowed and perfused transcardially with Hanks' balanced salt solution (HBSS). Brains were post-fixed in 4% paraformaldehyde for 48 h, then transferred to a 15% sucrose solution for 24 h and finally transferred to a 30% sucrose solution for 24 h. Brains were then flash frozen in Tissue-Tek Oct (Sakura, compound 4583) and stored at −80 °C until the time of sectioning. Brains were subsequently sectioned at −20 °C using a cryostat at the bregma position for each targeted brain. Sections were cut at 0.2 mm in a fourfold series interval. Five total sections were placed on Colorfrost Plus-treated adhesion slides (Thermo Fisher Scientific) and stored at −20 °C until the time of staining. Whole meninges were processed as previously described[123]. For immunofluorescence, sections were blocked in in a 10% normal horse serum solution, containing 0.1% Triton X-100, 1% glycine and 2% bovine serum albumin (BSA). Slides were incubated overnight at 4 °C with anti-Iba-1 (rabbit, 1:1,000, Wako). The following day sections were washed and incubated with an Alexa Fluor-647 goat anti-rabbit IgG (1:1,000, Abcam, cat. no. ab150075) for 1 h at room temperature. Sections were also stained with H&E (Abcam, cat. no. ab245880) and TUNEL (TUNEL Assay Kit, BrdU-Red, Abcam, cat. no. ab66110) according to their corresponding kit protocols. Iba-1- and TUNEL-stained slides were co-stained with DAPI mounting medium (Vector Laboratories, cat. no. UX-93952-24). FoxP3 GFP mice were used to visualize FoxP3 T_{reg} cells in the meninges and brain using the Cy2 channel of the microscope and CD3 was stained using Alexa Fluor-647 anti-mouse CD3 (BioLegend, cat. no. 17A2, 1:50). Images were taken using a Leica DMi8 wide-field microscope on the ×20 objective or the Zeiss LSM710 confocal microscope.

Image analysis

Analysis of the percentage Iba-1 and number of TUNEL-positive cells per surface area was performed on five photomicrographs per animal ($n = 4$ or 5). The sections analyzed were taken between 300 µm and 1,500 µm laterally from the coronal plane. Each scanned photomicrograph was used to produce images of the area of contusion. All the images were analyzed using ImageJ software (National Institutes of Health: https://imagej.nih.gov/ij). Images were split by color channel, the channel of interest was threshold using the Yen setting and the number of positive cells were quantified as previously described[124].

Serum biomarkers

Levels of cytokines in the serum of mice were measured with the V-PLEX Plus Proinflammatory Panel1 Mouse Kit (Meso Scale Discovery, cat. no. K15048G-1). All sample controls were diluted 1:2 and run as duplicates according to the manufacturer's protocol, as previously described[125].

Quanterix single-molecule array analysis

Levels of ubiquitin carboxy-terminal hydrolase L1 (UCH-L1) and GFAP were quantified in the serum using single-molecule array technology (SiMoA, Quanterix). The SiMoA Neurology 4-Plex B kit was run according to the manufacturer's directions. Briefly, samples were thawed, vortexed and centrifuged at 10,000*g* for 5 min. All samples were run at a 4× dilution, along with eight calibrators run neat and two controls also run at a 4× dilution. The data were validated using a calibration curve with $R^2 > 0.99$. For both UCHL-1 and GFAP, the dynamic range was 0–40,000 pg ml^{-1}, with a lower limit of quantification of 9.38 pg ml^{-1}.

Flow cytometry microglial sorting

For microglial cell sorting, mice were anesthetized with CO_2 until their respiration rate slowed and then transcardially perfused with 50 ml of HBSS containing heparin (1:1,000). After perfusion, the ipsilateral hemisphere was homogenized using a Dounce glass tissue homogenizer. Cells were separated through a Percoll (GE Healthcare Life Sciences) 30% gradient centrifugation. Cells were isolated from the Percoll layer and stained on ice for 30 min with combinations of phycoerythrin (PE)/cyanine7 anti-mouse CD11b (BioLegend, cat. no. M1/70, 1:100), allophycocyanin (APC)/cyanine7 anti-mouse CD45 (BioLegend, cat. no. 30-F11, 1:100), FITC anti-mouse Ly6C (BD Bioscience, cat. no. AL-21, 1:200) and APC anti-mouse 4D4 (ref. 51) (marking resident microglia; 1:1,000) in blocking buffer containing 0.2% BSA (Sigma-Aldrich) in HBSS. Cell sorting was performed using a FACSAriaIII cell sorter (Becton Dickson). Microglial cells were identified as $CD45^{+}CD11b^{+}Ly6C^{-}4D4^{+}$ and dead cells were also excluded based on 7-aminoactinomycin D (7-AAD; BD Bioscience) staining. Cells were sorted directly in 1.5-ml Eppendorf tubes and stored at −80 °C. Phagocytic positive microglia were sorted as $4D4^{+}$ Alexa-405^{+}.

Flow cytometry intracellular staining

Intracellular cytokine staining and cell isolation were done as previously described[126]. The meninges were carefully removed from the skull and the ipsilateral brain was further isolated. The enzyme dissociation mix used for the ipsilateral brain hemisphere and meninges was collagenase P (0.5 mg ml^{-1}; Sigma-Aldrich, cat. no. 11213865001) and DNase-1 (250 U ml^{-1}, Worthington, cat. no. LK003172) diluted in Roswell Park Memorial Institute (RPMI)-1640 with 10 mM Hepes. The samples were then finely minced and incubated in a room temperature shaker for 1 h. After enzyme dissociation, the cells were separated using Percoll (GE Healthcare Life Sciences) as described above. Cells isolated from the brain and meninges were incubated for only 2 h instead of the 4 h for cLN cells. Acquisition was performed on a Symphony (BD Biosciences) using DIVA software (BD Biosciences) and the data were analyzed with FlowJo software v.9.9 or v.10.1 (TreeStar Inc.). Intracellular staining antibodies used Zombie Aqua Fixable Viability Kit (BioLegend, cat. no. 423102, 1:1,000) or Zombie UV (BioLegend, cat. no. 423108, 1:1,000) was used to exclude dead cells. The staining antibodies used PE/cyanine7 anti-mouse CD11b (BioLegend, cat. no. M1/70, 1:300), APC/cyanine7 anti-mouse TCR-β (BioLegend, cat. no. H57-597, 1:100), BUV661 anti-mouse CD45 (30-F11, BD Biosciences, 1:200), PE anti-mouse CD4 (BioLegend, cat. no. GK1.5, 1:100), BUV805 anti-mouse CD8 (BD Biosciences, cat. no. 53-6.7, 1:100), FITC anti-mouse FoxP3 (eBioscience, cat. no. FJK-16s, 1:100), BV421 anti-mouse LAP (BioLegend, cat. no. TW7-16B4, 1:100), PE/Dazzle 594 anti-mouse IL-10 (BioLegend, cat. no. JES5-16E3, 1:100), BUV395 anti-mouse IL-17a (BD Biosciences, cat. no. TC11-18H10, 1:100), BV785 anti-mouse IFNγ (BioLegend, cat. no. XMG1.2, 1:100), BV605 anti-mouse Ly6G (BioLegend, cat. no. 1A8, 1:300), BV711 anti-mouse NK-1.1 (BioLegend, cat. no. PK136, 1:100), AF700 anti-mouse Ly6C (BioLegend, cat. no. HK1.4, 1:200), BV711 anti-mouse Ly6C (BioLegend, cat. no. HK1.4, 1:200) and APC anti-mouse 4D4 (ref. 47) (1:1,000) provided by Butovsky.

Flow cytometry FoxP3(GFP) T_{reg} cell sorting from the brain and blood

The ipsilateral brain hemisphere was processed with the same enzyme dissociation kit described above and then processed as the microglial cell sorting above. The sample was purified and enriched using CD4 cell isolation microbead kit (Miltenyi Biotech, cat. no. 130-104-454) on a magnetic MACS separator before sorting. Cell sorting was performed using FACSAriaIII cell sorter (Becton Dickson). APC/cyanine7 anti-mouse CD45 (BioLegend, cat. no. 30-F11, 1:100), APC anti-mouse CD4 antibody (BioLegend, cat. no. GK1.5, 1:100) and 7-AAD (BD Bioscience) was used to identify the live $CD4^{+}$ population and the FITC channel was used to identify the $FoxP3^{+}$ population. Each RNA-seq sample is a pool of 5 ipsilateral hemispheres and 20 sham brain hemispheres. The blood samples were collected in heparin-coated tubes and then transferred to 15-ml tubes where ACK lysis buffer was used to lyse the erythrocytes. The sample was then strained through a 70-µm filter and stained as decribed above. Each RNA-seq sample is a pool of five mice.

Quantitative PCR

RNA was extracted with RNeasy columns (QIAGEN), complementary DNA was prepared and used for qPCR (Applied Biosystems, cat. no. 437466) and the results were normalized to *Gapdh* (Mm99999915_g1). Applied Biosystems supplied: *Il10* (cat. no. Mm01288386_m1), *Il6* (cat. no. Mm00446190_m1), *Tnf* (cat. no. Mm00443258_m1), *Il1b* (cat. no. Mm00434228_m1), *Il2* (cat. no. Mm00434256_m1), *Il18* (cat. no. Mm00434226_m1), *Ifng* (cat. no. Mm01168134_m1), *Bdnf* (cat. no. Mm04230607_s1), *Gdnf* (cat. no. Mm00599849_m1), *Ccl5* (cat. no. Mm01302427_m1), *Cd14* (cat. no. Mm01158466_g1), *Mrc1 (Cd206)* (cat. no. Mn01329359_m1), *Tgfb1* (cat. no. Mm01178820_m1), *Il17a* (cat. no. Mn00439618_m1), *Cd86* (cat. no. Mm00444540_m1), *Clec7a* (cat. no. Mm01183349_m1), *Tlr2* (cat. no. Mm00442346_m1), *Cd33* (cat. no. Mm00491152_m1), *Cx3cr1* (cat. no. Mm00438354_m1) and *Il10ra* (cat. no. Mm00434151_m1). The $2^{-\Delta\Delta Ct}$ method was used to calculate the relative expression of each gene.

Isolation of primary neurons

Primary neuron isolation was carried out as previously described[51]. In short, primary neurons were prepared from embryos at age E18. Cell density was determined using a hemocytometer and cells were seeded. Dulbecco's modified Eagle's medium (DMEM) with 10% fetal bovine serum (FBS) was used for initial plating and the medium was changed to neurobasal supplemented with 1× B27 (Invitrogen) 3 h later. The medium was changed every 3 d.

Induction of apoptosis and labeling of neurons

Apoptosis and labeling of neurons were done as previously described[51]. Neurons were irradiated with ultraviolet light (302 nm) with an intensity of 6 × 15 W for 15 min. The apoptotic neurons were labeled with labeling dye (Alexa-405 NHS Ester, Life Technologies/Thermo Fisher Scientific). Neurons were resuspended at a density of 500,000 cells per 4 µl for stereotactic injections.

Stereotactic injections

Mice were anesthetized by intraperitoneal injection of ketamine (100 mg kg^{-1}). Apoptotic neurons or sterile Dulbecco's PBS (DPBS) were injected into the lesion of TBI mice at two depths of 1.5 mm and 2 mm. Then, 2 µl was injected at each depth using stereotaxic equipment (Harvard Apparatus). After recovery from surgery, animals were returned to their cages. Post-surgery (4 or 16 h), mice were euthanized by CO$_2$ inhalation and brains were processed for flow cytometry analysis of phagocytic microglia.

Adoptive transfer

Splenocytes and cLNs from FoxP3-GFP or 10BiT.FoxP3^{GFP} mice were purified and enriched using CD4 cell isolation microbead kit (Miltenyi Biotech, cat. no. 130-104-454) on a magnetic MACS separator before sorting. Cell sorting was performed using FACSAriaIII cell sorter (Becton Dickson). PE anti-mouse CD3 (BioLegend, cat. no. 17A2, 1:100), APC anti-mouse CD4 (BioLegend, cat. no. GK1.5, 1:100) and 7-AAD were used to identify the live CD4$^+$ population and the FITC channel was used to identify the FoxP3$^+$ population. For the 10BiT.FoxP3^{GFP}, PE anti-mouse Thy1.1 (BioLegend, cat. no. S20007C, 1:1,500) was used to identify the FoxP3$^+$Thy1.1$^+$ IL-10-producing FoxP3 T$_{reg}$ cells. All cells were injected i.p. at 2.5 million for total CD4, 1 million for CD4$^+$FoxP3$^+$ and 1 million for FoxP3$^+$Thy1.1$^+$ or FoxP3$^-$Thy1.1$^-$ populations.

In vitro cell culture

Sorted 4D4$^+$ microglia 24 h post-TBI were cultured as previously described[127] at 200,000 cells in a 24-well plate (Kemtec, cat. no. 4422A). The microglial culture medium was composed of 10% FBS (Gibco, cat. no. 10438026), 100 U ml^{-1} of penicillin–streptomycin mixture (Lonza, cat. no. DE17-602E), supplemented in DMEM/F-12 Glutamax medium (Gibco, cat. no. 10565018). FoxP3-GFP was treated with nasal aCD3 or the isotype control for 7 d and the splenic/cLN CD4$^+$FoxP3$^+$ and CD4$^+$FoxP3(GFP)$^-$ population, specifically from aCD3-treated animals, was placed in a lymphocyte culture medium composed of 10% FBS, 100 U ml^{-1} of penicillin–streptomycin mixture, 55 µM 2-mercaptoethanol (Gibco, cat. no. 21985023), 1% sodium pyruvate (Lonza, cat. no. BE13-115E) and 1% Hepes (Lonza, cat. no. BE17-737E), supplemented in RPMI-1640 medium (Gibco, cat. no. 11875119) and then placed on the top of the hanging cell culture 0.4-µm insert (Millicell, cat. no. PTHT24H48) at 600,000 cells per insert on top of the cultured microglia, and the assay was left for 72 h in a CO$_2$ Cell culture Incubator (InCusafe). There was a fourth group where IL-10-neutralizing antibody (BioXCell, cat. no. JES5-2A5) at a concentration of 50 µg ml^{-1} was added with the CD4$^+$FoxP3$^+$ which was cell sorted from nasal aCD3-treated mice After 72 h the microglia were lysed with buffer RLT and RNA was extracted with RNeasy columns (QIAGEN).

Bulk RNA-seq and analysis

Bulk RNA-seq was performed as previously described[59]. Briefly, 2,000 isolated microglia CD45$^+$CD11b$^+$Ly6C$^-$4D4$^+$ were lysed in 5 µl of TCL buffer + 1% 2-mercaptoethanol. Between 800 and 1,000 isolated CD4$^+$FoxP3(GFP$^+$) cells from the brain and blood were processed. Smart-Seq2 libraries were prepared and sequenced using the Broad Genomic Platform. The cDNA libraries were generated from sorted cells using the Smart-seq2 protocol5. RNA-seq was performed using Illumina NextSeq500 with a High Output v.2 kit to generate reads of 2× 38 bp. Sequencing data were demultiplexed and provided by the Broad Institute in FASTQ format. The processing of the bulk RNA-seq data (transcript assembly and quantification) was based on an established computational pipeline (HISAT, Stringtie and Ballgown)[128] and sequencing quality was assessed using FastQC. Reads were aligned to the 'mm10' reference genome. Transcript abundances were then imported into R (v.4.1.2) and converted to gene-level estimated counts using the 'tximport' package (v.1.22.0) from Bioconductor. Low abundance genes that achieved <10 counts aggregated across all samples were filtered out. Raw read counts were then normalized using DESeq2 (v.1.34.0). Differential gene expression was performed using DESeq2 with a significance cutoff of false discovery rate (FDR)-adjusted $P < 0.05$. Analyses that did not pass the FDR-correction cutoff were denoted with $P < 0.05$. Pairwise group comparisons were conducted using Wald's test with standard parameters, then log$_2$(fold-changes) were shrunk using the lfcShrink function in DESeq2. Gene expression comparisons of three or more groups were conducted using a likelihood ratio test (LRT). Heatmaps were created using ComplexHeatmap (v.2.10.1) or pheatmap (v.1.0.12) and clusters were identified via hierarchal clustering. Identified clusters were functionally annotated with Gene Ontology Biological Process (GOBP) gene-set terms using the enrichGO function of the clusterProfilerpackage (v.4.2.2), where GOBP terms with q-values < 0.05 were considered significantly enriched.

Pathway analysis

GSEA was performed using the clusterProfiler package and the resulting enriched terms with q-values < 0.05 were visualized through dot plots and bar plots, which were generated using the ggplot2 and ggpubr (v.0.6.0) packages. For IPA (https://digitalinsights.qiagen.com/products-overview/discovery-insights-portfolio/analysis-and-visualization/qiagen-ipa), DEGs from pairwise comparisons with corresponding log$_2$(fold-changes) and FDR-adjusted P values were used as input. Biological networks were generated in IPA based on canonical pathways and biological functions, as outlined in our group's previous work[59].

Statistical and reproducibility

Statistical analysis was performed using GraphPad Prism v.9 software. Data are presented as mean ± s.e.m and two-sided Student's t-tests (unpaired), two-factor, repeated-measure, two-way analysis of variance (ANOVA) (group × time) or one-way ANOVA, followed by Tukey's multiple-comparison analysis was used to assess statistical significance between the groups. All *n* and *P* values and statistical tests are indicated in the figure legends. No statistical methods were used to predetermine sample sizes, but our sample sizes are similar to those reported in previous publications[15,23]. Data distribution was assumed to be normal, but this was not formally tested. Data for each experiment were collected and processed randomly and animals were assigned randomly to various experimental groups as well. The investigators were blinded to allocation during experiments and outcome assessment. No animals or data points were excluded from the analyses. Each experiment was repeated 2–3 times.

Reporting summary

Further information on research design is available in the Nature Portfolio Reporting Summary linked to this article.

Data availability

The Smartseq2 RNA-seq data that support the findings of the present study have been deposited into Gene Expression Omnibus under SuperSeries, accession no. GSE276761. The datasets included in the present study are available as Supplementary Data.

Code availability

The present study did not develop any new code. All software and packages employed are publicly accessible and fully documented in Methods.

References

110. Kaiser, T. & Feng, G. Tmem119-EGFP and Tmem119-CreERT2 transgenic mice for labeling and manipulating microglia. *eNeuro* https://doi.org/10.1523/ENEURO.0448-18.2019 (2019).
111. Bermpohl, D., You, Z., Lo, E. H., Kim, H. H. & Whalen, M. J. TNF alpha and Fas mediate tissue damage and functional outcome after traumatic brain injury in mice. *J. Cereb. Blood Flow Metab.* **27**, 1806–1818 (2007).
112. Kraeuter, A. K., Guest, P. C. & Sarnyai, Z. The open field test for measuring locomotor activity and anxiety-like behavior. *Methods Mol. Biol.* **1916**, 99–103 (2019).
113. Vorhees, C. V. & Williams, M. T. Morris water maze: procedures for assessing spatial and related forms of learning and memory. *Nat. Protoc.* **1**, 848–858 (2006).
114. Wu, L. et al. Repetitive head injury in adolescent mice: a role for vascular inflammation. *J. Cereb. Blood Flow Metab.* **39**, 2196–2209 (2019).
115. Jarvis, B. B. et al. New macrocyclic trichothecenes from *Baccharis megapotamica*. *J. Nat. Prod.* **50**, 815–828 (1987).
116. Natarajan, R., Northrop, N. & Yamamoto, B. Fluorescein isothiocyanate (FITC)-Dextran extravasation as a measure of blood-brain barrier permeability. *Curr. Protoc. Neurosci.* **79**, 9.58.1–59.58.15 (2017).
117. Ben-Zvi, A. et al. Mfsd2a is critical for the formation and function of the blood-brain barrier. *Nature* **509**, 507–511 (2014).
118. Li, J. et al. Retro-orbital injection of FITC-dextran combined with isolectin B4 in assessing the retinal neovascularization defect. *BMC Ophthalmol.* **21**, 208 (2021).
119. Li, S. et al. Retro-orbital injection of FITC-dextran is an effective and economical method for observing mouse retinal vessels. *Mol. Vis.* **17**, 3566–3573 (2011).
120. Yang, S. et al. Anesthesia and surgery impair blood-brain barrier and cognitive function in mice. *Front. Immunol.* **8**, 902 (2017).
121. Wu, L. et al. Genetic inhibition of RIPK3 ameliorates functional outcome in controlled cortical impact independent of necroptosis. *Cell Death Dis.* **12**, 1064 (2021).
122. Fedorov, A. et al. 3D slicer as an image computing platform for the quantitative imaging network. *Magn. Reson. Imaging* **30**, 1323–1341 (2012).
123. Louveau, A., Filiano, A. J. & Kipnis, J. Meningeal whole mount preparation and characterization of neural cells by flow cytometry. *Curr. Protoc. Immunol.* **121**, e50 (2018).
124. Izzy, S. et al. Repetitive traumatic brain injury causes neuroinflammation before tau pathology in adolescent P301S mice. *Int. J. Mol. Sci.* **22**, 907 (2021).
125. Mallory, K. L. et al. Messenger RNA expressing PfCSP induces functional, protective immune responses against malaria in mice. *NPJ Vaccines* **6**, 84 (2021).
126. Rezende, R. M. et al. gammadelta T cells control humoral immune response by inducing T follicular helper cell differentiation. *Nat. Commun.* **9**, 3151 (2018).
127. Xie, L., Choudhury, G. R., Winters, A., Yang, S. H. & Jin, K. Cerebral regulatory T cells restrain microglia/macrophage-mediated inflammatory responses via IL-10. *Eur. J. Immunol.* **45**, 180–191 (2015).
128. Pertea, M., Kim, D., Pertea, G. M., Leek, J. T. & Salzberg, S. L. Transcript-level expression analysis of RNA-seq experiments with HISAT, StringTie and Ballgown. *Nat. Protoc.* **11**, 1650–1667 (2016).

Acknowledgements

S.I. reports grants from the National Institute of Neurological Disorders and Stroke (grant no. 5K08NS123503-03), Department of Defense (grant no. HT9425-24-1-0635), a 2021 Neurocritical Care Society research grant and 2023 Stepping Strong Innovator Awards. S.I. and H.W. report a grant from the Department of Defense Multidisciplinary University Research Initiatives Program (grant no. W911NF-23-1-0276). We thank the NeuroTechnology Studio at Brigham and Women's Hospital for providing instrument (Leica DMi8 Widefield Fluorescence Microscope and Zeiss LSM710 Confocal) access and consultation on data acquisition and data analysis. A Brigham Research Institute Pilot imaging microgrant was received.

Author contributions

S.I. designed and performed experiments and wrote the manuscript. T.Y. designed and performed experiments. R.M.R. and T.G.M. designed and supervised experiments and wrote the manuscript. M.A., H.A.E.-H., T.C., M.G.D.O., K.-J.L., M.L.B., L.C.B., D.L., W.N.B., A.C.D., T.L., F.M., J.-H.L., G.P.D.N., J.D.B., M.K. and K.C. performed experiments. R.K. sorted cells for RNA-seq experiments. O.A., P.D.S. and O.B. analyzed RNA-seq data. R.M., F.J.Q. and O.B. supervised the project. H.L.W. supervised the project and wrote the manuscript. All authors edited or commented on the manuscript. The author(s) read and approved the final manuscript.

Competing interests

H.L.W. is on the scientific advisory board of Tiziana Life Sciences.

Additional information

Extended data is available for this paper at https://doi.org/10.1038/s41593-025-01877-7.

Supplementary information The online version contains supplementary material available at https://doi.org/10.1038/s41593-025-01877-7.

Correspondence and requests for materials should be addressed to Howard L. Weiner.

Peer review information *Nature Neuroscience* thanks John Lukens, Edward Needham and Michal Schwartz for their contribution to the peer review of this work.

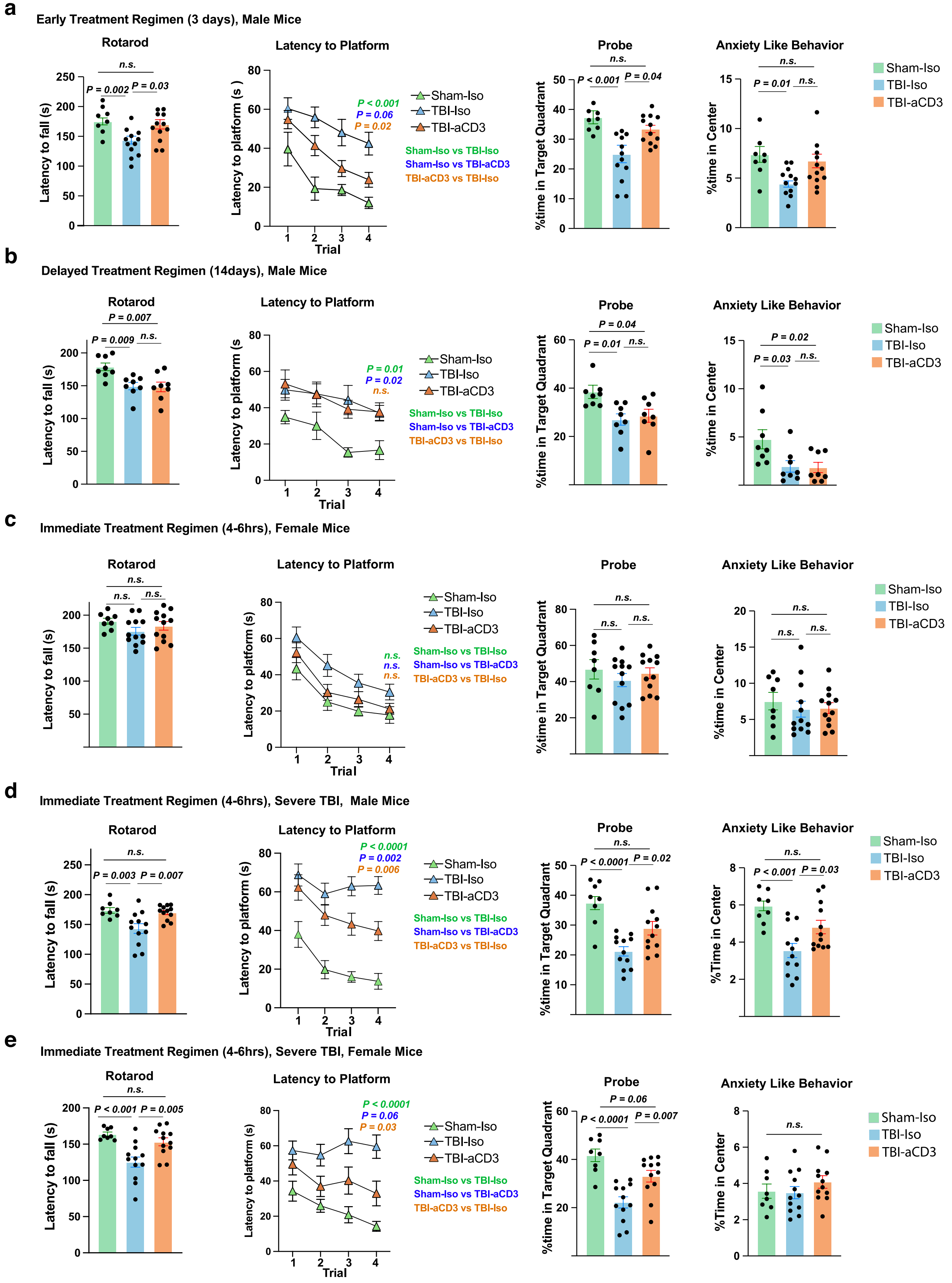

Extended Data Fig. 1 | See next page for caption.

Extended Data Fig. 1 | Nasal anti-CD3 improves behavioral outcomes at different treatment regimens and TBI severities. (a) Behavioral testing in the early treatment regimen for males of rotarod, Morris water maze, probe trial, and anxiety like behavior that is measured by the open field was assessed between (Sham-Iso *n* = 8, TBI-Iso *n* = 12, and TBI-aCD3 *n* = 12) groups in the early and **(b)** delayed treatment regimen for males and **(c)** immediate for females. Morris water maze analyzed by two-factor repeated measures two-way ANOVA (group x time); others by one-way ANOVA with Tukey's multiple comparisons. Data shown as mean ± SEM. **(d)** Behavioral testing in the immediate treatment regimen for males in severe TBI (Depth: 1.5 mm, Diameter: 3.0 mm of the impact tip) of rotarod, Morris water maze, probe trial, and anxiety like behavior that is measured by the open field was assessed between (Sham-Iso *n* = 8, TBI-Iso *n* = 12, and TBI-aCD3 *n* = 12) groups in males and **(e)** females. Morris water maze analyzed by two-factor repeated measures two-way ANOVA (group x time); others by one-way ANOVA with Tukey's multiple comparisons. Data shown as mean ± SEM. All data are biological replicates and are representative from two independent experiments. *n.s.* = non-significant.

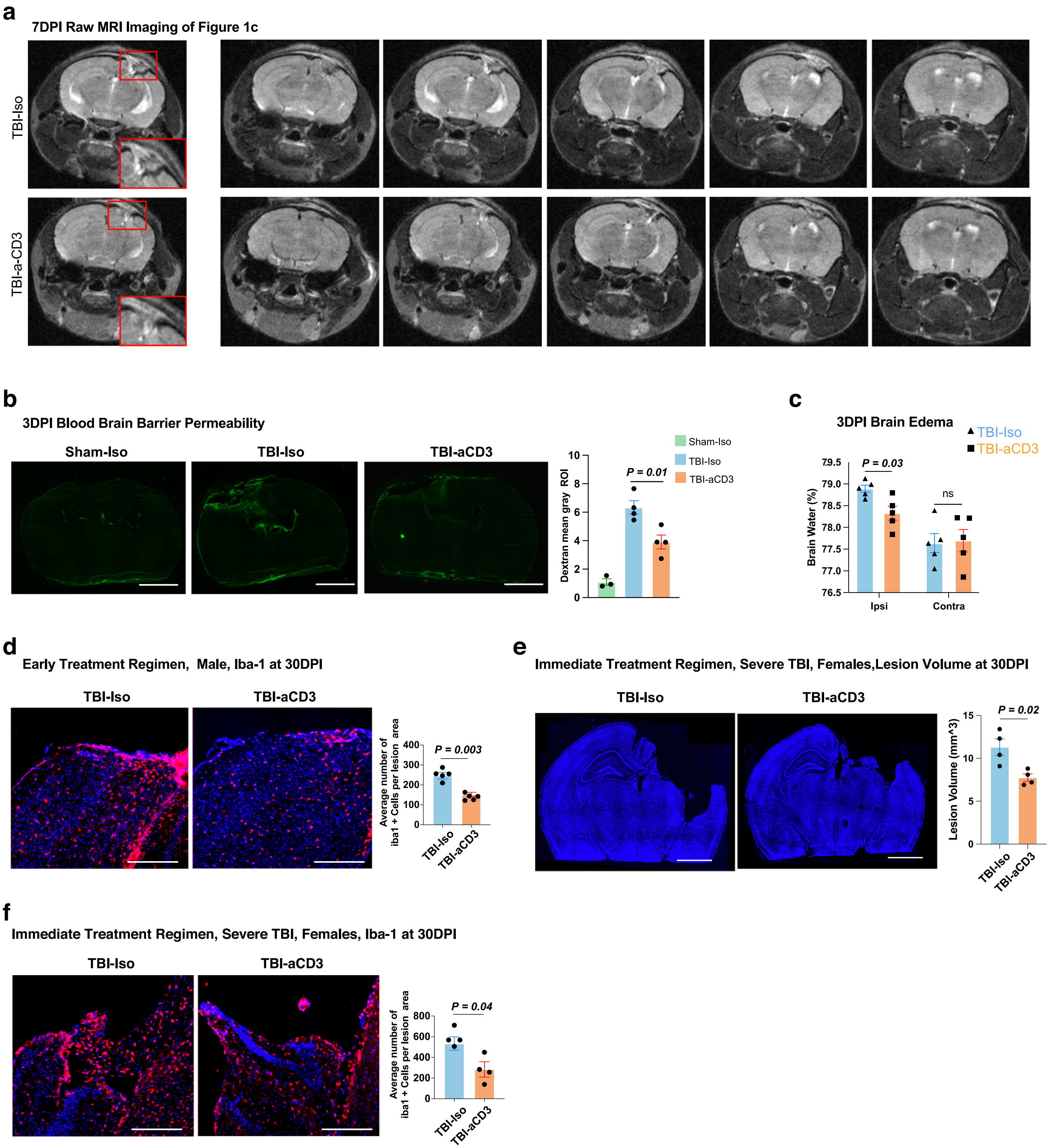

Extended Data Fig. 2 | See next page for caption.

Extended Data Fig. 2 | Nasal anti-CD3 ameliorates pathological outcomes at different treatment regimens and TBI severities. (a) Unedited 3-Tesla serial images Magnetic resonance imaging (MRI) taken 7 days post-TBI of (Fig. 1c). **(b)** Dextran 70-kDa (Green) for measurement of blood-brain barrier permeability between the groups (3days post-TBI). Scale bars are 1000 um. Data is shown as mean ± SEM, (Sham-Iso *n* = 3, TBI-Iso *n* = 4, and TBI-aCD3 *n* = 4) and analyzed by one-way ANOVA with Tukey's multiple comparisons. **(c)** Brain edema was analyzed on day 3 post-TBI and % water content was measured between the ipsilateral and contralateral hemispheres. Data shown as mean ± SEM and *n* = 3-4 mice/group were used. Data was analyzed by two-sided unpaired Student's t-test. **(d)** Immunofluorescence staining of Iba-1 30-days post-TBI for early treatment in males at the peri-contusional cortex for DAPI (blue) and Iba-1 (red). Scale bars are 250 um. Five sections of each sample were prepared and the area around the contusion was captured and the number of Iba-1 positive cells around the contusion were quantified by Image J. Data shown as mean ± SEM and *n* = 5 mice/group were used. Data was analyzed by two-sided unpaired Student's t-test. **(e)** Brain sections were stained with DAPI (blue) at 30 days post severe TBI in females and lesion volume was measured by image J software. Data shown as mean ± SEM and *n* = 4 mice/group were used. Data was analyzed by two-sided unpaired Student's t-test. Scale bars are 1000 um. **(f)** Immunofluorescence staining of Iba-1 30 days post severe TBI in females in the at the peri-contusional cortex for DAPI (blue) and Iba-1 (red). Scale bars are 250 um. Five sections of each sample were prepared and the area around the contusion was captured and the number of Iba-1 positive cells around the contusion were quantified by Image J. Data shown as mean ± SEM and *n* = 4 mice/group were used. Data was analyzed by two-sided unpaired Student's t-test. All data are biological replicates and are representative from two independent experiments. *n.s.* = non-significant. DPI indicates Days Post Injury.

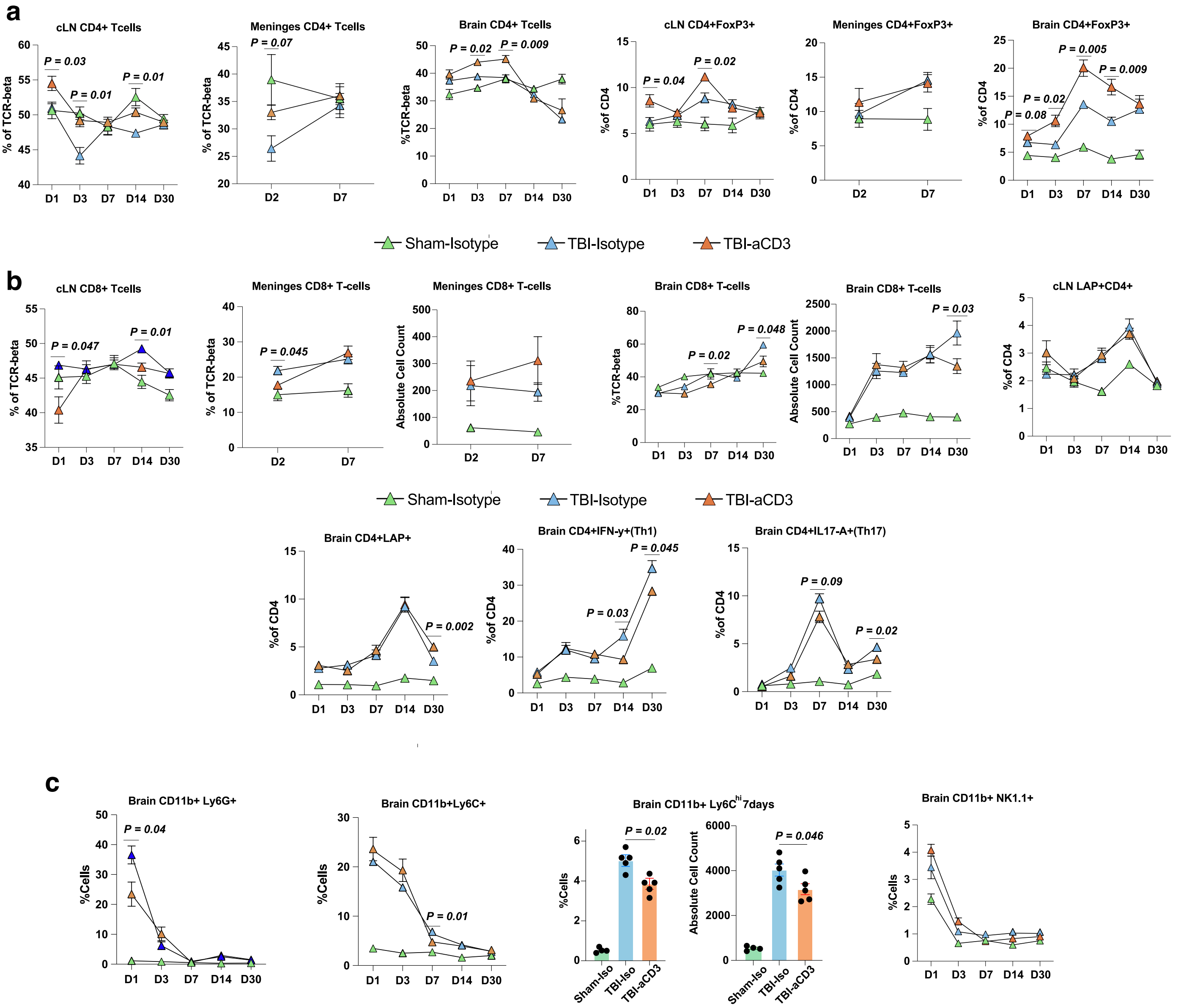

Extended Data Fig. 3 | Nasal anti-CD3 ameliorates adaptive immune response following TBI. **(a)** Flow cytometry analysis and quantification of CD4 + T cells, CD4+FoxP3 + and **(b)** CD8 + T cells, CD4 + LAP + , Th1, and Th17 at 1,3,7,14, and 30 days post TBI and nasal anti-CD3 treatment in the cervical lymph nodes, meninges, and Ipsilateral brain hemisphere. (Sham-Iso *n* = 4, TBI-Iso *n* = 6, TBI-aCD3 *n* = 6). Data shown as mean ± SEM and analyzed by one-way ANOVA with Tukey's multiple comparisons for every individual timepoint **(c)** Flow cytometry analysis and quantification of neutrophils, monocytes, classical monocytes (7 days post-TBI), and NK cells at 1,3,7,14, and 30 days post TBI and nasal anti-CD3 treatment in Ipsilateral brain hemisphere. (Sham-Iso *n* = 4, TBI-Iso *n* = 6, TBI-aCD3 *n* = 6). Data shown as mean ± SEM and analyzed by one-way ANOVA with Tukey's multiple comparisons for every individual timepoint. All data are biological replicates and are representative from two independent experiments.

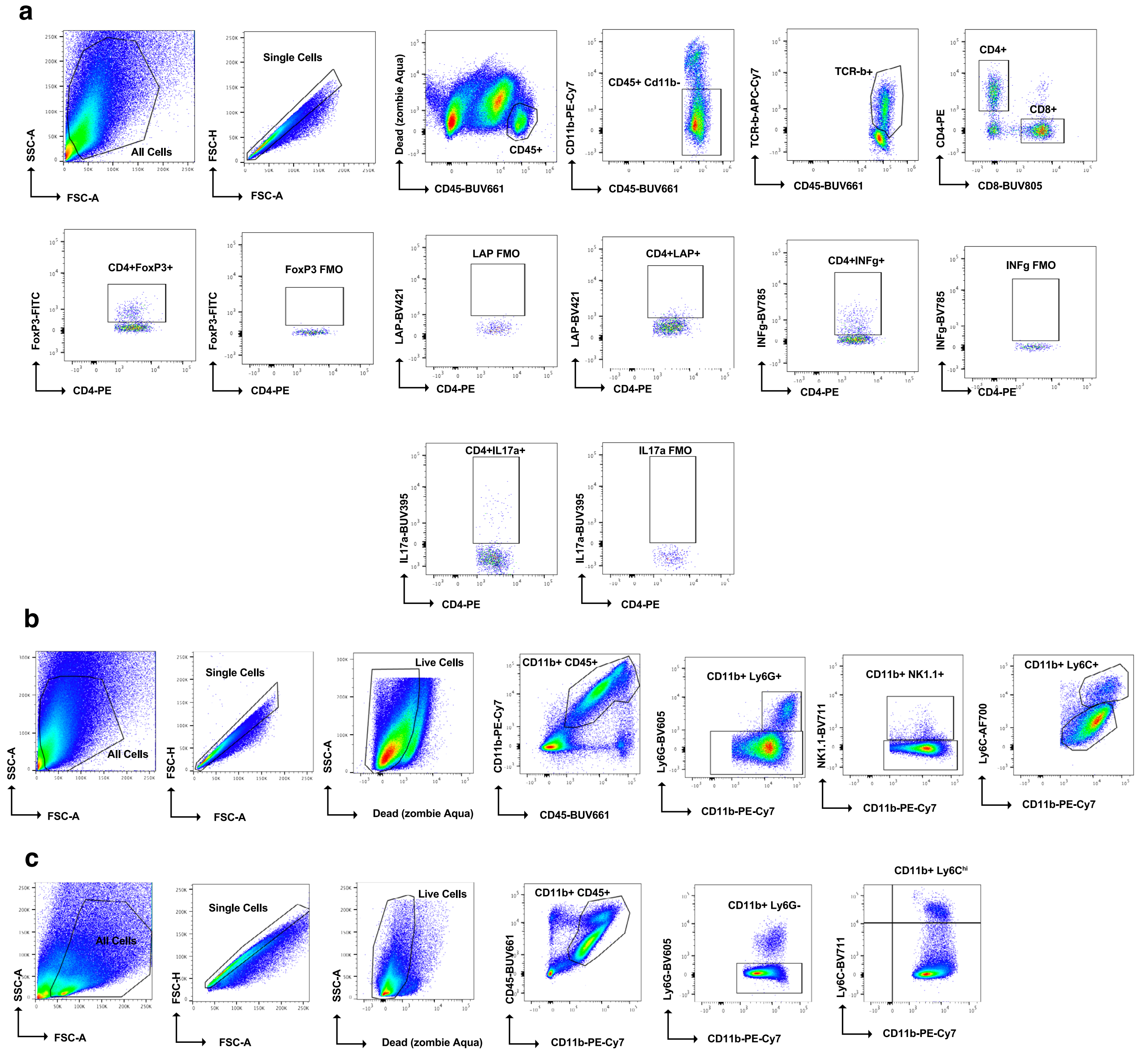

Extended Data Fig. 4 | Gating strategy of different immune cells in TBI. **(a)** Gating strategy used to identify the different T-cell substypes. **(b)** Gating strategies used to identify different CD11b+ infiltrating cells and (**c**) CD11b+Ly6Chi monocytes.

https://doi.org/10.1038/s41593-025-01877-7

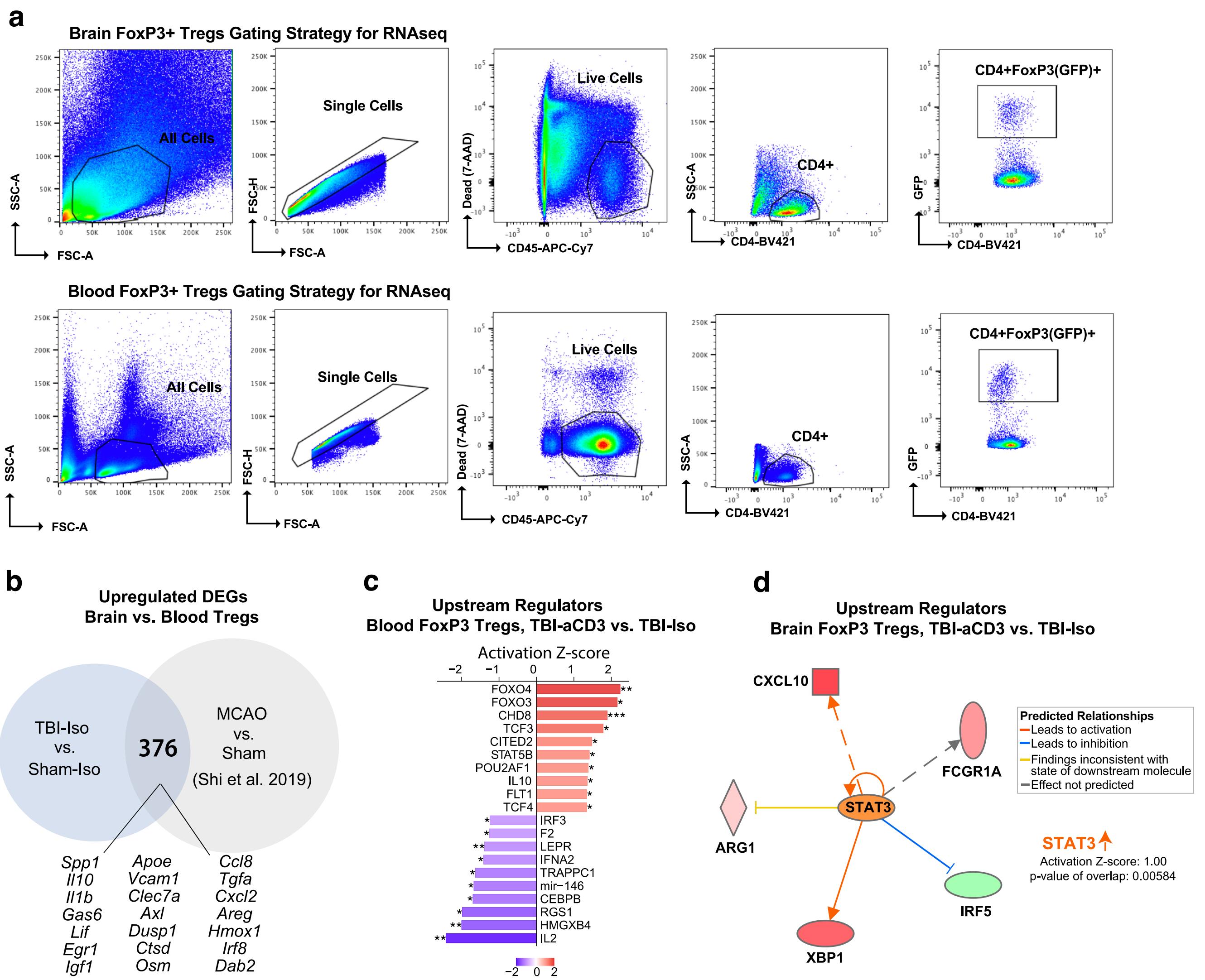

Extended Data Fig. 5 | Nasal anti-CD3 induces a unique immune modulatory signature in FoxP3 Tregs. **(a)** Gating strategy used to identify and sort $CD4^+FoxP3(GFP)^+$ from the ipsilateral hemisphere of the brain and blood. **(b)** Overlap in differentially expressed genes in injured brain vs. sham blood Treg cells after injury with another study investigating the transcriptomic effects of stroke in brain vs. blood Treg cells[23]. **(c)** Selected top predicted regulators using IPA based on DEGs in TBI-aCD3 vs. TBI-Iso blood Treg cells at 7 days post-TBI identified using DESeq2 analysis (two-sided Wald test, FDR-corrected $P < 0.05$). One-sided Fisher's exact test. * $P < 0.05$, ** $P < 0.01$, *** $P < 0.001$. Results with FDR-corrected $P < 0.05$ were selected. **(d)** Predicted upstream regulator using IPA analysis based on DEGs of brain Tregs in TBI-aCD3 vs. TBI-Iso identified using DESeq2 analysis (two-sided Wald test, FDR-corrected $P < 0.05$). Due to the low number of $FoxP3^+$ cells recruited to the brain, and ethical considerations, we limited the study to two biological replicates, following practices from previous studies in the field[23]. Despite this limitation, the consistent and robust results observed support the validity of our findings.

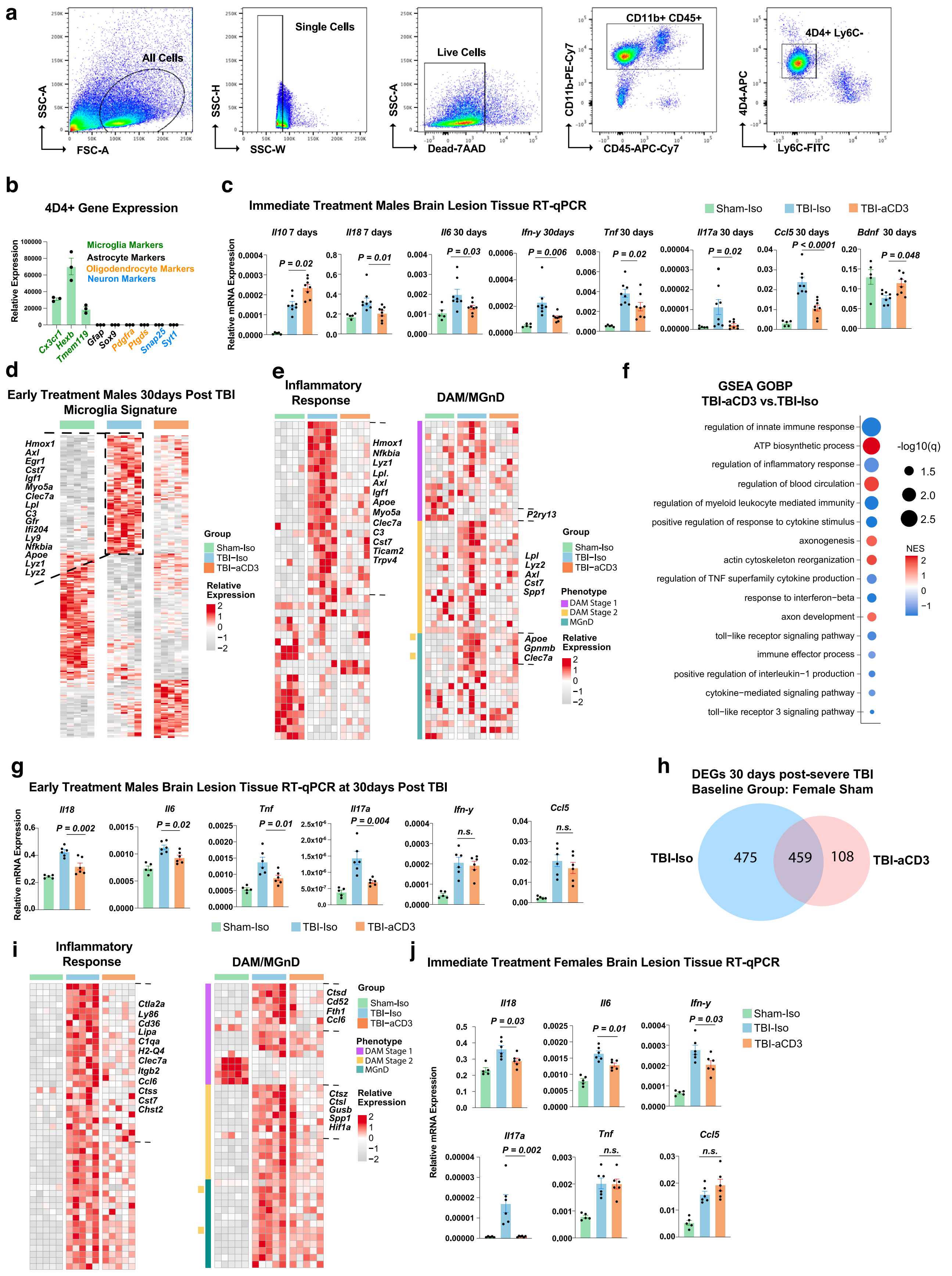

Extended Data Fig. 6 | See next page for caption.

Extended Data Fig. 6 | Nasal anti-CD3 modulates chronic microglial response after TBI for different treatment regimens and TBI severities. **(a)** Gating strategy for microglia. **(b)** Relative expression of cell types in Sham-Iso microglia (*n* = 3). **(c)** RT- qPCR of ipsilateral hemisphere 7 and 30 days post-TBI (immediate treatment males). Expression was normalized to GAPDH and presented relative to Sham-Iso. Data shown as mean ± SEM, (Sham-Iso *n* = 6, TBI-Iso *n* = 8, TBI-aCD3 *n* = 8) and analyzed by one-way ANOVA with Tukey's multiple comparisons. **(d)** Heatmap signature of DEGs 30 days post-TBI (early treatment males) identified using DESeq2 analysis (two-sided likelihood ratio test, *n* = 5 mice/group, FDR-corrected P < 0.05). **(e)** Heatmap of genes in inflammatory response and genes of disease-associated microglia (DAM) and neurodegenerative microglia (MGnD) 30 days post-TBI (early treatment males). Genes identified with an FDR-corrected p-value < 0.05 using DESeq2 analysis are bolded (two-sided likelihood ratio test, n = 5 mice/group). **(f)** GSEA analysis of GO Biological Processes (BP) comparing TBI-aCD3 vs. TBI-Iso groups 30 days post-TBI (early treatment male mice). NES, normalized enrichment score. **(g)** RT- qPCR of ipsilateral hemisphere 30 days post-TBI (early treatment males). Expression normalized to GAPDH and presented relative to Sham-Iso. Data shown as mean ± SEM, (Sham-Iso *n* = 5, TBI-Iso *n* = 6, TBI-aCD3 *n* = 6) and analyzed by one-way ANOVA with Tukey's multiple comparisons. **(h)** Venn diagram of DEGs in comparisons with Sham-Iso microglia group as baseline 30 days post-severe TBI (immediate treatment female mice): TBI-Iso, and TBI-aCD3. **(i)** Heatmap genes involved in inflammatory response and (DAM) and (MGnD) at 30 days following severe TBI (immediate treatment females). Genes identified with FDR-corrected p-value < 0.05 using DESeq2 analysis are bolded (two-sided likelihood ratio test, n = 5 mice/group). **(j)** RT-qPCR of ipsilateral hemisphere 30 days post-severe TBI (immediate treatment female). Expression was normalized to GAPDH and presented relative to Sham-Iso. Data shown as mean ± SEM, (Sham-Iso *n* = 5, TBI-Iso *n* = 6, TBI-aCD3 *n* = 6) and analyzed by one-way ANOVA with Tukey's multiple comparisons. All data are biological replicates and are representative from two independent experiments. *n.s.* = non-significant.

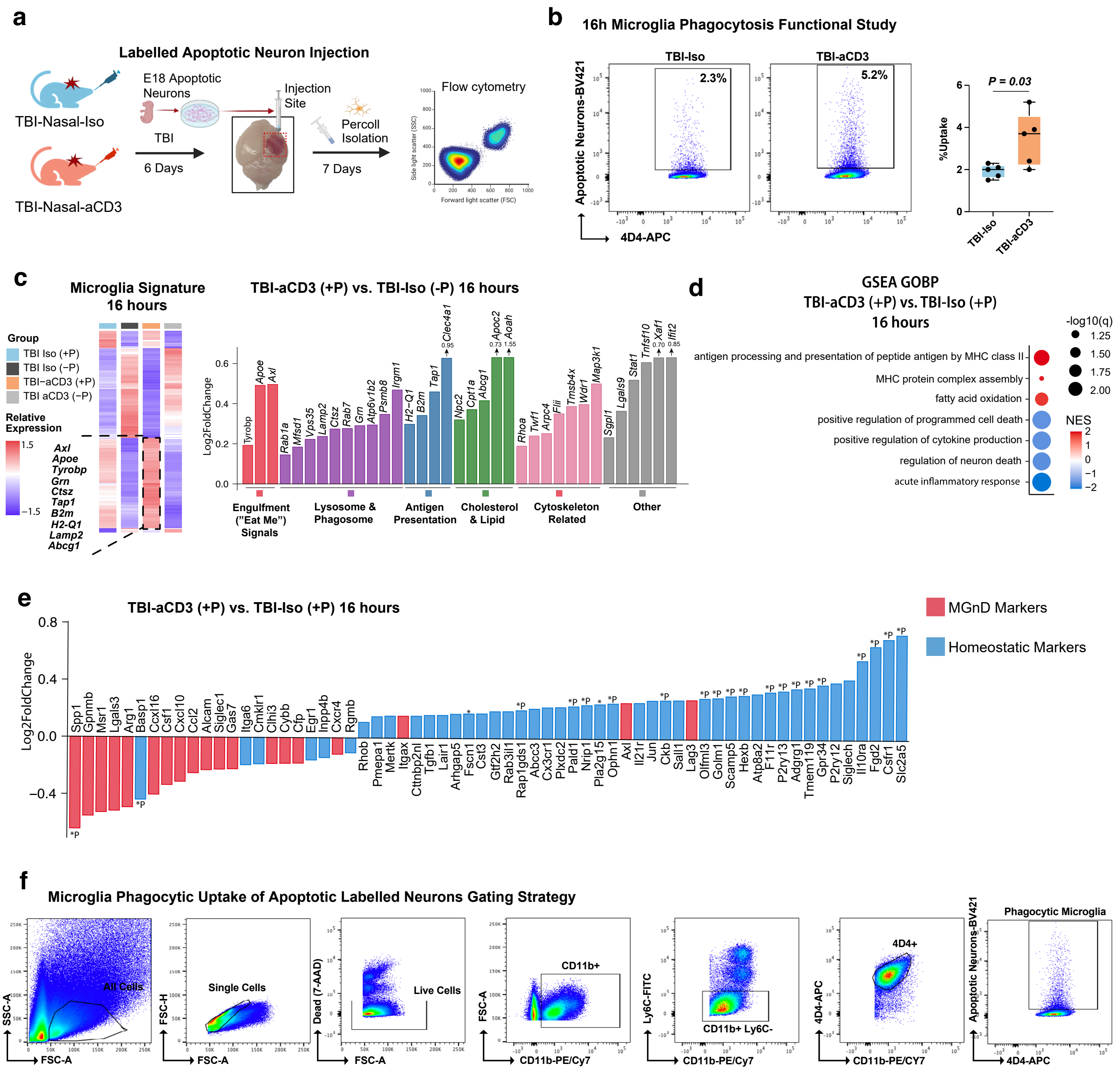

Extended Data Fig. 7 | Nasal anti-CD3 increases expression of phagocytosis machinery at 16 hours post injection of apoptotic neurons. (a) Schematic presenting phagocytosis functional study. Created with BioRender.com. **(b)** *In-vivo* phagocytosis functional experiment where mice were injected with labelled apoptotic neurons and sacrificed 16 h post injection. Gating strategy showing phagocytic positive microglia in TBI-Iso and TBI-aCD3 animals. Data shown as box plots (min, max, interquartile range, median) and *n* = 5 mice/group were used. Data was analyzed by two-sided unpaired Student's t-test. **(c)** Clustered heatmap of select DEGs of aggregated samples for phagocytic (+ P) and non-phagocytic (-P) microglia at 7 days following TBI and 16 hours post-injection of apoptotic neurons using DESeq2 analysis (two-sided likelihood ratio test, *n* = 5-6 mice/group, FDR-corrected P < 0.05). Identified genes pertinent to microglial phagocytosis and related functions are visualized through bar plots with log2-fold changes in phagocytic TBI-aCD3 microglia compared to non-phagocytic TBI-Iso microglia. **(d)** GSEA analysis of GO Biological Process (BP) comparing phagocytic TBI-aCD3 microglia to phagocytic TBI-Iso microglia at 7 days following TBI and 16 hours post-injection of apoptotic neurons. NES, normalized enrichment score. **(e)** Bar plots of select microglial homeostatic and neurodegenerative microglia (MGnD) markers in phagocytic TBI-aCD3 microglia compared to phagocytic TBI-Iso microglia at 7 days following TBI and 16 hours post-injection of apoptotic neurons. DEGs indicated with an asterisk: FDR-corrected P < 0.05; DEGs indicated with "*P": P < 0.05 (DESeq2 analysis, two-sided Wald test, n = 5 mice/group). **(f)** Gating strategy showing how phagocytic microglia cells were identified. All data are biological replicates and are representative from two independent experiments. *n.s.* = non-significant.

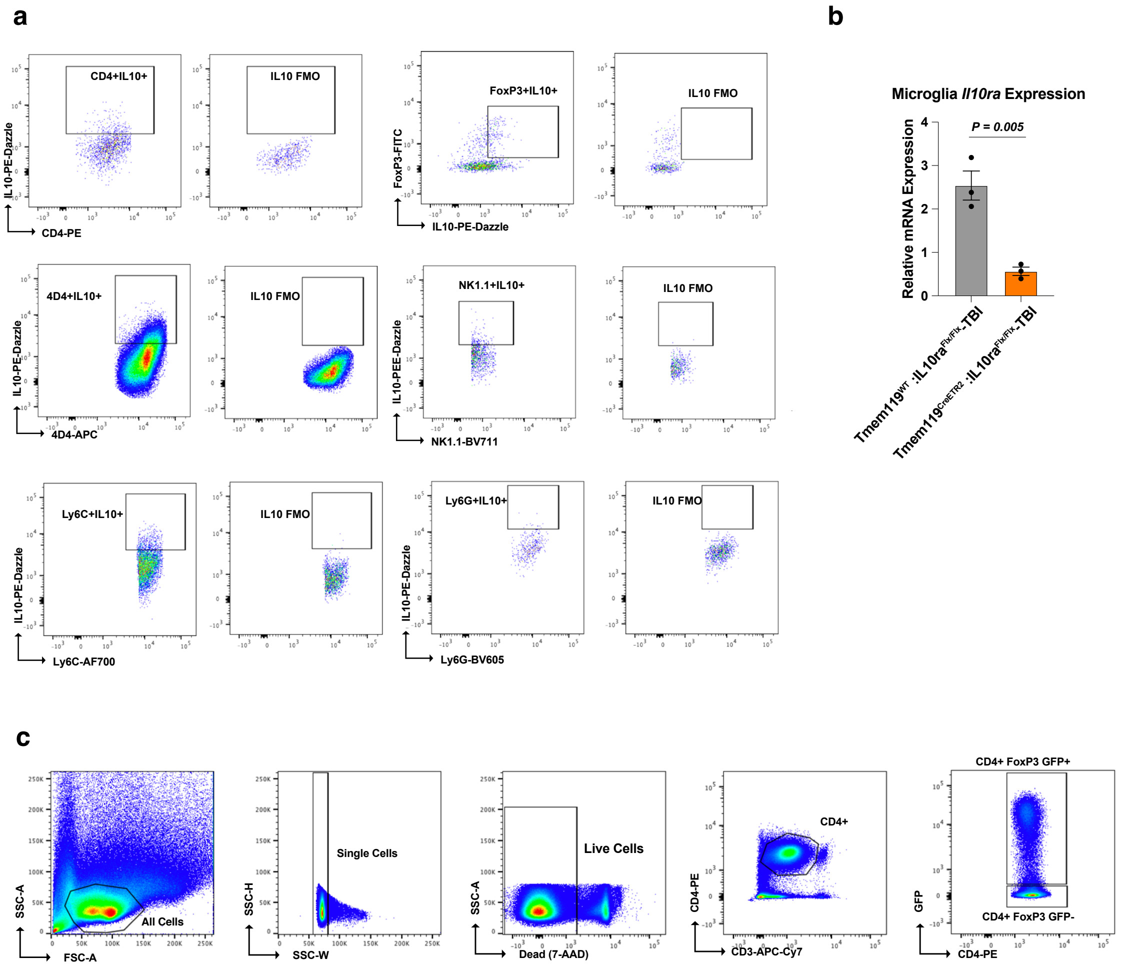

Extended Data Fig. 8 | Gating strategy of IL-10 production, tamoxifen induced microglia specific IL10ra reduction in gene expression, and FoxP3(GFP)+ gating strategy. **(a)** Gating strategy for IL-10 expression on CD4 + , FoxP3 + , 4D4+ microglia, NK1.1 + , Ly6C + , and Ly6G+ cell and their fluorescence minus one (FMO) control. **(b)** Bar plot of Quantitative PCR of microglia sorted from the ipsilateral hemisphere at 7 days post TBI for microglia specific IL-10ra knockout Tmem119^{CreETR2}:IL-10ra$^{Flx/Flx}$ and their littermate controls Tmem119^{WT}:IL-10ra$^{Flx/Flx}$. Mice were treated with tamoxifen for 5 straight days and were given a 2-week rest period before TBI. Expression was normalized to GAPDH. Data shown as mean ± SEM, $n = 3$ mice/group. Data was analyzed by two-sided unpaired Student's t-test. The data are biological replicates and are representative from three independent experiments. **(c)** Gating strategy showing CD4$^+$FoxP3 GFP$^+$ and the population of CD4$^+$FoxP3 GFP$^-$ from the spleen/cLN that was selected for the adoptive transfer experiments in Fig. 6 and Extended Data Fig. 9.

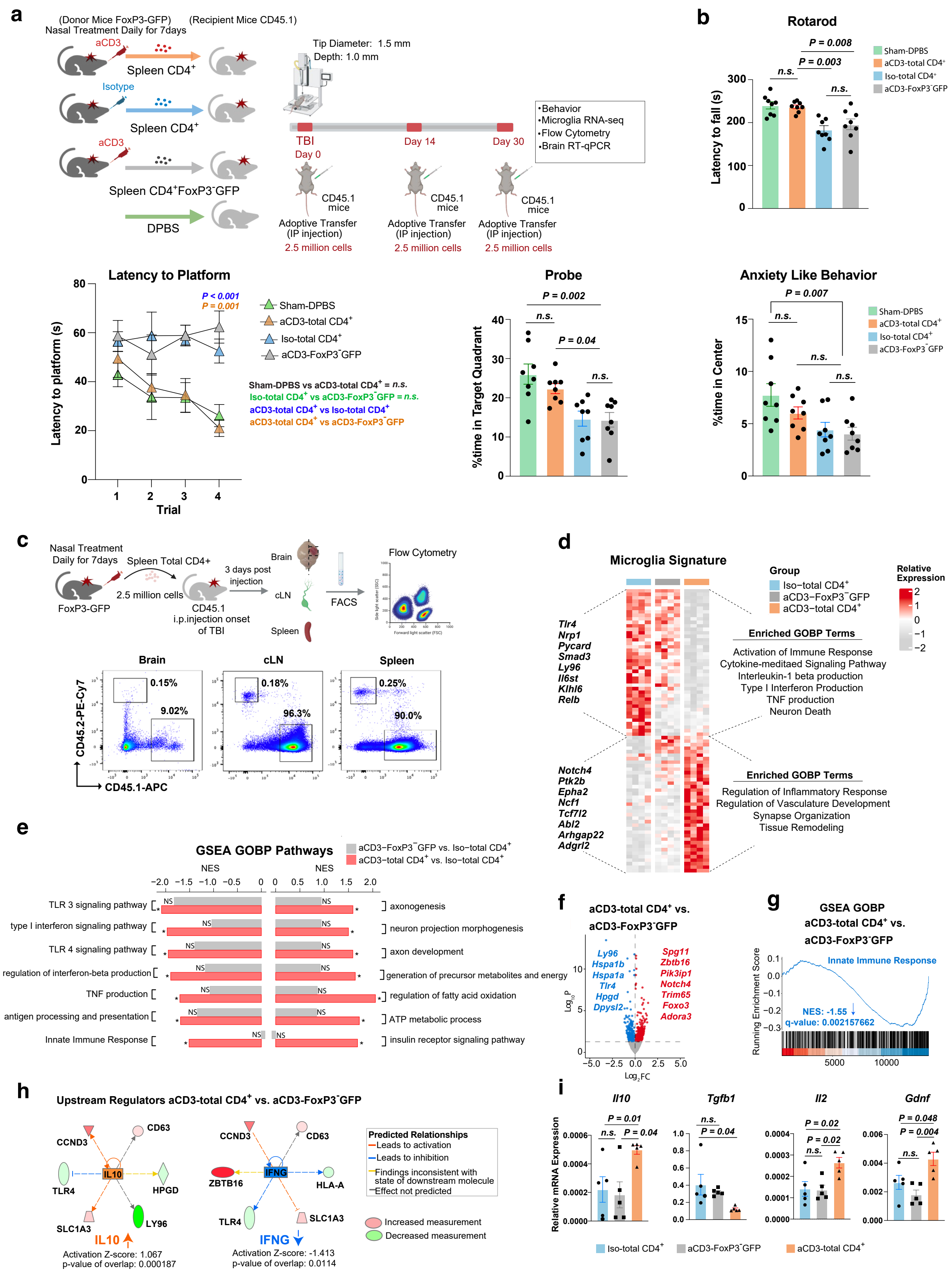

Extended Data Fig. 9 | See next page for caption.

Extended Data Fig. 9 | Nasal anti-CD3 induced Total CD4 + T-cells ameliorate microglial response and improved behavioral outcomes at chronic TBI. **(a)** Schematic representing experimental timeline of adoptive transfer experiment. Created with BioRender.com. **(b)** Behavioral testing of rotarod, Morris water maze, probe trial, and anxiety like behavior (measured by the open field) was assessed between WT Sham (DPBS treated, baseline), Iso-total CD4$^+$, aCD3-total CD4$^+$, and aCD3-FoxP3$^-$GFP groups. Morris water maze analyzed by two-factor repeated measures two-way ANOVA (group x time); others by one-way ANOVA with Tukey's multiple comparisons. Data shown as mean ± SEM. **(c)** Visual representing an experiment where splenic CD4$^+$ cells from 7 days treated TBI (FoxP3-GFP) animals were injected into untreated, but TBI-injured (CD45.1) animals and the %CD45.2 cells were analyzed by fluorescence-activated cell sorting (FACS) at 3 days after injection. Flow cytometry gating of brain, cervical lymph node, and spleen of (CD45.1) animals showing the percent of CD45.2 cell infiltration. $n = 5$ mice and the brain was a pool of 5 ipsilateral hemispheres. Created with BioRender.com. **(d)** Heatmap of DEGs from microglia 30 days following TBI and adoptive transfer identified using DESeq2 analysis (two-sided likelihood ratio test, $n = 4$ mice/group, FDR-corrected $P < 0.05$). Clusters of genes were functionally annotated using enriched GO Biological Process (BP) terms (q-value < 0.05). **(e)** GSEA analysis of GO Biological Process (BP) 30 days post-TBI based on the following comparisons: aCD3-Total CD4$^+$ vs. Iso-Total CD4$^+$, and aCD3-FoxP3$^-$GFP vs. Iso-total CD4$^+$. Asterisk (*) indicates enriched terms (q-value < 0.05). NES, normalized enrichment score; NS, not significant. **(f)** Volcano plot of DEGs in aCD3-total CD4$^+$ vs. aCD3-FoxP3$^-$GFP 30 days post-TBI identified using DESeq2 (two-sided Wald test, n = 4 mice/group). Labeled genes have an FDR-corrected $P < 0.05$. **(g)** GSEA analysis of GO Biological Process (BP) comparing aCD3-total CD4$^+$ vs. aCD3-FoxP3$^-$GFP 30 days post-TBI. NES, normalized enrichment score**. (h)** Predicted top upstream regulators using IPA analysis based on DEGs in aCD3-total CD4$^+$ vs. aCD3-FoxP3$^-$GFP 30 days post-TBI. **(i)** RT- qPCR of ipsilateral hemisphere 30 days post-TBI and expression normalized to GAPDH. Data shown as mean ± SEM, $n = 5$ mice/group and analyzed by one-way ANOVA with Tukey's multiple comparisons. All data are biological replicates and are representative from two independent experiments. *n.s.* = non-significant.

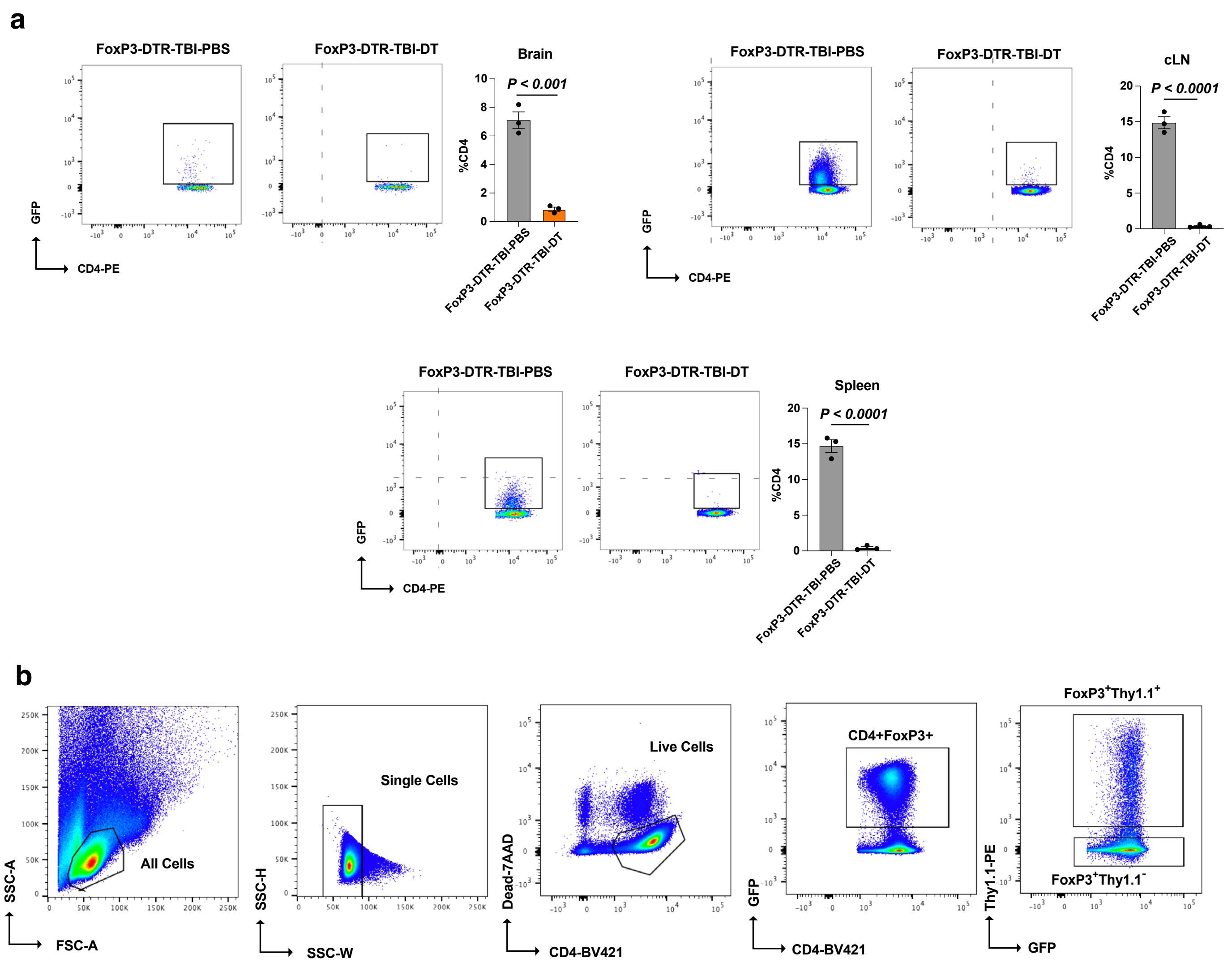

Extended Data Fig. 10 | Validation of FoxP3 depletion in FoxP3-DTR mice following Diphtheria toxin (DT) injection and Gating strategy of FoxP3$^+$Thy1.1$^+$ IL-10 producing FoxP3 Tregs. (a) Flow cytometry gating showing depletion of FoxP3$^+$ Tregs after DT injection compared to DPBS injected for FoxP3-DTR mice 7 days post-TBI in the ipsilateral brain hemisphere, cLN, and spleen. DT was injected 3 days prior to TBI and was given every third day to sustain FoxP3 depletion. Data shown as mean ± SEM, *n* = 3 mice/group. Data was analyzed by two-sided unpaired Student's t-test. The data are biological replicates and are representative from three independent experiments. **(b)** Gating strategy showing FoxP3$^+$Thy1.1$^+$ and FoxP3$^+$Thy1.1$^-$ from the spleen/cLN of dual reporter 10BiT.FoxP3^{GFP} mice that was selected for the adoptive transfer experiments for Fig. 7.

Corresponding author(s): Howard L. Weiner

Last updated by author(s): Nov 14, 2024

Reporting Summary

Nature Portfolio wishes to improve the reproducibility of the work that we publish. This form provides structure for consistency and transparency in reporting. For further information on Nature Portfolio policies, see our Editorial Policies and the Editorial Policy Checklist.

Statistics

For all statistical analyses, confirm that the following items are present in the figure legend, table legend, main text, or Methods section.

n/a	Confirmed	
☐	☒	The exact sample size (*n*) for each experimental group/condition, given as a discrete number and unit of measurement
☐	☒	A statement on whether measurements were taken from distinct samples or whether the same sample was measured repeatedly
☐	☒	The statistical test(s) used AND whether they are one- or two-sided *Only common tests should be described solely by name; describe more complex techniques in the Methods section.*
☐	☒	A description of all covariates tested
☐	☒	A description of any assumptions or corrections, such as tests of normality and adjustment for multiple comparisons
☐	☒	A full description of the statistical parameters including central tendency (e.g. means) or other basic estimates (e.g. regression coefficient) AND variation (e.g. standard deviation) or associated estimates of uncertainty (e.g. confidence intervals)
☐	☒	For null hypothesis testing, the test statistic (e.g. *F*, *t*, *r*) with confidence intervals, effect sizes, degrees of freedom and *P* value noted *Give P values as exact values whenever suitable.*
☐	☒	For Bayesian analysis, information on the choice of priors and Markov chain Monte Carlo settings
☐	☒	For hierarchical and complex designs, identification of the appropriate level for tests and full reporting of outcomes
☒	☐	Estimates of effect sizes (e.g. Cohen's *d*, Pearson's *r*), indicating how they were calculated

Our web collection on statistics for biologists contains articles on many of the points above.

Software and code

Policy information about availability of computer code

Data collection	1.RNA-seq. Samples were processed for cDNA generation and Illumina Nextera XT library construction. Sequencing data was generated using 2x38 bp paired end sequencing on the NextSeq500. 2.Flow cytometry. acquisition was performed on FACSSymphony A5 (BD Biosciences) using DIVA software. 3.Immunofluorescence. Images were acquired using a Leica DMi8 widefield microscope and Zeiss LSM710 Confocal. 4.RT-qPCR. Data were collected using a Vii 7 real-time PCR system. 5.Cell sorting. Cells were sorted using FACSAria II. 6.Behavioral data acquisition. Noldus EthoVision XT software v.17.0.
Data analysis	1.RNA-seq. RNA-seq reads was assessed using FastQC quality control tool. Reads were concatenated then trimmed using Trimmomatic. The RNA reads were aligned to the mouse mm10 reference genome using HISAT2. HISAT2-generated SAM files were sorted and converted into BAM files using Samtools. The sorted reads were assembled into transcripts using StringTie104. Next, StringTie-generated transcript lengths and abundance estimates were converted into count matrices using Tximport. Differential gene expression analysis was performed with false discovery rate (FDR)-adjusted P values using DESeq2. Data visualization was performed in R (version 4.0.3). 2.Flow cytometry. Data were analyzed with FlowJo software version 10. 3.Immunofluorescence. Images were processed using Fiji. 4.RT-qPCR. Quantitative PCR data were analyzed by the delta-delta Ct method. 5. Statistical analysis.Statistical analysis was performed using GraphPad Prism 9 software.

For manuscripts utilizing custom algorithms or software that are central to the research but not yet described in published literature, software must be made available to editors and reviewers. We strongly encourage code deposition in a community repository (e.g. GitHub). See the Nature Portfolio guidelines for submitting code & software for further information.

Data

Policy information about availability of data

All manuscripts must include a data availability statement. This statement should provide the following information, where applicable:

- Accession codes, unique identifiers, or web links for publicly available datasets
- A description of any restrictions on data availability
- For clinical datasets or third party data, please ensure that the statement adheres to our policy

The Smartseq2 RNA-sequencing data that support the findings of this study have been deposited into Gene Expression Omnibus (GEO) under SuperSeries GSE276761.

Research involving human participants, their data, or biological material

Policy information about studies with human participants or human data. See also policy information about sex, gender (identity/presentation), and sexual orientation and race, ethnicity and racism.

Reporting on sex and gender	N/A
Reporting on race, ethnicity, or other socially relevant groupings	N/A
Population characteristics	N/A
Recruitment	N/A
Ethics oversight	N/A

Note that full information on the approval of the study protocol must also be provided in the manuscript.

Field-specific reporting

Please select the one below that is the best fit for your research. If you are not sure, read the appropriate sections before making your selection.

☒ Life sciences ☐ Behavioural & social sciences ☐ Ecological, evolutionary & environmental sciences

For a reference copy of the document with all sections, see nature.com/documents/nr-reporting-summary-flat.pdf

Life sciences study design

All studies must disclose on these points even when the disclosure is negative.

Sample size	In our study, 3-12 mice were used per group and every experiment was reproduced at least twice, which is commonly used for in vivo studies to alleviate unnecessary animal suffering. No sample calculation size was performed but was chosen in accordance with previous studies in the field: -Roth, T. L. et al. Transcranial amelioration of inflammation and cell death after brain injury. -Nature 505, 223-228 (2014), Kramer, T. J. et al. Depletion of regulatory T cells increases T cell brain infiltration, reactive astrogliosis, and interferon-gamma gene expression in acute experimental traumatic brain injury. J Neuroinflammation 16, 163 (2019) Brain and blood samples are pools of 5 mice, and sham-Iso brain samples are pools of 20 mice. Due to the low number of FoxP3$^+$ cells recruited to the brain, and ethical considerations, we limited the study to two biological replicates, following practices from previous studies in the field for blood and treg sequencing: -Shi, L. et al. Treg cell-derived osteopontin promotes microglia-mediated white matter repair after ischemic stroke. Immunity 54, 1527-1542 e1528 (2021
Data exclusions	Outliers were excluded as determined by the following: Any value that is 1.5 x IQR greater than the third quartile is designated as an outlier and any value that is 1.5 x IQR less than the first quartile is also designated as an outlier.
Replication	All experiments were performed at least twice to assure rigor and reproductibility, and all attempts at replication were successful.
Randomization	Mice were randomly assigned to the experimental groups. For in-vitro experiments, cells from the randomly assigned mice were sorted with each mouse and each well in the culture was from a different biological replicate.
Blinding	For all experiments the investigator was blinded to the different groups. Experimenter was also blinded to the different well conditions in the in-vitro experiement.

Reporting for specific materials, systems and methods

We require information from authors about some types of materials, experimental systems and methods used in many studies. Here, indicate whether each material, system or method listed is relevant to your study. If you are not sure if a list item applies to your research, read the appropriate section before selecting a response.

Materials & experimental systems

n/a	Involved in the study	
☐	☒	Antibodies
☒	☐	Eukaryotic cell lines
☒	☐	Palaeontology and archaeology
☐	☒	Animals and other organisms
☒	☐	Clinical data
☒	☐	Dual use research of concern
☒	☐	Plants

Methods

n/a	Involved in the study	
☒	☐	ChIP-seq
☐	☒	Flow cytometry
☐	☒	MRI-based neuroimaging

Antibodies

Antibodies used

in-vivo/vitro antibodies:
hamster IgG CD3-specific antibody (clone 145-2C11.BioXCell), hamster IgG control antibody (BioXCell), monoclonal anti-IL-10R blocking antibody (clone 1B1.3A, BioXCell), IL-10 neutralizing antibody (JES5-2A5; BioXCell).

Flow Cytometry:
Zombie Aqua Fixable Viability Kit (Biolegend, #423102, 1:1000) or Zombie UV (Biolegend, #423108, 1:1000) was used to exclude dead cells. The staining antibodies used PE/Cyanine7 anti-mouse CD11b (M1/70, Biolegend, 1:300), APC/Cyanine7 anti-mouse TCR-beta (H57-597, Biolegend, 1:100), BUV661 anti-mouse CD45 (30-F11, BD Biosciences, 1:200), PE anti-mouse CD4 (GK1.5, Biolegend, 1:100), BUV805 anti-mouse CD8 (53-6.7, BD Biosciences 1:100), FITC anti-mouse FoxP3 (FJK-16s, eBioscience, 1:100), BV421 anti-mouse LAP (TW7-16B4, Biolegend, 1:100), PE/Dazzle 594 anti-mouse IL-10 (JES5-16E3, Biolegend, 1:100), BUV395 anti-mouse IL-17a (TC11-18H10, BD Biosciences, 1:100), BV785 anti-mouse IFN-g (XMG1.2, Biolegend, 1:100), BV605 anti-mouse Ly6G (1A8, Biolegend, 1:300), BV711 anti-mouse NK-1.1 (PK136, Biolegend, 1:100), AF700 anti-mouse Ly6C (HK1.4, Biolegend, 1:200), BV711 anti-mouse Ly6C (HK1.4, Biolegend, 1:200), and APC anti-mouse 4D4 (1:1000) provided by Dr. Butovsky.

For Cell Sorting:
PE/Cyanine7 anti-mouse CD11b (M1/70, Biolegend, 1:100), APC/Cyanine7 anti-mouse CD45 (30-F11, Biolegend, 1:100), FITC anti-mouse Ly6C (AL-21, BD Bioscience, 1:200) and APC anti-mouse 4D4 (marking resident microglia; 1:1000. APC/Cyanine7 anti-mouse CD45 (30-F11, Biolegend, 1:100), APC anti-mouse CD4 antibody (GK1.5, Biolegend, 1:100), and 7-AAD (BD Bioscience.

Tissue Staining:
Anti Iba1 (rabbit,1:1000, Wako), 647 goat anti-rabbit IgG (1:1000, Abcam, ab150075) haematoxylin and eosin (HE; Abcam, ab245880), and TUNEL (TUNEL Assay Kit - BrdU-Red, Abcam, ab66110),DAPI mounting media (Vector Laboratories, UX-93952-24). Alexa Flour 647 anti-mouse CD3 (17A2, Biolegend, 1:50).

Validation

Antibody dilutions were used as recommended by the manufactures. All antibodies employed in this study are well characterized and broadly used by the research community. Validation of all primary antibodies for the species and applications can be found at the website of the company, for example, Biolegend, Abcam, and BD Biosciences where the antibodies were purchased. Microglia staining 4D4 antibody was developed in our laboratory and has been extensively used. Krasemann, S. et al. The TREM2-APOE Pathway Drives the Transcriptional Phenotype of Dysfunctional Microglia in Neurodegenerative Diseases. Immunity 47, 566-581 e569 (2017). Butovsky, O. et al. Modulating inflammatory monocytes with a unique microRNA gene signature ameliorates murine ALS. J Clin Invest 122, 3063-3087 (2012).

Animals and other research organisms

Policy information about studies involving animals; ARRIVE guidelines recommended for reporting animal research, and Sex and Gender in Research

Laboratory animals

Studies were performed using 8-12-week-old C57BL6J mice (000664, Jackson Laboratories), B6.CD45.1 mice (002014, Jackson Laboratory), FoxP3-GFP mice (023800, Jackson Laboratory), FoxP3-DTR mice (016958, Jackson Laboratory), IL10-KO mice (002251Jackson Laboratory), Tmem119-CreETR2 mice (031820, Jackson Laboratory), IL-10raFlx mice (028146, Jackson Laboratory), and 10BiT.FoxP3GFP (kindly provided by Dr. Vijay Kuchroo). All mice were housed under specific pathogen free conditions, with food and water ad libitum. All animals were housed in temperature (20 ºC) - and humidity (60 %)-controlled rooms, maintained on a 12-h/12-h light/dark cycle (lights on at 7:00 AM). Mice were euthanized by CO2 inhalation. The Institutional Animal Care and Use

	Committee (IACUC) at Harvard Medical School and Brigham and Women's Hospital has all experimental procedures involving animals.
Wild animals	No wild animals were used in the study.
Reporting on sex	Both males and females were used.
Field-collected samples	No field-collected samples were used in the study.
Ethics oversight	All experiments were reviewed and overseen by the institutional animal use and care committee at Brigham and Women's Hospital in accordance with NIH guidelines for the humane treatment of animals. IACUC Protocol number: 2018N000028.

Note that full information on the approval of the study protocol must also be provided in the manuscript.

Plants

Seed stocks	N/A
Novel plant genotypes	N/A
Authentication	N/A

Flow Cytometry

Plots

Confirm that:

☒ The axis labels state the marker and fluorochrome used (e.g. CD4-FITC).

☒ The axis scales are clearly visible. Include numbers along axes only for bottom left plot of group (a 'group' is an analysis of identical markers).

☒ All plots are contour plots with outliers or pseudocolor plots.

☒ A numerical value for number of cells or percentage (with statistics) is provided.

Methodology

Sample preparation	Flow cytometry microglial sorting For microglial cell sorting, mice were anesthetized with CO2 until respiration rate slowed and then transcardially perfused with 50mL hanks balanced salt solution (HBSS) containing heparin (1:1000). Following perfusion, the ipsilateral hemisphere homogenised using a dounce glass tissue homogeniser. Cells were separated through Percoll (GE Healthcare Life Sciences) 30% gradient centrifugation. Cells were isolated from the Percoll layer and stained on ice for 30 min with combinations of PE/Cyanine7 anti-mouse CD11b (M1/70, Biolegend, 1:100), APC/Cyanine7 anti-mouse CD45 (30-F11, Biolegend, 1:100), FITC anti-mouse Ly6C (AL-21, BD Bioscience, 1:200) and APC anti-mouse 4D4 (marking resident microglia; 1:1000) in blocking buffer containing 0.2% bovine serum albumin (BSA, Sigma-Aldrich) in HBSS. Cell sorting was performed using FACSAriaIII cell sorter (Becton Dickson). Microglial cells were identified as CD45+CD11b+ Ly6C-4D4+ and Dead cells were also excluded based on 7-AAD (BD Bioscience) staining. Cells were sorted directly in 1.5mL Eppendorf tubes and stored at -80°C. Phagocytic positive microglia was sorted as 4D4+ Alexa405+. Flow cytometry Intracellular Staining Intracellular cytokine staining and cell isolation was done as previously described. The meninges were carefully removed from the skull and the ipsilateral brain was further isolated. The enzyme dissociation mix used for the ipsilateral brain hemisphere and meninges was Collagenase P (0.5 mg/mL, Sigma cat. 11213865001) and DNAse-1 (250 U/mL, Worthingon cat. LK003172) diluted in RPMI-1640 with 10 mM HEPES. The samples were then finely minced and incubated in a room temp shaker for 1 hour. Following the enzyme dissociation, the cells were separated using Percoll (GE Healthcare Life Sciences) as described above. Cells isolated from the brain and meninges were only incubated for 2 hours instead of the 4 hours for cLN cells. Acquisition was performed on a Symphony (BD Biosciences) by using DIVA software (BD Biosciences) and data were analyzed with FlowJo software versions 9.9 or 10.1 (TreeStar Inc.). Intracellular staining antibodies used Zombie Aqua Fixable Viability Kit (Biolegend, #423102, 1:1000) or Zombie UV (Biolegend, #423108, 1:1000) was used to exclude dead cells. The staining antibodies used PE/Cyanine7 anti-mouse CD11b (M1/70, Biolegend, 1:300), APC/Cyanine7 anti-mouse TCR-beta (H57-597, Biolegend, 1:100), BUV661 anti-mouse CD45 (30-F11, BD Biosciences, 1:200), PE anti-mouse CD4 (GK1.5, Biolegend, 1:100), BUV805 anti-mouse CD8 (53-6.7, BD Biosciences 1:100), FITC anti-mouse FoxP3 (FJK-16s, eBioscience, 1:100), BV421 anti-mouse LAP (TW7-16B4, Biolegend, 1:100), PE/Dazzle 594 anti-mouse IL-10 (JES5-16E3, Biolegend, 1:100), BUV395 anti-mouse IL-17a (TC11-18H10, BD Biosciences, 1:100), BV785 anti-mouse IFN-g (XMG1.2, Biolegend, 1:100), BV605

anti-mouse Ly6G (1A8, Biolegend, 1:300), BV711 anti-mouse NK-1.1 (PK136, Biolegend, 1:100), AF700 anti-mouse Ly6C (HK1.4, Biolegend, 1:200), BV711 anti-mouse Ly6C (HK1.4, Biolegend, 1:200), and APC anti-mouse 4D4 (1:1000) provided by Dr. Butovsky.

Flow cytometry FoxP3(GFP) Tregs Sorting from the brain and blood

The ipsilateral brain hemisphere was processed with the same enzyme dissociation kit described above and then processed as the microglia cell sorting above. The sample were purified and enriched using CD4 cell isolation microbead kit (Militenyi Biotech, #130-104-454) on a magnetic MACS separator prior to sorting. Cell sorting was performed using FACSAriaIII cell sorter (Becton Dickson). APC/Cyanine7 anti-mouse CD45 (30-F11, Biolegend, 1:100), APC anti-mouse CD4 antibody (GK1.5, Biolegend, 1:100), and 7-AAD (BD Bioscience) was used to identify the live CD4+ population and the FITC channel was used to identify the FoxP3+ population. Each RNA sequencing sample is a pool of 5 ipsilateral hemispheres and 20 sham brain hemispheres. The blood samples were collected in heparin coated tubes and then transferred to a 15 mL tubes where ACK lysis buffer was used to lyse the erythrocytes. The sample was then strained through a 70 um filter and stained as decribed above. Each RNA sequencing sample is a pool of 5 mice.

Instrument

Flow cytometry acquisition was performed on FACSSymphony A5 (BD Biosciences) using DIVA software.
Cell were sorted using FACSAria III (Becton Dickson)

Software

Flow cytometry data were analyzed with FlowJo software version 10.

Cell population abundance

Gating Ly6C negative and CD11b positive yielded a cell population which was >95% positive for 4D4, a microglia-specific marker, which gates were drawn for and positive cells taken for analysis.

Gating strategy

Microglial cells were identified as CD45+CD11b+ Ly6C-4D4+ and Dead cells were also excluded based on 7-AAD (BD Bioscience) staining. Phagocytic positive microglia was sorted as 4D4+ Alexa405+

For FoxP3 Tregs were selected based on Dead cells were also excluded based on 7-AAD and CD4+ cells were gated then GFP+ cells were sorted as FoxP3 Tregs.

For Intracellular staining Dead cells were excluded with zombie aqua and CD45+ cells were gated, then CD11b+ was excluded followed by gating on TCR-b+ cells, Followed by gating both CD4+ and CD8+ T-cells. Different subtypes of CD4+ T cells were gated on CD4 and were chosen to be positive for that population based on an FMO for that marker.

Detailed gating strategies and FMOs are found in extended Data Fig 4,5,6,7,8, and 9.

☒ Tick this box to confirm that a figure exemplifying the gating strategy is provided in the Supplementary Information.

Magnetic resonance imaging

Experimental design

Design type

One week post-TBI mice went through MRI imaging to measure the lesion volume of the injury.

Design specifications

Imaging was done using 7.0T Bruker BioSpect®USR. In brief, mice were gently handled and placed in isoflurane anesthesia chamber. Then mice were placed inside the imaging apparatus with their nose in front of tubes releasing 2% of isoflurane. Electrocardiogram (ECG) leads were placed on the animal's paws and a pneumatic pillow sensor will be placed under the abdomen for continuous ECG and respiratory rate monitoring of the anesthetized animal. These waveforms were closely monitored throughout MRI scanning by the MRI operator. The animal was placed on an MRI compatible bed, which will be placed inside the magnet for imaging. The imaging sessions last between 15-60 minutes. Mice were then returned to their cages and were monitored continuously after being returned to their cages prior to returning to a fully alert status. The. Following parameters were obtained to generate the T2 sequence images: Slice Thickness: 0.5mm, Repetition Time:3000ms, Echo Time: 50ms, Number of Averages: 3, Spacing Between Slices:0.5mm, Echo Train Length: 8, Acquisition Matrix: 200x200, Flip Angle:90, Field of View: 20mm. Serial Images were viewed and analyzed using the 3D Slicer platform

Behavioral performance measures

The MRI was used to quantify lesion volume by obtaining T2 sequences, and behavioral performance measures were not required to be obtained for that purpose.

Acquisition

Imaging type(s)	Structural
Field strength	7T
Sequence & imaging parameters	The following parameters were obtained to generate the T2 sequence images: Slice Thickness: 0.5mm, Repetition Time:3000ms, Echo Time: 50ms, Number of Averages: 3, Spacing Between Slices:0.5mm, Echo Train Length: 8, Acquisition Matrix: 200x200, Flip Angle:90, Field of View: 20mm.
Area of acquisition	The whole brain was used.

Diffusion MRI ☐ Used ☒ Not used

Preprocessing

Preprocessing software	3D Slicer platform
Normalization	DICOM files were opened and serial images of the whole brain was obtained to analyze the TBI lesion volume
Normalization template	No data was normalized
Noise and artifact removal	The animal was well-sedated where noise and artifact removal were not required.
Volume censoring	The animal was well-sedated and positioned in which volume censoring was not needed.

Statistical modeling & inference

Model type and settings	A statistical model was not used and only lesion volumes were directly calculated from the T2 sequences.
Effect(s) tested	No statistical effects were tested and only lesion volumes were directly calculated from the T2 sequences.

Specify type of analysis: ☐ Whole brain ☒ ROI-based ☐ Both

Anatomical location(s): The area of lesion was measured and analyzed using the Slicer 3D platform

Statistic type for inference (See Eklund et al. 2016)	Statistical inference was not used since lesion volumes were directly calculated from the T2 sequences.
Correction	Correction was not required since lesion volumes were directly calculated from the T2 sequences.

Models & analysis

n/a	Involved in the study	
☒	☐	Functional and/or effective connectivity
☒	☐	Graph analysis
☒	☐	Multivariate modeling or predictive analysis